Particle manipulation in plasma device & Dynamics of binary complex plasma

Ke Jiang

München 2011

Particle manipulation in plasma device & Dynamics of binary complex plasma

Ke Jiang

Dissertation
an der Fakultät für Physik
der Ludwig–Maximilians–Universität
München

vorgelegt von
Ke Jiang
aus Dalian, P.R.China

München, den 31.05.2011

Erstgutachter: Prof. Gregor Morfill
Zweitgutachter: Prof. Hartmut Zohm
Tag der mündlichen Prüfung: 01.08.2011

I think physicists are the Peter Pans of the human race. They never grow up and they keep their curiosity.

Isidor Isaac Rabi

It is not the possession of truth, but the success which attends the seeking after it, that enriches the seeker and brings happiness to him.

Max Planck

Stands at the sea... wonders at wondering... I... a universe of atoms... an atom in the universe.

Richard Feynman

Contents

Acknowledgements

Firstly I would like to thank my supervisor, Prof. Gregor Morfill, for his supervision and encouragement and for offering me the opportunity to perform research and giving me the freedom to choose topics at the Max-Planck-Institute for Extraterrestrial Physics. His deep thinking and humor have shown me that research can be so entertaining. Besides, his comments and suggestions are part of what constructed the final form of this thesis.

Secondly, I would like to thank Dr. Yangfang Li, for his everyday company and friendship, as well as the vast amount of knowledge he passed onto me in experimental physics. His unconditional contribution is a key element in the success of building the striped electrode chamber. His suggestions lead this thesis toward the current shape.

I am also deeply grateful to the following colleagues without whom the completion of this thesis would not be possible: I thank Dr. Hubertus Thomas for reading the thesis and providing very useful suggestions; Dr. Alexei Ivlev for many helpful discussions on lane formation and phase separation, and for sharing his profound knowledge on physics; Dr. Lujing Hou for his constant encouragement and fruitful discussions about numerical simulations ever since my undergraduate study; Dr. Tetsuji Shimizu and Dr. Uwe Konopka for their help in building the experimental apparatus, for passing their mechanical skills onto me and for being humorous though in different ways; Dr. Vladimir Nosenko for being gentle and encouraging all the time and for many intensive discussions about Mach cones; Dr. Robert Sütterlin for fruitful discussions about binary complex plasmas and for his great support for computers; Dr. Philip Brandt for helping me polish the German abstract; Chengran Du for his efforts on analyzing my simulation results for the lane formation topic in chapter 3.

I would also like to thank my current and former colleagues in complex plasma group in MPE for helpful discussions, parties, table tennis, *etc*: Alexander, Boris, Christina, Christoph, Dong, Guido, Herwig, Julia, Jin, Katinka, Lisa, Lénaïc, Michael, Martin, Mikhail, Mierk, Markus, Milenko, Manis, Peter, Pintu, Roman, Ralf, Slobodan, Sergey (both young and old), Satoshi, Tobias, Thomas, Tetyana, and Victoria.

Thanks goto Angelika and Elsbeth for their support to address administrative issues. Thanks must also goto engineers in our group, Bernd Steffes, Florian Huber and Günter Stadler for their technical support in the laboratories.

I am grateful to Dr. Felix Cheung for his help in improving my academic writing since my graduate study and providing valuable suggestions for this thesis.

I would also like to take this opportunity to thank Prof. Younian Wang for giving me

the first lesson on plasma physics at *Dalian University of Technology*.

Lastly, I am in great debts to my beloved grandparents who raised me up and supported my study unconditionally. I would also like to thank my wife Ning for her love, patience, and for understanding me spending most of the time on physics. I thank my daughter Luna for dispersing my life into different colors starting with lots of "PHDs" (Pretty Heavy Diapers).

Zusammenfassung

Ein komplexes Plasma ist eine Suspension von nano- bis mikrometergrößen Staubteilchen in einem Plasma mit Ionen, Elektronen und neutralen Gasmoleküle. Die Staubteichen erhalten einige tausend von Elektronen-Ladungen durch die Aufnahme von umgebenden Elektronen und Ionen, folglich interagieren diese über ein dynamisch abgeschirmtes Coulomb-Potential.

Staubpartikel in einem komplexen Plasma können durch eine niedrige Frequenz mit elektrostatischer Verzerrung gesteuert werden. Wir untersuchten die Transportgeschwindigkeiten der Teilchen, indem wir Frequenz und Phase von der angelegten Spannung einer segmentierten Elektrode modulierten. Wir benutzen zudem eine Molekulardynamik-Simulation die unsere experimentellen Beobachtungen wiedergab, unter den gleichen Bedingungen wie in unabhängigen "Particle-in-cell"-Simulationen. Wir fanden, dass der Transport von Staubteilchen durch niederfrequente Modulation in unseren Simulationen in guter Übereinstimmung mit den experimentellen Befunden ist. So ist es zum Einen ein Ziel dieser Arbeit eine potentielle Technik zu erarbeiten, die zum Problem der Staub-Kontamination in Plasma-Processing-Reaktoren beiträgt und zum Anderen soll ein Setup entworfen werden, in dem große zwei-dimensionale Systeme aus komplexen Plasmen untersucht werden knnen, sodass Radeffekte zu vernachlässigen sind.

Dann gingen wir daran, die Nicht-Additivität eines komplexen Plasmas mit zwei verschiedenen Größen von Staubpartikeln (binäre komplexe Plasmen) zu studieren. Für Staubteilchen vom Typ 1 und Typ 2 ist die 1-2 (Inter-Spezies-) Wechselwirkung immer mehr repulsiv als das geometrische Mittel von 1-1- und 2-2- Wechselwirkungen. Diese Asymmetrie in der gegenseitigen Wechselwirkung wird als positiv nicht-additiv bezeichnet. Wir fanden heraus, dass zwei Typen von Teilchen in fluid-fluid-Phasen separieren; das Wachstum hierbei folgt einem einfachen Potenzgesetz mit einem Exponenten von rund 1/3 bis die Stärke der Kopplung gering genug ist, um dann, in guter Übereinstimmung dem Lifshitz-Slyozov-Wachstumsgesetz für das initiale diffuse Regime der Phasenseparation zu folgen. Wir benutzen Langevin-Dynamik-Simulationen um den Einfluss von nicht-additiver Wechselwirkung auf die "Lane-Formation" zu testen. Wir zeigten ein Crossover aus normalen Modus-Laning zu einer Entmischung dominieren Modus-Laning. Zudem fanden wir, dass die "Lane-Formation" stark durch die exakte räumliche Konfigurationen beeinflusst wird, bei einem erheblichen Kontakt-Moment zwischen zwei verschiedenen komplexen Plasmen.

Wir verwendeten auch Hydrodynamik, um die Entwicklung von Mach-Kegeln in komplexen Plasmen in untersuchen. Unser Hydrodynamik-modell konnte die Kompressions-Wellen in Mach-Kegeln, die in Experimenten an Bord der Internationalen Raumstation beobachte wurden, erklären.

Abstract

A complex plasma is a suspension of nano- to micron-sized dust particles immersed in a plasma with ions, electrons and neutral gas molecules. Dust particles acquire a few thousands of electron charges by absorbing the surrounding electrons and ions, and consequently interact with each other via a dynamically-screened Coulomb potential.

Dust particles in a complex plasma can be controlled through a low frequency electrostatic distortion. We studied the transport velocity of the particles as we modulate the frequency and phase of the applied voltage by a segmented electrode. We used molecular dynamics to simulate our experimental observations, using plasma conditions from independent particle-in-cell simulations. We found that the transport of dust particles controlled by low-frequency modulation in our simulations are in good agreement with our experimental findings. This work is in the aim of, on one hand, providing a potential technique for addressing the dust contamination issues in plasma processing reactors and on the other hand, providing a setup for investigating large two-dimensional complex plasma systems where boundary effects can be avoided.

We then proceeded to study the non-additivity effect in a complex plasma containing two different sizes of dust particles (binary complex plasma). For dust particles of type 1 and 2, the 1-2 (inter-species) interaction is always more repulsive than the geometric mean of 1-1 and 2-2 interactions. This asymmetry in the mutual interaction is called positive non-additivity. We used Langevin dynamics simulations for the Yukawa interacting particles characterized by positive non-additivity. We found that the two types of particles can separate into fluid-fluid phases and the growth of characteristic domain length follows a simple power law with an exponent of about 1/3 until the coupling strength is small enough, which is in a good agreement with the Lifshitz-Slyozov growth law for the initial diffusive regime of phase separation. We then used Langevin dynamics simulations to probe the influence of non-additive interactions on lane formation. We revealed a crossover from normal laning mode to a demixing dominated laning mode. In addition, we found that the lane formation is strongly influenced by the exact spatial configurations at the very moment of contact between two different complex plasmas.

We also used hydrodynamics to model the evolution of Mach cones in complex plasmas. The hydrodynamic model was able to reproduce a compressional-wave Mach cone observed onboard the International Space Station.

Chapter 1

Introduction

1.1 Complex plasma

Plasma is one of the four classical states of matter [41]; the other three states are solid, liquid and gas. When a solid is heated to its melting temperature, it turns into a liquid. When a liquid is heated to its boiling temperature, it turns into a gas. When a gas is heated to its ionization temperature, the gas atoms dissociate themselves into free electrons and heavier positive ions – collectively known as plasma. Plasma was first identified by Sir William Crookes (see picture in Fig. 1.1a) in 1879 and described as *radiant matter* [28]. The term of plasma was first assigned to describe an ionized gas by Lewi Tonks and Irving Langmuir (see picture in Fig. 1.1b) in 1929 [167].

A complex plasma is different to a normal plasma in that it contains an additional ingredient – dust particles [19, 40, 118, 130, 151, 152, 168, 169]. The dust particles, typically micron-sized, could absorb or lose electrons from or to their environment depending on the conditions. Compared to ions and electrons, the dust particles oscillate at a much lower frequency and their dynamics are much easier to observe. Because of this, complex plasma also provides a unique opportunity to study many phenomena in real time.

The field of complex plasmas has been attracting attentions since the observation of the formation of spokes in Saturn's B ring (see Fig. 1.2a), which was first observed by *Voyager* spacecraft in 1981 [155] and by *Cassini* spacecraft [113] again in 2006. The appearance of darkness in backscattered light and brightness in forward-scattering cannot be explained by gravitational force alone, but are speculated to be composed of electrostatically levitated dust particles inside a short-lived, dense plasma near the ring [45]. In 1994, a series of experimental realizations of *plasma crystal* (charged dust particles form lattice structure in a hexagonal shape, as can be seen in Fig. 1.2b) were reported in radio-frequency (RF) discharge plasmas in laboratories [25, 59, 164]. At that time, it captured the interest of many scientists because the introduction of dust particles brought new understanding to plasma physics and solid state physics. Nowadays, complex plasma physics has developed into a substantial research field in its own right and established its importance in both the fundamental research (non-Newtonian liquids, self-organization at the kinetic level, phase

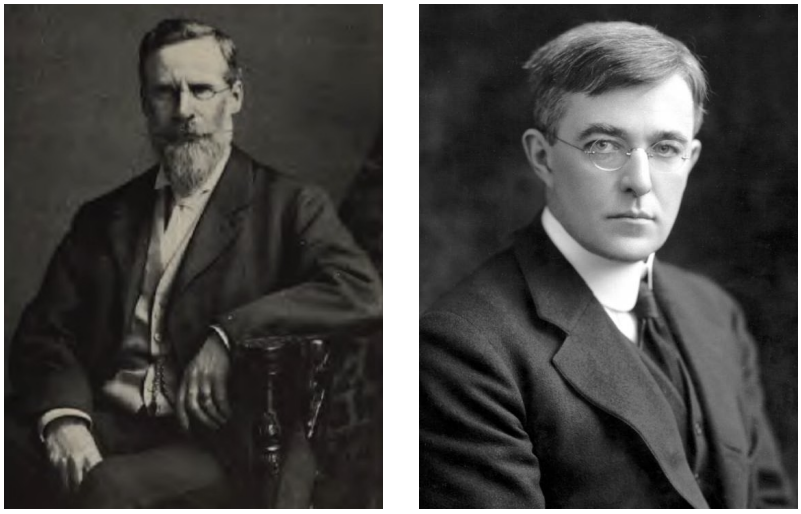

(a) (b)

Figure 1.1: Two pioneers of plasma physics: (a) Picture of William Crookes from Ref. [177]; and, (b) Picture of Irving Langmuir from *Linus pauling and the nature of the chemical bond: A documentary history website.*

transitions *etc.*) and the applications (particle contamination in plasma processes, such as etching, thin film deposition and fusion devices) [118].

1.1.1 Examples of complex plasmas

Complex plasma in space

Complex plasmas are ubiquitous in space environments [159]. In the early days, the space plasmas containing dust particles started to draw attention of astronomers about a century ago because they obscure objects which astronomers want to observe [168]. When the field of infrared astronomy began in the late 60's, those previously annoying dust particles were realized to be important for astrophysical processes, such as the formation of stars and planets [168]. The study of dust particles then became an important research topic in many branches of astronomy and astrophysics [49, 175]. In Fig. 1.3a, dust particles distributed in the spiral arms from a face view of the *Whirlpool Galaxy* (also known as M51). The *Sombrero Galaxy* (also known as M104) in the constellation Virgo is a spiral galaxy with a huge amount of dust particles forming a prominent ring as can be seen in an edge-on view in Fig. 1.3b. According to the infrared spectroscopy from Ref. [16], the dust ring is the primary site of star formation within this galaxy.

The interstellar space is also filled with a huge amount of gas and dust particles [172]. In some regions of space, when the concentration of gas and particles is high enough, clouds form. Most of the time these clouds are very thin so that they are invisible. At other times they are dense enough to be seen and are called *nebulae*, such as the *Carina Nebula* in Fig.

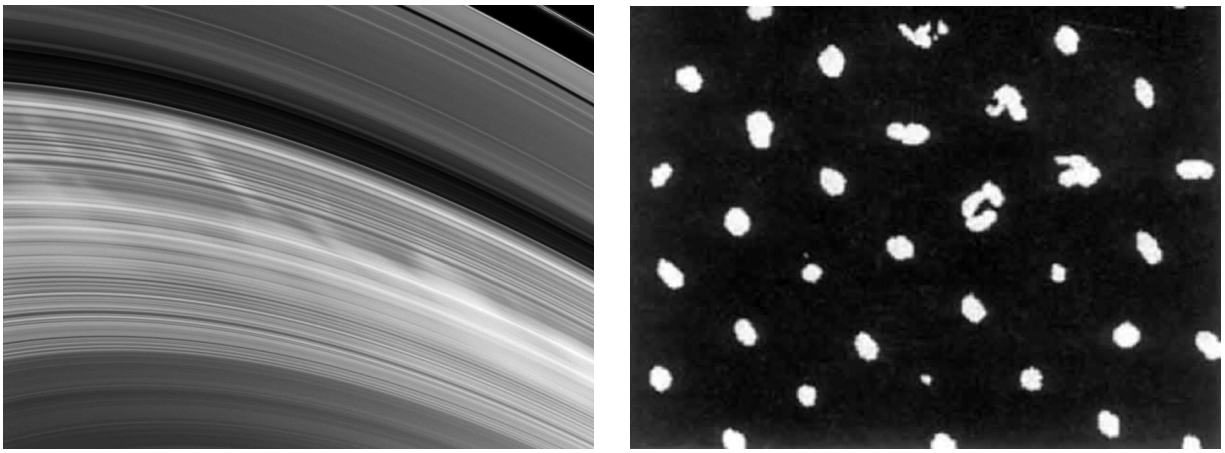

(a) (b)

Figure 1.2: Two important events for complex plasma: (a) The observation of the formation of spokes in Saturn's B ring. Credit: *Cassini Imaging Team, ISS, JPL, ESA, NASA*; and, (b) The experimental discovery of "plasma crystal" in a RF discharge plasma by Hubertus Thomas *et al.* The white dots are dust particles imaged by camera with laser scattering technique. Hexagonal lattice structure are evident in the figure. Reproduced from Ref. [165].

1.3c, which reveals radiant dust and brilliant star clusters. A nebula will either absorb or reflect the starlight. It was theoretically estimated that without the presence of cosmic dusts, the Milky Way would shine so brightly that human beings could read books at night on the Earth.

In our own solar system, dust particles can be found in the zodiacal light, the planetary rings, and comet tails. The existence of dust in the early solar nebula has been advocated by the Nobel Laureate Hannes Alfvén in 1954 [62]. The coagulation of the dust particles in the solar nebula leads to the formation of *planetesimals* from which comets and planets started to form. The origins of the dust particles in the solar system are mainly micrometeoroids and space debris. The properties of such dust particles depends on their origins and surroundings. Dust particles in a number of different regions of our solar system will be briefly presented in the following paragraphs.

Dust in comet: A comet is a relatively small, rocky, and icy body in the Solar System. When it is close enough to the Sun, a visible coma and sometimes also a tail can be displayed, due to the effects of solar radiation and the solar wind upon the nucleus of the comet. Comet nuclei are collections of ice and dust, ranging from a few hundred meters to tens of kilometers [62].

Dust in zodiacal light: This phenomenon was first investigated by astronomer Giovanni Domenico Cassini in 1683. Zodiacal light is faint because the sunlight scattered by cosmic dust in the zodiacal cloud can easily be concealed by either moonlight or light pollution. Though the zodiacal light decreases in intensity with distance from the Sun, it is

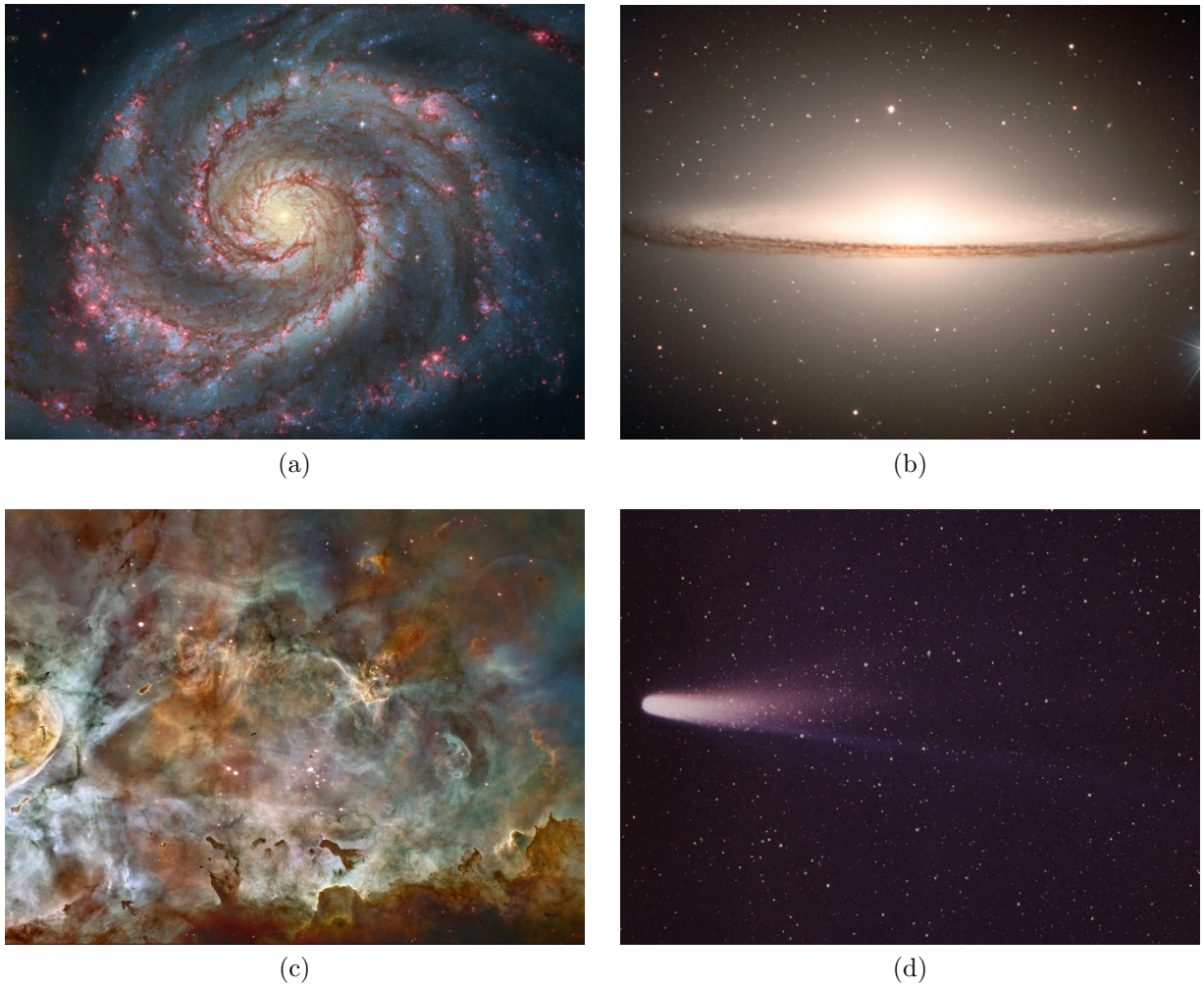

(a) (b)

(c) (d)

Figure 1.3: Examples of dusty plasmas in space: (a) The Whirlpool galaxy M51 contains dust in its spiral arms (Courtesy NASA/ESA); (b) Dust rings of the Sombrero galaxy M104, seen by Very Large Telescope, expressing a striking feature that huge amounts of dust crosses in front of the bulge of the galaxy (Courtesy ESO); (c) Carina nebula reveals glowing dust and brilliant star clusters (Courtesy NASA/ESA); and, (d) Comet Halley on 8 March 1986 (Courtesy Dr. William Liller).

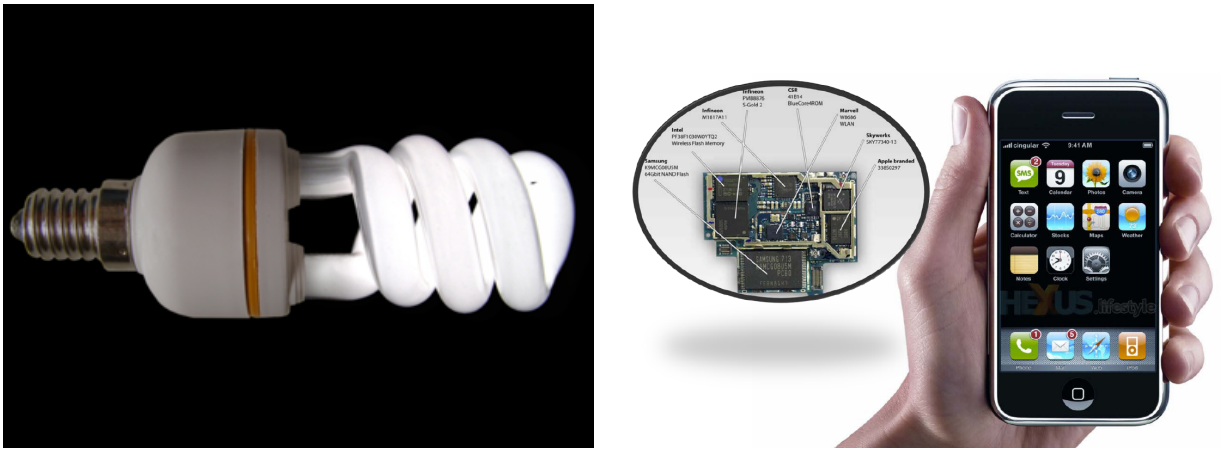

(a) (b)

Figure 1.4: Plasma processing related products in our daily life: (a) Fluorescent light bulb; and, (b) *iPhone*, designed and marketed by *Apple Inc*, as an example of smartphones. The inset shows the chips used inside the smartphone from plasma etching technologies.

still possible to observe it as a clear band shape on very dark nights. In fact, the zodiacal light covers the entire sky, being responsible for 60% of the total skylight on a moonless night.

Dust in planetary rings: Micron to sub-micron sized dust particles can be found in the outer diffuse planetary rings of planets in our solar system, such as Jupiter, Saturn, Uranus and Neptune [62]. The ring structure of Saturn was first found by the *Voyager* and then confirmed by the *Hubble Space Telescope* and the *Cassini* spacecraft. One of the most interesting features observed in the Saturn's ring system was the Spokes in the B ring as shown in Fig. 1.2a [45, 113, 155, 156]. The formation and evolution of spokes are explained by Ref. [45]. Jupiter's ring system, which is also formed by dust particles, was discovered by Voyager 1 in 1979 and subsequently probed in details by Voyager 2. Besides, comet dusts were found in Uranus and Neptune's rings as well [50].

Dust in Earth's atmosphere: Dust particles have been observed in the Earth's atmosphere and often play an important role in several phenomena that they are involved due to their abilities to reflect/absorb energy and to influence the dynamics of the atmosphere, which potentially may lead to the climate changes [148]. One famous example is the strong radar reflectivity of noctilucent cloud at frequencies from 50 MHz to 1.3 GHz. This behavior might be due to the presence of ice particles in the Earth's atmosphere being coated with a very thin metal film, which makes the cloud more reflective to radar [142].

Dust on Lunar surface: The lunar surface is covered with a thin layer of dust particles which is temporally exposed to solar wind plasma, and UV radiation. Thus the dust particles are charged by absorbing electrons, ions and solar UV photons and stick to any surface they approach. There are several observations that indicate that complex plasma processes are responsible for the mobilization and transport of the lunar soil [26].

Complex plasma in industry

The plasma processing poses a great importance in our daily life. High-pressure lamps illuminate our streets and serve as light sources in modern data projectors; Fluorescent light bulb used at homes as seen in Fig. 1.4a; chips of computers and smartphones as seen in Fig. 1.4b are produced with plasma technologies; plasma-enhanced chemical vapor deposition processes result in computer monitors and solar cells.

Plasma is important for three reasons in the semiconductor fabrication steps in the production of semiconductor chips. For instance in etching process, firstly, electrons can be used to dissociate and activate the input gas. Secondly, the etch rate can be enhanced by ion bombardment, which can break the bonds on the surface or/and give energy to processes for chemical reactions, allowing the etchant atoms, usually Cl or F, to combine with substrate atoms to form volatile molecules. And thirdly, the electric field of the plasma sheath straightens the orbits of the bombarding ions so that the etching can be anisotropic, allowing the creation of features approaching nanometer dimensions. However, dust particles up to μm size can be grown in plasma because there are many precursors for the particles to grow from many reactions. Grown dust particles are notorious in plasma-assisted processing because they introduce defects into the final products. For instance, dust particles grown (as shown in Fig. 1.5a) inside the plasma device formed ring structures on top of the wafers [143]. When the plasma is turned off, the particles may fall onto the wafer, contaminating it. A scanning electron microscope (SEM) images taken in *Hitachi* has shown how the photoresist patterns were damaged by dust particles (as shown in Figs. 1.5b and 1.5c). Although great attentions had been paid to minimize dust contamination of the clean room, it was discovered that the particles actually formed and grew inside the plasma chamber: grown particles formed from chemically reactive gases; fragments chipped off by etching; macroscopic particles due to sputtering [19, 143]. In 1986, Spears *et al.* reported that a silane plasma was contaminated by micron-sized particles visualized using laser light scattering [158]. Subsequently it was reported that in plasma enhanced chemical vapor deposition, grown dust particles may decrease the deposition rate and the quality of the silicon film [149]. Nowadays dust particles have been commonly understood as one of the major contamination issues. The removal of such particles poses a major technological challenge [145] for plasma-assisted processing and will be the very issue that we try to address in **chapter 2**, where a new technique will be proposed and tested for particle removal in a plasma device.

Complex plasma in nuclear fusion devices

Similar as in industry, dust particles are noxious in fusion devices as well. The presence of dust in nuclear fusion devices, mainly due to plasma-wall interactions, can lead to numerous safety and operational issues [170, 178] including high chemical reactivity of dust, tritium retention[1] and transport by dust, plasma contamination with dust material, discharge termination by large particles, damage of the first wall and diagnostic instruments by

[1]Radioactive tritium are captured and trapped in the dust particles.

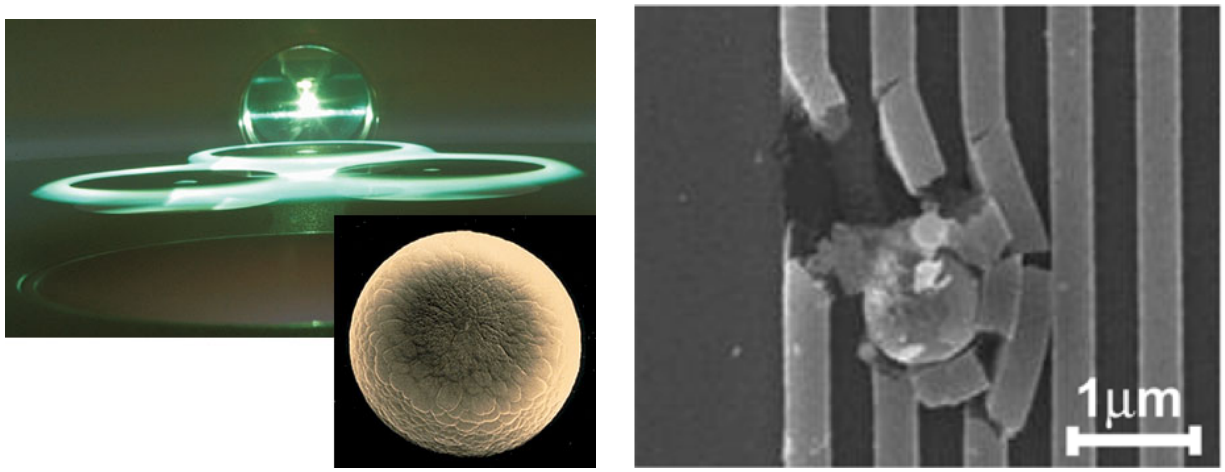

(a)

(b)

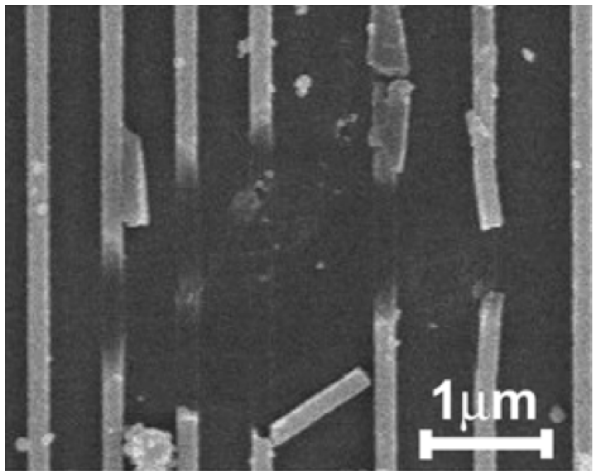

(c)

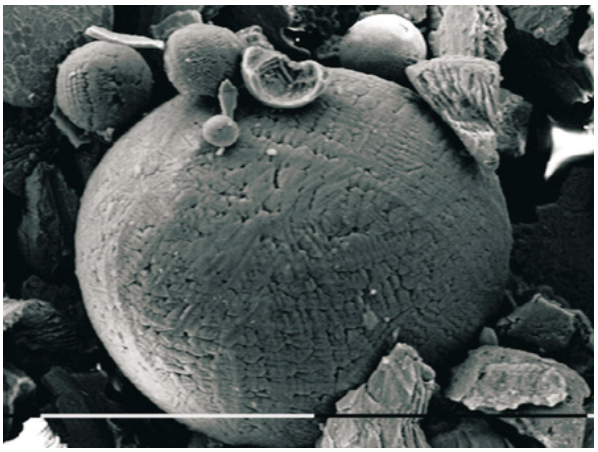

(d)

Figure 1.5: Dust particles in semiconductor manufacturing and fusion devices: (a) Dust particles forming rings on top of the silicon wafers in a plasma processing device. (Inset) An electron microscope image of a 20 μm diameter particle from such a dust cloud. Reproduced from Refs. [108, 143]; (b) An electron microscope image taken by Kobayashi in *Hitachi* of photoresist pattern damage due to the collision with dust particles. Reproduced from Ref. [83]; (c) An electron microscope image taken by Kobayashi in *Hitachi* of photoresist pattern damage due to the collision with dust particles. Reproduced from Ref. [83]; and, (d) Iron particles from fusion device. Reproduced from Ref. [178].

high speed dust particles, *etc.* [117, 154]. According to recent statistics by Rosanvallon and co-workers [134], the International Thermonuclear Experimental Reactor (ITER) is expected to produce 100 kg tungsten, 100 kg beryllium and 200 kg carbon dust particles during one year of operation. Particles are often found in the bottom of fusion devices after operations. An iron spherical particles from fusion device is presented as an example in Fig. 1.5d. The particles not only consist of fragments of the wall or debris from diagnostic devices, but also of very fine grained particles. Dust particles may retain a large fraction of hydrogen which will lead to considerable tritium inventories. The thermophoretic forces or repetitive evaporation and condensation may lead to accumulation of dust particles at cold areas and the migrations of dust particles may fill spaces unexpectedly and hence lead to safety issues [178]. The particle speed in a fusion device may go beyond km/s (hypervelocity regime) according to the study by Morfill *et al.* [117] with silica aerogel for dust capture experiments. This kind of fast dust particles has been commonly agreed as a severe safety issue and the dust contamination problem in fusion device has not yet been fully resolved.

1.1.2 Basic properties of complex plasmas

In this section, the basic properties of complex plasmas will be discussed, starting from important physical quantities, spatial and temporal scales, and closing by a short summary.

Laboratory experiments in complex plasmas are often performed in low-temperature plasmas with ionization rate normally $\ll 1$. Normally the electron temperature goes up to a few eV, while the temperature of ions and neutral gas are usually at room temperature (300 K).

When dust particles are introduced into a plasma, they will be charged (The details of charging mechanisms is shown in Appendix A.) and afterwards shielded by a charge cloud with a characteristic length of *Debye length* λ_D, which describes the combined shielding effect of electrons and ions [22]. Another two important length scale in complex plasmas are dusty particle radius r_d and the average inter-particle distance a. a is determined by the number density of dust particles n_d as $a = (4\pi n_d/3)^{-1/3}$ and is also called *Wigner-Seitz radius*. Normally $r_d \ll \lambda_D$ holds in complex plasma experiemnts, one can treat the dust from a particle dynamics point of view when $r_d \ll \lambda_D < a$, in which case it is just isolated shielded dust particles in a plasma. Otherwise, collective effect of dust particles is no longer negligible when $r_d \ll a < \lambda_D$, in which case the mixture of dust particles and background plasma can be treated as fluid [151]. In order to obtain λ_D, *Poisson equation* is solved within the framework of far-field approximations, assuming Boltzmann distribution of electrons and ions. According to Refs. [22, 150], λ_D is given by

$$\frac{1}{\lambda_D^2} = \frac{1}{\lambda_{De}^2} + \frac{1}{\lambda_{Di}^2}, \tag{1.1}$$

where $\lambda_{De} = \sqrt{T_e/(4\pi n_e e^2)}$ and $\lambda_{Di} = \sqrt{T_i/(4\pi n_i e^2)}$ are the electron and ion Debye length, respectively, T_e and T_i are the electron and ion temperature in the unit of eV, n_e

and n_i are the densities of electrons and ions. In the case of low temperature plasmas and assuming dust particles are negatively charged, one has $T_e \gg T_i$ and $n_e \ll n_i$, namely, $\lambda_{De} \gg \lambda_{Di}$, which leads to $\lambda_D \simeq \lambda_{Di}$. This means that the build-up shielding distance mainly depends on ions (T_i and n_i). On the other hand, the ions in the *sheath*[2] are directed towards the wall with high velocity and contribute much less for shielding dust particles than the electrons in this case, thus we have $\lambda_D \simeq \lambda_{De}$. Under typical parameters in complex plasma experiments, such as $T_e = 3$ eV, $T_i = 300$ K and $n_i \simeq n_e = 10^9$ cm^{-3}, one has $\lambda_{Di} = 37.8$ μm, $\lambda_{De} = 407.2$ μm, and $\lambda_D = 37.6$ μm. It is worthy mentioning that, any deviation from equal densities of electrons and ions tend to be smoothed by Debye shielding. Therefore, a plasma instinctually tends to be quasineutral. The equilibrium *quasineutrality* [152] condition in complex plasma is expressed as

$$n_e \pm Z_d n_d = Z_i n_i, \tag{1.2}$$

where Z_d is the number of elementary charge on a single dust particle. In the case of negatively charged dust particles, the sign before $Z_d n_d$ is "+". Z_i is the number of elementary charge on a single ion and it is assumed that $Z_i = 1$ in this thesis unless otherwise defined. $P = Z_d n_d / n_e$ introduced by Havnes [55] is normally used to describe the strength of electron density depletion due to dust charging. When most of the ambient electrons around a particle are bombarded onto the dust grain, one has $Z_d n_d \sim n_i \gg n_e$ ($P \gg 1$), the system can be treated as a two-component plasma, containing dust particles and positive ions. It should be stressed that in this particular case, injecting new dust particles ends up with sharing charge with other neighboring grains and consequently leads to the decrease of charge on each particle. On the other hand, with small P ($P \ll 1$), the dust particles are isolated grains embedded in the plasma and no significant depletion of electrons takes place. In the presence of UV light, dust particles can be positively charged (details in Appendix A) and the sign before term $Z_d n_d$ should be "−".

Complex plasma as a many-particle systems can be in gas, liquid, and solid state even at room temperature. Complex plasma system in thermodynamical equilibrium can be characterized by two dimensionless parameters [118]. These are the coupling parameter Γ and the screening parameter κ defined as

$$\Gamma = \frac{|\langle V_d \rangle|}{\langle K_d \rangle} = \frac{Q_d^2}{aT_d} \tag{1.3}$$

and

$$\kappa = \frac{a}{\lambda_D}, \tag{1.4}$$

respectively, where K_d is the kinetic energy of a single particle, and V_d is the mean interaction energy of two nearest neighbors. Interestingly, distinct values of Γ separate qualitatively different behaviors of complex plasma: from weak coupling (ideal gas-like) at

[2] *Sheath* was named by Irving Langmuir to describe a positive space close to the walls generating a potential barrier confining the electrons in the plasma, the resulting field decelerates the electrons approaching the walls while accelerates the ions towards the walls [94].

$\Gamma \ll 1$, over fluid-like at $1 \ll \Gamma \ll \Gamma_c$, to crystalline state at $\Gamma \gg \Gamma_c$ (Γ_c is the critical value of Γ when crystal formation occurs because particles do not have sufficient kinetic energy to escape from the local minima of the total potential. Examples of strongly correlated complex plasma are *plasma crystals* in 2D [25, 59, 106, 164] and *Yukawa balls* in 3D [9, 10].

To summarize, we list the unique properties of complex plasmas under typical experimental conditions as follows:

- Dust particles size is about $r_d \simeq 0.3 - 30$ μm and hence are often individually observable by laser scattering techniques. So physics in complex plasmas can be studied at the individual particle level.
- The characteristic length scales (*e.g.*, Debye length $\lambda_D \simeq 20 - 200$ μm, mean particle separation $a \simeq 1 - 2000$ μm) are a few 100 μm so that complex plasma systems are normally up to a few centimeters in size which allows three-dimensional optical diagnostics.
- The characteristic dynamical time scales for dust particles $\tau \simeq 1/\omega_{pd}$ (*e.g.*, frequency of dust particle oscillations $\omega_{pd} \simeq 1 - 100$ Hz) are in the range of tens of milliseconds, allowing full single-particle resolution of particle dynamics.
- Damping for dust particles due to dust-neutral collision is easily manipulated in complex plasma experiments by modifying the pressure in the vacuum chamber, which allows us to study from weakly damped system to relatively strongly damped system.
- Different dimensions of complex plasma systems are accessible, which allows us to study surface physics and mesoscopic physics (*e.g.*, complex plasma films like Membranes).
- The huge charge (with Z_d in Eq.(1.2) $\sim 10^3 - 10^5$) carried by dust particles result in a high coupling strength between the dust particles, that can easily place complex plasma in fluid or solid state by tuning the ambient plasma conditions, the interparticle distance and temperature of dust particles.
- Microparticles in complex plasmas can be manipulated in various ways: *e.g.*, applying external electric field or magnetic field, applying directed gas flow, heating up the electrode for thermal gradients, or using laser radiation pressure force, *etc.*(see the following section for more details)

1.2 Dust particle manipulation and removal in plasma device

Dust particles have become a technologically important subject for plasma-assisted material processing. In many cases, especially in the fabrication of electronic circuits, *e.g.*,

plasma vapor deposition, grown dust particles can be considered as a main source of defects in the final products. Therefore, the challenge to remove these fine particles is one of the motivations for the extensive study of dusty plasma in recent decades [152]. Current methods for particle manipulation will be reported in this section and forces can be used for dust manipulation will be discussed in details as well.

1.2.1 Current particle manipulation methods

Methods for removing dust particles from processing plasmas have been investigated by many authors [7, 15, 74, 75, 89, 97, 129, 135] by manipulating various forces acting on them, such as gravitational force, ion drag force, neutral drag force, thermophoretic force as well as laser radiation pressure force [152].

The NFP-Collector (Negatively charged fine particle collector) has been proposed for collection and removal of fine particles in complex plasmas [89, 139]. The collector is a simple electrode with a hole, which is biased with voltage higher than the floating potential in plasmas. Microparticles, immersing in plasmas, approach the collector in the presence of force balance among particles, being pulled into the collector. Similar technique has been used by simply inserting a positively biased metal tube into the plasma during the preparation of silicon dioxide thin films in a plasma-enhanced chemical vapor deposition reactor [146]. This system effectively removes particles during operation and provides clean film without particle contamination. However the particle removal system reduces the rate of film growth by about 40%.

O'Hanlon and co-workers have shown theoretically and experimentally that the neutral drag force induced by a directed gas flow can be strong enough to remove particles from their trap locations [129]. It was also proposed and tested by Momonoi *et al.* [114] using gas flow for particle cleaning during semiconductor manufacturing. Particles are removed by the viscous friction of the gas flow, which can be increased by narrowing the gas-flow space along the wafer surface.

It was proposed to use thermophoresis to remove particles from a discharge [74]. A series of experiments were performed by Jellum by varying the temperature of water circulated through planar, parallel electrodes. They found that particles suspended in the discharge moved away from a heated electrode towards a cooled one. This method can also be used to compensate the gravitational force in order to achieve "microgravity condition" for complex experiments on the Earth [136].

It was also proposed to use localized secondary plasmas for the manipulation and removal of fine particles in plasma [8]. In Ref. [8], *segmented electrode* is used for modifying the sheath locally.

1.2.2 Forces used for dust particle manipulation

In order to understand the dynamics of dust particles, it is crucial to know the behavior of particles in the presence of different forces exerting on dust particles. The dynamics of

a single particle immersed in plasma can be mainly expressed as

$$m_d \frac{\mathrm{d}\mathbf{v}_d}{\mathrm{d}t} = \mathbf{F}_g + \mathbf{F}_{ion} + \mathbf{F}_N + \mathbf{F}_E + \mathbf{F}_L + \mathbf{F}_{th} + \mathbf{F}_R, \tag{1.5}$$

where $\mathbf{F}_g$ is the gravitational force, $\mathbf{F}_{ion}$ and $\mathbf{F}_N$ are the ion and neutral drag force respectively, $\mathbf{F}_E$ is the electrostatic force, $\mathbf{F}_L$ is the Lorentz force, $\mathbf{F}_{th}$ is the thermophoretic force, and $\mathbf{F}_R$ is the radiation pressure force. The other forces are out of the scope of this thesis since they are normally neglected in complex plasma physics (*e.g.*, electron drag force). The origin and proportionality to particle radius r_d of forces in Eq. 1.5 are summarized in Table 1.1 and will be discussed in details in the following paragraphs.

Name	**Origin**	**Scaling of r_d**
Gravitational force $\mathbf{F}_g$	gravity	r_d^3
Electric force $\mathbf{F}_E$	electric field	r_d
Lorentz force $\mathbf{F}_L$	magnetic field	r_d
Neutral drag force $\mathbf{F}_N$	streaming neutrals	r_d^2
Ion drag force $\mathbf{F}_{ion}$	streaming ions	r_d^2
Thermophoretic force $\mathbf{F}_{th}$	temperature gradient	r_d^2
Radiation pressure force $\mathbf{F}_R$	electromagnetic radiation	r_d^2

Table 1.1: Overview of forces on dust particle: the origin and proportionality to particle radius r_d.

In ground-based experiments, the force from the gravitational field is one of the dominant forces. The gravitational force $\mathbf{F}_g$ is expressed as

$$\mathbf{F}_g = \frac{4\pi r_d^3}{3} \rho_d \mathbf{g}, \tag{1.6}$$

assuming a spherical particle. $\mathbf{g}$ is the acceleration due to gravity and ρ_d is the dust mass density [3]. $\mathbf{F}_g$ is always directed downward and scales with r_d^3.

Here we consider dust particles immersed in a plasma in the presence of non-zero macroscopic filed (*e.g.*, in the pre-sheath region of a discharge). Although the sheath around a dust particle shields it from the ambient plasma, it does not screen the dust particle from an externally applied electric field [30, 52]. Daugherty *et al.* [30] analytically solved the linearized Poisson equation and obtained the following description of electrostatic force $\mathbf{F}_E$ for a dust particle in an electric field $\mathbf{E}_0$, provided the dust particle in a uniform plasma

$$\mathbf{F}_E = Q_d \mathbf{E}_0 + Q_d \mathbf{E}^*, \tag{1.7}$$

[3] Dust particles used in experiments conducted in chapter 2 and chapter 4 are $\rho_d = 3.95$ g/cm^3 for Al_2O_3 and $\rho_d = 1.57$ g/cm^3 for melamine-formaldehyde (MF) particles, respectively.

where Q_d is the charge on the dust particle. The first term of the expression above is the electrostatic force experienced by a dust particle under the external field $\mathbf{E}_0$ under vacuum circumstance. The second term correspond to the dipolar force due to the polarization of the surface charge [19]. In other words, the polarized surface charges on the dust create an electric field $\mathbf{E}^*$ which in turn exerts an electric force $\mathbf{F}_p^* = Q_d\mathbf{E}^*$ (the second term on the right-hand-side) on the dust particle with

$$\mathbf{F}_p^* = Q_d\mathbf{E}_0\frac{r_d^2/\lambda_D^2}{3(1+r_d/\lambda_D)}. \tag{1.8}$$

In the limit of $r_d/\lambda_D \ll 1$, which generally holds for complex plasma experiments with small size particles, one has $\mathbf{E}^*/\mathbf{E} \sim 0$ and Eq. (1.7) reduces to

$$\mathbf{F}_E = Q_d\mathbf{E}_0, \tag{1.9}$$

which means the electrostatic force experienced by dust particle in electric field $\mathbf{E}_0$ in a unform plasma can be well approximated by the case in a vacuum situation. In other words, the plasma does not shield the dust particle from the bulk electric field and reduce the electrostatic force [19]. The charge of the dust particles is proportional to their radius, thus $\mathbf{F}_E \propto r_d$. The situation for dust particle immersed in a nonuniform plasma was studied by Refs. [51, 52]. A polarization force arises from a plasma density gradient or a Debye length gradient and toward the opposite direction of the external electric field $\mathbf{E}_0$. In this case, the Debye length is spatially dependent and the Debye sheath around the dust particle is deformed [19]. $\mathbf{F}_E$ exerted on a dust particle in these conditions can be expressed as

$$\mathbf{F}_E = Q_d\mathbf{E}_0 + \mathbf{F}_p, \tag{1.10}$$

and the polarization force $\mathbf{F}_p$ is [81]

$$\mathbf{F}_p = -\frac{Q_d^2}{2}\frac{\nabla\lambda_D}{\lambda_D^2}, \tag{1.11}$$

where $\lambda_D = \lambda_D(r)$ is the linearized Debye length, and $\nabla\lambda_D$ is its gradient. The first term in Eq. (1.10) is the conventional electric force, while the second term $\mathbf{F}_p$ is the polarization force arising due to plasma polarization around the grain. The ratio between these two terms $\mathbf{F}_p/Q_d\mathbf{E}_0$ is on the order of r_d/λ_D [19] and is therefore negligible under normal complex plasma conditions ($r_d \ll \lambda_D$). The effect of the polarization force on the propagation of dust acoustic waves in complex plasmas is investigated by Khrapak *et al.* recently [81]. It is shown that polarization interaction results in a decrease of the dust acoustic phase velocity. The effect becomes more pronounced as the grain size increases. The difference between $\mathbf{F}_p^*$ in Eq. (1.8) and $\mathbf{F}_p$ in Eq. (1.11) comes from different polarization mechanism. The direction of $\mathbf{F}_p^*$ is along the external applied field $\mathbf{E}_0$, while $\mathbf{F}_p$ is always on the opposite direction of $\mathbf{E}_0$. It is noteworthy that $\nabla\lambda_D$ can either be a result of plasma density gradient or plasma temperature gradient.

The Lorentz force $\mathbf{F}_L$ acting on a point charge Q_d with velocity $\mathbf{v}_d$ is given by

$$\mathbf{F}_L = Q_d \mathbf{v}_d \times \mathbf{B}, \tag{1.12}$$

Here, $\mathbf{B}$ represents the magnetic flux density. The influence of the magnetic field is only important if one of the particle species in the plasma is magnetized: its collision frequency with the neutral background gas is much smaller than its gyro-frequency, and it can thus complete many gyro-rotations before being disturbed by a collision with a neutral particle. Due to their small mass, the plasma electrons are easier to magnetize than ions or dust particles. The Lorentz force $\mathbf{F}_L$ scales with r_d.

The neutral drag force arises from the rate of momentum exchange between the dust particles and neutrals during their collision. Two regimes separated by Knudsen number [4] are considered [124, 152]. These are the hydrodynamic regime ($Kn \ll 1$) and the kinetic regime ($Kn \gg 1$). In the hydrodynamic regime, the neutral drag force can be estimated from Stokes's law and is found to be proportional to the speed and radius of the dust particle. In the kinetic regime, classical gas theory may be used [12]. The neutral drag force $\mathbf{F}_N$ for a spherical dust grain of radius r_d with velocity $\mathbf{v}_d$ is expressed as

$$\mathbf{F}_N = -\gamma_{Ep} m_d (\mathbf{v}_d - \mathbf{v}_n) = -\delta_{Ep} \frac{4\pi}{3} r_d^2 \rho_n u_n (\mathbf{v}_d - \mathbf{v}_n), \tag{1.13}$$

where $\rho_n = m_n N_n$, $\mathbf{v}_n$, $u_n = \sqrt{8T_n/\pi m_n}$ are the mass density, drifting velocity and thermal velocity of the neutrals (normally we have $|\mathbf{v}_n| \ll u_n$). Eq. (1.13) is applicable when $Kn \gg 1$ and $\mathbf{v}_d \ll u_n$. γ_{Ep} is the dust-neutral collision frequency in the unit of s^{-1} and can be written as [34]

$$\gamma_{Ep} = \delta_{Ep} \frac{4\pi}{3} r_d^2 \frac{\rho_n u_n}{m_d}. \tag{1.14}$$

δ_{Ep} is a dimensionless coefficient introduced by Epstein [34] and determined by the nature of collision mechanism, *i.e.*, *specular reflection* and *diffusive reflection*. In the limiting case, δ_{Ep} has the value as

$$\delta_{Ep} = \begin{cases} 1 & \text{:specular reflection;} \\ 1 + \pi/8 & \text{:perfect diffusive reflection.} \end{cases} \tag{1.15}$$

δ_{Ep} in complex plasma was measured by Liu *et al.* [100] with a laser acceleration method and a vertical resonance method, which yielded $\delta_{Ep} = 1.26 \pm 0.13$ and $\delta_{Ep} = 1.44 \pm 0.19$, respectively. Konopka [85] analyzed the horizontal oscillation of melamine-formaldehyde (MF) particles in argon and krypton plasmas at room temperature and gave $\delta_{Ep} = 1.48 \pm 0.05$. δ_{Ep} given by Konopka will be used in this PhD thesis.

[4] The Knudsen number ($Kn = l_n/r_d$) is a dimensionless number defined as the ratio of the neutral mean free path length, l_n, to a representative physical length scale, which in complex plasma study is the radius of a dust particle, r_d, in the neutral background. The number is named after Danish physicist Martin Knudsen (1871-1949).

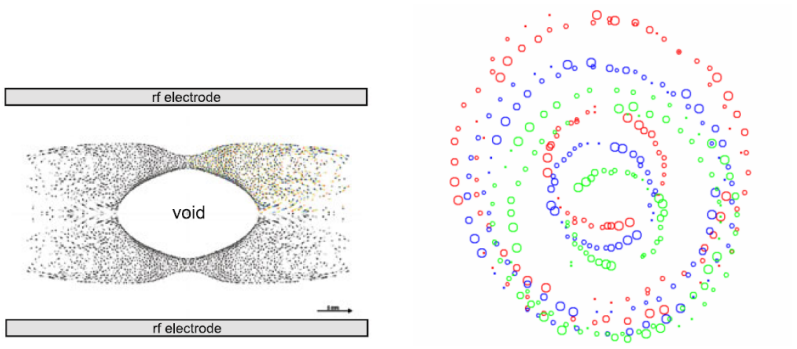

(a) (b)

Figure 1.6: Phenomena in complex plasmas due to ion drag force: (a) Dust free region in the center of a RF-driven parallel plate discharge under microgravity (inverted image). The motion of the dust particles becomes visible from the superposition of 150 video frames covering 3 s. Reproduced from [116]; and, (b) Particles in the cluster followed a circular trajectory during rotation when the magnetic field strength was 30 Gauss (red circles), 60 Gauss (blue circles) and 90 Gauss (green circles). Reproduced from [23].

Eq. (1.13), on one hand, can be used to calculate the force that a neutral flow with velocity v_n exerts on a dust particle at rest ($\mathbf{v}_d = 0$), on the other hand it can also be adopted when dust particle moves with velocity through a neutral gas at rest ($\mathbf{v}_n = 0$). In the former case, the neutral drag force acts as an acceleration force, for instance $\mathbf{F}_N$ was used to blow dust particles away from the discharge area by O'Hanlon [129], while in the latter case, $\mathbf{F}_N$ is simply a damping force decelerating the particle's motion. Note that $\mathbf{F}_N$ scales with r_d^2.

The ion drag force results from the momentum transfer from flowing ions to a negatively charged dust particle [21, 71, 80, 152]. The ion drag force is responsible for a number of fascinating phenomena occurred in complex plasma such as *void formation* [11, 43, 46, 103, 110, 116, 166] (see Fig 1.6a) and *crystal rotation* [23, 66, 87, 140] in the presence of the magnetic field (see Fig 1.6b). The momentum is transferred from ion flow to dust particles in the following two ways [14], through direct impacts and through Coulomb collisions between ions and the negatively charged dust particles. The total ion drag force can be expressed as

$$\mathbf{F}_{ion} = \mathbf{F}_{coll} + \mathbf{F}_{Coul}, \tag{1.16}$$

where $\mathbf{F}_{coll}$ represents the collection force and $\mathbf{F}_{Coul}$ is the contribution from Coulomb collision.

Assuming a single dust particle with radius r_d immerses in a neutral gas environment in the presence of a temperature gradient, dT/dx, the gas molecules on the hot side of the particle have higher average thermal speeds than those on the cold side, thus more momentum are transferred to the particle on the hot side than the cold side. This leads

to a thermophoretic force directed from the higher temperature region toward to the cold temperature region [152]. It was first observed in complex plasma by Ref. [74]. In the limit of dust temperature $T_d < 500$ K, the thermophoretic force, $\mathbf{F}_{th}$, can be expressed as follows [56, 163]

$$\mathbf{F}_{th} = -\frac{32}{15}\frac{r_d^2}{u_n}\kappa_T\frac{dT}{dx}, \tag{1.17}$$

where κ_T is the translational thermal conductivity of the neutral gas, $u_n = \sqrt{8T_n/\pi m_n}$ is the thermal velocity of the neutral molecules, m_n is the mass of neutral molecules and T_n is the gas temperature in the energy unit of eV, dT/dx is the temperature gradient, where T is in temperature unit. It is evident that the thermophoretic force scales with r_d^2 since it is the particle surface which face the bombarding gas molecules. When a dust particle is

exposed to the electromagnetic radiation, it is subject to the radiation pressure force [151]

$$\mathbf{F}_R = \frac{\pi r_d^2 I_0}{c}\hat{\mathbf{e}}, \tag{1.18}$$

where I_0 is the photon energy flux along the direction $\hat{\mathbf{e}}$, and c is the speed of light in vacuum. This approximate expression is valid when all photons are absorbed by the dust grain and the dust grain is much larger than the wavelength of the radiation. Laser, which serves as a source for radiation pressure force, is commonly used in complex plasma experiments for particle manipulation, such as melting/heating of plasma crystal [127, 128], Mach cone excitation [107, 125], and Coulomb explosion [88]. Such a radiation pressure force is also important in the space for submicron particles that are close to the Sun, which have been observed by the Pioneer 8, 9 and Ulysses spacecrafts in the solar wind [48]. The radiation pressure force scales with the surface of the dust particle: $\mathbf{F}_R \propto r_d^2$.

1.3 Binary complex plasmas

Binary mixtures have been a long historical topic due to their much richer phase diagram, structures and dynamics properties than the single component ones, and its application in food industry and alloys productions. It has been studied in many different system such as colloids [2, 33], polymer blends [31, 84] and alloys [77].

Recently, complex plasmas with different types of dust-particles (or multi-component complex plasmas) are gaining more and more attention [53, 72, 119, 161, 162, 179], and physicists in this field realized that binary complex plasma, *i.e.*, complex plasma consisting of mixtures of two different sized dust particles can also serve as a model system to study various phenomena for binary mixtures such as phase separation, lane formation, *etc.*

Recent studies with binary complex plasmas under microgravity conditions [72, 119, 161, 162, 179] have demonstrated their promising prospects, as so many interesting phenomena have been observed, such as classic tunneling by Ref. [119], lane formation as in Fig. 1.7a by Ref. [161, 162] and phase separation as in Fig. 1.7b by Ref. [179]. In **chapter 3**.

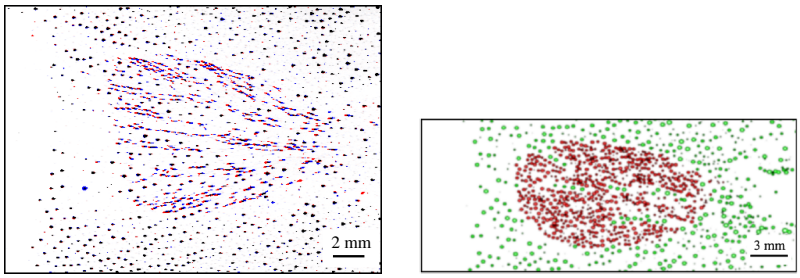

(a) (b)

Figure 1.7: Phenomena in binary complex plasma: (a) Lane formation in complex plasmas. A short burst of small (3.4 μm) particles is injected into a cloud of big (9.2 μm) background particles. From [161, 162]; and, (b) Phase separation in binary complex plasmas. The figure illustrates one experiment performed under microgravity conditions in the PK-3 Plus chamber (in argon discharge at a pressure of 30 Pa), with particles of 9.2 and 3.4 μm diameter. Small particles (colored in red) were injected into a stationary cloud of big particles (colored in green) and formed a spheroidal droplet which moved slowly towards the center of the chamber (to the right). From [179].

1.3.1 Phase separation

Phase separation, in which different types of particles tend to separate from each other, is a ubiquitous phenomenon in many different systems of multi-component mixtures, such as molecular fluids and colloidal suspensions, and has been a long-standing research topic in physics, because of both its fundamental and practical importance. It can be stimulated by either the interplay between individual particles, such as the interaction non-additivity or external perturbations, such as shear flow, temperature gradient and electric field. The phase separation is a scaling phenomenon with the average domain size, L, following a power law and is sequenced to a series of domain growth regimes with different growth exponents peculiar to each regime:

$$L \propto \begin{cases} t^{1/3} & \text{:Diffusive regime;} \\ t & \text{:Viscous regime;} \\ t^{2/3} & \text{:Inertial regime.} \end{cases} \tag{1.19}$$

The diffusive regime obeys the power law with growth exponent of 1/3 [99], where diffusion is the dominant mechanism driving like particles to accumulate in the formation of tiny clusters. After the formation of clear interfaces between unlike particles, the minimization of interfacial energy becomes the dominant mechanism. This regime is termed as viscous regime with domain growth follows a linear scaling law [153]. The last regime with growth exponent of 2/3 is known as inertial regime [78], where the segregation is dominated by inertia due to the increase of the Reynolds number.

In complex plasmas, phase separation was first reported in experiment by Morfill *et al.* [119] and later by Sütterlin *et al.* [161], both under microgravity conditions. Ivlev *et al.*

[72] has recently shown a theoretical model in a binary complex plasma; the inter-particle interaction is always asymmetrical, *i.e.*, for point particles of type "1" and "2", the 1-2 (inter-species interaction) is more repulsive/attractive than the geometric mean of 1-1 and 2-2 interactions. This asymmetry in the mutual interaction between different species is called "interaction non-additivity", and in the case of complex plasma, one has always a positive non-additivity. According to the theory, such an interaction non-additivity leads to a spinodal region, where the fluid phase separation (spinodal decomposition) could happen, and this region overlaps with typical experimental conditions of complex plasmas in laboratory. This explains well the phase separation phenomena observed in recent experiments and also makes binary complex plasma a promising model system for studying the kinetics of phase separation.

1.3.2 Lane formation

The formation of lanes is a ubiquitous phenomenon occurring in nature when two species are moving toward and penetrating into each other. Couzin [27] has found that the movement rules of individual ants on trails can lead to a collective choice of direction and the formation of distinct traffic lanes that minimize congestion. This phenomenon can also be found in human beings walking on the street that they occupy specific region where lanes are formed and traffic flow is maximized. Lane formation also draws considerable interest in different branches of physics. When two different species of particles are driven into each other, like-driven particles form "stream lines" and move collectively in lanes, which depends on the details of the particle interactions and their dynamics [133]. Typically, the lanes exhibit a considerable anisotropic structural order accompanied by an enhancement of their (unidirectional) mobility. The phenomenon is commonly known from pedestrian dynamics in highly crowded pedestrian zones [60], where people heading in the same directions form lanes to pass the zebra crossings. It also occurs in different systems of driven particles, such as colloidal dispersions [33, 96], lattice gases [141], and molecular ions [123]. In other words, it is a ubiquitous generic process of considerable interest in different branches of physics. It is also a genuine nonequilibrium transition [141] which depends on the details of the particle interactions and their dynamics [133]. Recently, particle laning was also observed in complex plasmas [160–162] as shown in Fig.1.7a.

1.4 Simulating the complex plasma

Computer simulation represents a complementary approach to experimental and theoretical studies, and it has become invaluable tools in numerous disciplines of physical science. In complex plasma physics, various simulation methods have been used to study different topics: molecular dynamics (MD) simulations for Mach cones [102, 107] and crystallization [82]; particle-in-cell (PIC) simulations for ion drag force [70], ion focusing [111, 112] and pairwise interaction between dust particles in plasma [92]; fluid simulation for void modeling [43, 93]; Langevin dynamics (LD) simulations for self-diffusion [68], wave spectra [67],

and crystallization [54]; Monte Carlo (MC) simulations for phase transitions [147].

The MD simulation is a widely applied approach, which deals with all microscopic degrees of freedom explicitly, *i.e.*, the equations of motion are solved for each particle in the system. In some cases, the dynamics of objects in the system has a big timescale gap, namely, some degrees of freedom evolve fast while others are slow (*e.g.*, electron dynamics and ion dynamics). Sometimes the dynamics of the fast degrees of freedom is not the topic for research, whereas their effect on the slow phenomena should be studied. The most prominent example for such a system is a Brownian particle in a solvent. Many systems with a solvent environment fall into this class, *e.g.*, colloidal systems [101], polymer solutions [47], and complex plasmas [118] which is the very subject in this thesis. Since there are usually a large number of solvent particles in these systems, it is rather inefficient to simulate the fast degrees of freedom explicitly. Therefore techniques that reduce the degrees of freedom are favorable, such as Langevin dynamics or Brownian dynamics [6], where the fast degrees of freedom are substituted by stochastic terms in the equation of motion and Langevin equation, instead of Newton's equation is numerically solved. In complex plasma physics, it had been pointed out by Ref. [181] that the Brownian motions of particles are not negligible in typical laboratory conditions since random agitation arising from asymmetric molecular bombardment is commonly noticeable.

Therefore LD simulation is more favorable for simulating dust particle dynamics in complex plasma physics. The advantages of LD simulation are that it is possible to store the phase-space trajectories of particles and provide time evolution information of the investigated systems. From the phase-space coordinates of the particles, it is possible to derive static, dynamic as well as transport properties and to obtain information about the collective excitations.

In this section I will discuss about the equations of motion for dust particle first and then describe the details of Langevin dynamics simulations. Some applications of LD simulation will be presented in **chapter 2** and **3**.

1.4.1 Equations of motion for dust particles

In complex plasma, dust particle motion can be very well described by the Langevin equation [40],

$$\dot{\mathbf{r}}_i = \mathbf{v}_i, \tag{1.20}$$

$$\dot{\mathbf{v}}_i = -\gamma \mathbf{v}_i + \frac{1}{m_i}\mathbf{F}_i + \frac{1}{m_i}\mathbf{R}_i, \tag{1.21}$$

where, m_i[5], $\mathbf{v}_i$ and $\mathbf{r}_i$ are, respectively, the mass, velocity and position of the ith dust particle. γ is the neutral gas damping frequency and $\gamma = \gamma_{Ep}$ in the context of complex plasma (see Eq. (1.14) for details about the damping force arise from neutral drag force), *i.e.*, the so-called Epstein drag coefficient which was introduced by Epstein [34].

[5]It should be noted here in this section subscript i denote the ith particle in the system, instead of physical quantities attributed to *ions* which are used in the sections 1.1.2.

$\mathbf{F}_i = -\sum \nabla\phi + \mathbf{F}_{ext}$ in Eq. (1.21) is the deterministic force comprised of inter-particle interactions and external force fields such as those discussed in the sections above and listed in table (1.1). The inter-particle interactions in complex plasma are often approximated to Yukawa potential [86]. The last term, $\mathbf{R}_i$, is a stochastic force representing the random kicks from surrounding media molecules. It is commonly described by a delta-correlated stationary Gaussian process with zero-mean satisfying

$$\langle \mathbf{R}_i(0)\mathbf{R}_i(t)\rangle = 2\gamma k_B T m_i \delta(t). \tag{1.22}$$

Here, δ is the Dirac delta function, k_B is Boltzmann constant and T the system temperature. The stochastic force and friction are related through the fluctuation-dissipation theorem [95]. (Technically speaking, the cooling by friction should cancel the heating by noise).

1.4.2 Langevin dynamics simulations

The Langevin equation is a stochastic differential equation and can be integrated over a short time Δt, assuming the deterministic force $\mathbf{F}_i$ is only a function of time and can be extended by using Taylor series, thus solving the equation in a step by step manner [4, 5, 35, 95, 171]. Since we have assumed that the stochastic force $\mathbf{R}_i$ in Eq. (1.21) is a Gaussian white noise and that γ is constant, then the two dynamic variables, $\mathbf{r}_i(t)$ and $\mathbf{v}_i(t)$, are actually normally distributed random variables themselves. Consequently, according to the Normal linear transform theorem [95], $\mathbf{r}_i(t)$ and $\mathbf{v}_i(t)$ are completely determined by their instantaneous means (vectors) and variances (scalars), and can be expressed, respectively, as follows

$$\begin{aligned} \mathbf{r}_i &= \bar{\mathbf{r}}_i + \sqrt{\mathrm{Var}(r)}\mathbf{N}_r, \\ \mathbf{v}_i &= \bar{\mathbf{v}}_i + \sqrt{\mathrm{Var}(v)}\mathbf{N}_v. \end{aligned} \tag{1.23}$$

Here, $\mathbf{N}_r$ and $\mathbf{N}_v$ are random vectors following standard normal distribution (*i.e.*, having the mean 0 and variance 1). The subscripts v and r indicate that they are associated with the velocity and position, respectively. Since the velocity and position are not independent, but rather jointly distributed normal variables, the updating formulae Eq. (1.23) can be further written as [64, 95]

$$\begin{aligned} \mathbf{r}_i &= \bar{\mathbf{r}}_i + \sigma\mathbf{N}_1 + \sqrt{\mathrm{Var}(r) - \sigma^2}\mathbf{N}_2, \\ \mathbf{v}_i &= \bar{\mathbf{v}}_i + \sqrt{\mathrm{Var}(v)}\mathbf{N}_1, \end{aligned} \tag{1.24}$$

where $\sigma = \mathrm{Cov}(v,r)/\sqrt{\mathrm{Var}(v)}$. Note here the covariance $\mathrm{Cov}(v,r)$, the variances $\mathrm{Var}(\mathbf{r})$ and $\mathrm{Var}(\mathbf{v})$ are given as [64, 95],

$$\begin{aligned}
\mathrm{Cov}(v,r) &= \frac{k_B T}{m_i \gamma}\left(1 - 2e^{-\gamma\Delta t} + e^{-2\gamma\Delta t}\right), \\
\mathrm{Var}(\mathbf{r}) &= \frac{2\Delta t k_B T}{m_i \gamma}\left(1 - 2\frac{1-e^{-\gamma\Delta t}}{\gamma\Delta t} + \frac{1-e^{-2\gamma\Delta t}}{2\gamma\Delta t}\right), \\
\mathrm{Var}(\mathbf{v}) &= \frac{k_B T}{m_i}\left(1 - e^{-2\gamma\Delta t}\right),
\end{aligned} \tag{1.25}$$

where unit normals N_1 and N_2 are now statistically independent of each other. There are plenty of ways for generating normal random variables, *e.g.*, the Box-Muller method [20], the acceptance-complement ratio method [63] *etc.* As for the instantaneous means in Eq. (1.24), $\bar{\mathbf{r}}_i$ and $\bar{\mathbf{v}}_i$ are obtained by any algorithm suitable for conventional MD simulations as listed in table 1.2

Accuracy	**Numerical integration algorithm**
First order methods	Eular
Second order methods	Verlet, Velocity-Verlet, Leapfrog, Beeman
Higher order methods	Runge-Kutta, Gear's method

Table 1.2: Different integration methods commonly used in MD simulations.

Langevin dynamics can not only be used as a method to reduce the degrees of freedom, but also be used as a thermostat to imply MD simulation in the canonical ensemble (NVT) along with other techniques like velocity rescaling, Nosé-Hoover thermostat, Nosé-Hoover chains, and the Berendsen thermostat [6, 17, 42, 61, 131]. It can also cope with energy sources and sinks, which makes it possible to apply external forces to the system. In this way it is possible to simulate non-equilibrium situations, *e.g.*, shear flow, driven systems such as lane formation in **chapter 3**. Langevin dynamics simulations are therefore very suitable for simulating complex plasma physics and indeed have been widely used in studying many phenomena which complex plasmas host.

Though strictly defined in [17] that *Brownian dynamics* is only the non-inertia limit of the Langevin dynamics (The inertia term on the left-hand-side of Eq. (1.21) is neglected which means the system is "over-damped".), I shall in this thesis stick to the less strict terminology as suggested in Refs. [6], where Langevin dynamics and Brownian dynamics are the same concept.

Chapter 2

Striped electrode: toward particle manipulation in a meter-sized plasma device.

The results of this chapter have been published in the following papers which are attached to this thesis.

- K. Jiang, Y.-F. Li, T. Shimizu, U. Konopka, H. M. Thomas, and G. E. Morfill, *Controlled particle transport in a plasma chamber with striped electrode*, Phys. Plasmas 16, 123702 (2009).
- Y.-F. Li, U. Konokpa, K. Jiang, T. Shimizu, H. Höfner, H. M. Thomas, and G. E. Morfill, *Removing dust particles from a large area discharge*, Applied Physics Letters 94, 081502 (2009).

The objectives, methods, and results of these two papers listed above are summarized in sections 2.1 to 2.3, respectively.

2.1 Objectives

The purpose of this chapter is twofold: to provide a system for investigating large two-dimensional complex plasmas and to investigate techniques for providing clean environments in plasma processing reactors.

Dust particles have become a technologically important subject for plasma-assisted material processing. In many cases, especially in the fabrication of electronic circuits and in plasma vapor deposition, grown dust particles can be considered as a main source of defects in the final products. The formation of the dust particles was observed in several plasma processes [73, 143, 144, 158, 174, 178]. It was first indicated by Spears *et al.* that a silane plasma was contaminated by micron-size particles visualized using laser light scattering [158]. Subsequently it was reported by Watanabe that in a plasma

enhanced chemical vapor deposition (PECVD) process grown dust particles play a negative role on the deposition rate and the quality of the silicon film [174]. Dust particles were also observed in etching [143] and sputtering processes [73, 144], as well as in nuclear fusion devices [134, 154, 178]. The challenge to remove these dust particles is one of the motivations for the extensive study of complex plasma in recent decades [152].

Methods for removing dust particles from processing plasmas have been investigated by many authors and described in section 1.2 by manipulating various forces, however, how to transport dust particle across meter-sized electrodes remains a technological issue.

2.2 Methods

Experimental apparatus

The striped electrode chamber is a modified parallel-plate CCP chamber with an inner diameter of 80 cm and a height of 40 cm (A sketch for the device is provided in Fig. 2.1). The base pressure is about 10^{-6} mbar in this study. The chamber contains two stainless steel electrodes. The upper one, connected to a 13.56 MHz RF generator through a matching unit, has a frame shape structure with three 48 cm $\times$ 16 cm openings to allow visual and mechanical accesses from the top. The lower stripe electrode consists 100 stripes which are electrically insulated with each other. Each strip is connected independently to one channel of a multichannel voltage function generator. For each generator channel, different waveform, frequency, dc-bias, amplitude, and phase angle can be chosen separately. Both electrodes are rectangle shapes with the size of 48.8 cm $\times$ 52.5 cm and the distance between them is adjustable from 3 cm to 13 cm. The chamber is normaly operated with argon at pressures between 1 Pa and 100 Pa and RF powers between 20 W and 1000 W. A photograph of the experimental system is shown in Fig. 2.2.

Vacuum system

The chamber is normally evacuated by a turbomolecular pump, a mechanical booster pump and a rotary pump, which are shown in the bottom of Fig. 2.1 as Pump1, Pump2 and Pump3. All three are used to pre-evacuate the chamber and achieve base pressure before the experiments. The rotary pump and the mechanical booster pump are employed to maintain a certain pressure with applied gas during the experiments. The argon gas flow is maintained by a mass-flow controller (MKS type 1479A). The flow rate is kept below 3 sccm (standard cubic centimeters per minute) during experiments. The working gas pressure is maintained by a pressure controller (MKS type 651C) connecting to a throttling valve (MKS type 253B). The pressure is measured by a Baratron manometer (MKS type 627B) from the top of the chamber.

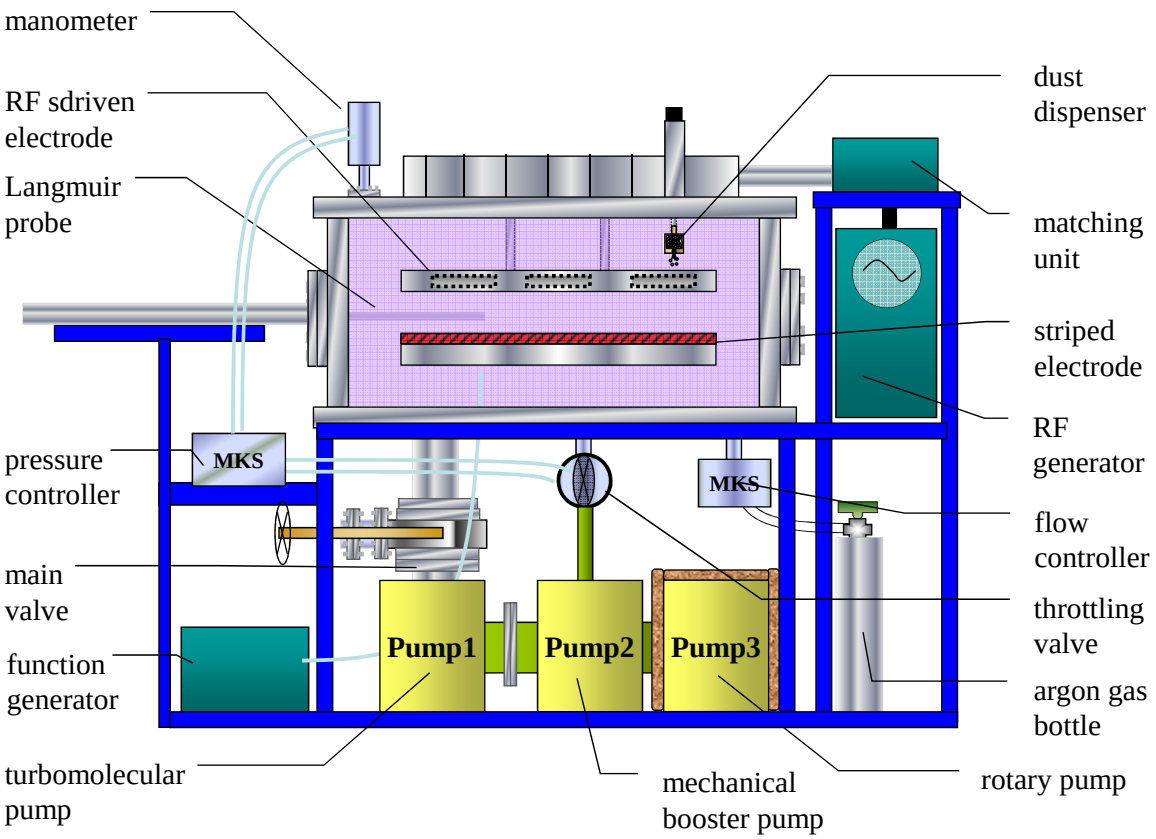

Figure 2.1: Sketch of the striped electrode device.

Lower striped electrode

The lower striped electrode consists of 100 electrically insulated stainless steel stripes of 5 mm × 488 mm as shown in Fig. 2.3. Each stripe is connected individually to one channel of a multichannel function generator which has 104 channels. The function generator can generate waveforms with dc-biases of ± 100 V and frequencies up to 100 Hz. This enables us to choose waveforms, frequencies, dc-biases, amplitudes, and phase angles for each stripe independently.

Dust dispenser and microparticles

Particles used in the experiments are grown particles and/or injected particles. When the injected particles are used, three different types of dust particles are normally introduced into the chamber. They are Al_2O_3 particles with density of 3.95 g/cm^3 and diameters of 1 μm and 3 μm; melamine formaldehyde (MF) particles with density of 1.57 g/cm^3 and diameters of 3 μm and polymethyl methacrylate (PMMA) particles with density of 1.19 g/cm^3 and diameters of 17 μm. PMMA particles of 17 μm in diameter taken by optical microscope are shown in Fig. 2.4a.

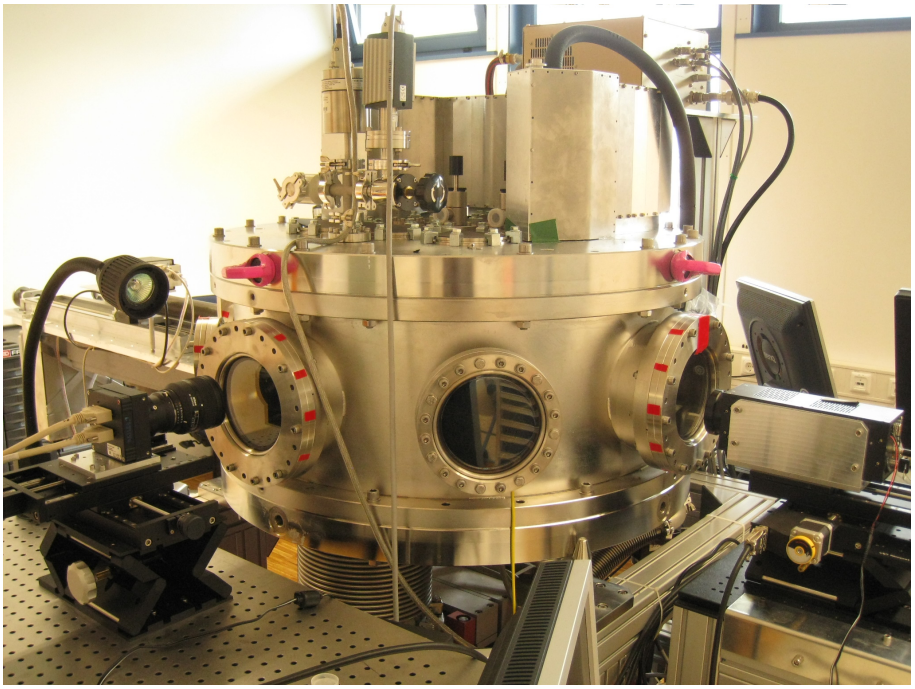

Figure 2.2: Photograph of the striped electrode device.

The particles are injected inside the chamber by a dispenser as shown in Fig. 2.4b, which is a small container, mounted on a metallic arm and placed in the discharge. The container has a mesh, through which the dust particles drop out when the dispenser is shaken. The size of the mesh holes is a few times larger than the diameter of the particles.

Particles imaging system

A laser sheet with central wavelength of 680 nm and power of 200 mW is aligned perpendicular to the electrode. The laser light is scattered by levitated particles between the electrodes. In order to obtain particle positions, a camera (Basler A404k) equipped with an interference filter and macro lens (Nikon AF 85 mm f/1.4D IF) is used to record the light scattered by dust particles. A digital video capture card (DVR Express CLFC) is installed in the computer and connected to the camera for the storage of images which will be used afterwards for analysis. The imaging system can resolve particle dynamics with the frame rate of up to 96.

2.3 Results

The utilization of the striped electrode enables us to generate a moving distortion or potential traps in front of the electrode, thus it provides a method to transport/remove dust particles over large distances without generating significant disturbances in the plasma region. The dependence of the particle transport in the electric field generated by the striped

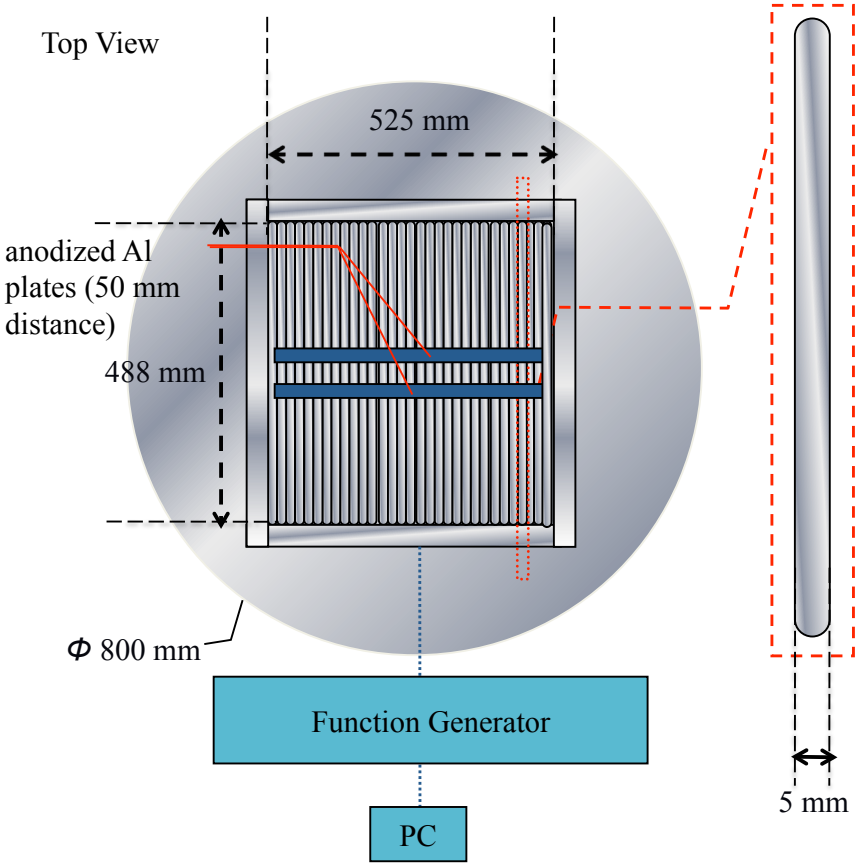

Figure 2.3: Sketch of the striped electrode.

electrode was studied experimentally and numerically. It was found that the transport efficiency of the dust particles is strongly dependent on the amplitude, dc-bias, frequency, and phase shift of the applied signals on the stripes. Three distinct transport regimes were also found both in the experiments and the simulations. The dust particles exhibited only a local oscillation when the potential profile was slightly modulated. At a very strong modulations, all the dust particles were fully trapped and transported with the velocity of the traveling potential distortions. In an intermediate case, both transport and local oscillations were observed. Results from the simulation based on the method described in chapter 1.4 show a qualitative agreement with our experimental findings.

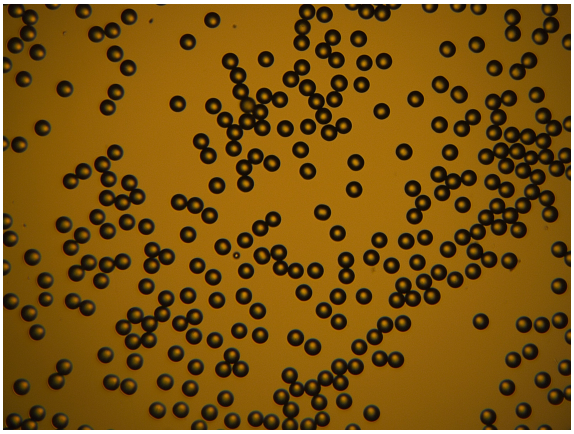

(a)

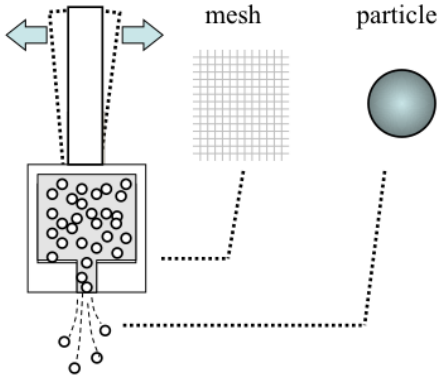

(b)

Figure 2.4: Dust particles and dispenser: (a) PMMA particles with the mean size of 17 μm in diameter; (b) Sketch of the dust dispenser.

Chapter 3

Dynamics of binary complex plasmas: Demixing and laning

The results of this chapter can been seen in the following papers which are attached to this thesis.

- **Ke Jiang**, L.-J. Hou, A. V. Ivlev, Y.-F. Li, C.-R. Du, H. M. Thomas, G. E. Morfill, and K. R. Sütterlin, *Initial stages in phase separation of binary complex plasmas: Numerical experiments*, Europhysics Letters 93, 55001 (2011).
- **Ke Jiang**, L.-J. Hou, A. V. Ivlev, Y.-F. Li, K. R. Sütterlin, H. M. Thomas, and G. E. Morfill, *Demixing in Binary Complex Plasma: Computer Simulation*, accepted by IEEE at May 1, 2011.
- **Ke Jiang**, C.-R. Du, K. R. Sütterlin, A. V. Ivlev, and G. E. Morfill, *Lane formation in binary complex plasmas: Role of non-additive interactions and initial configurations*, Europhysics Letters 92, 65002 (2010).

The objectives, methods, and results of these three papers listed above are summarized below in sections 3.1 to 3.3, respectively.

3.1 Objectives

In this chapter, Langevin dynamics simulations (details in chapter 1.4) are employed to study two intriguing phenomena in binary complex plasmas, namely phase separation (demixing) and lane formation (laning).

Recently, binary complex plasma (complex plasmas with two different sized dust particles) are gaining more and more attention [53, 72, 119, 161, 162, 179], as both demixing and laning have been observed in recent microgravity experiments on board ISS (International Space Station) [161, 162]. The work presented in this chapter is particularly motivated by these recent experimental findings.

3.2 Methods

Langevin dynamics simulations are employed to study phase separation and lane formation in binary complex plasmas. For both big and small particles in the binary mixture of complex plasmas we assume that they can be treated as point-like charge and that they interact with each other via pairwise Yukawa or screened Coulomb potential with the same screening length λ, but different magnitudes ε_{ij}. The general form of inter-particle interaction can be written as

$$\phi_{ij}(r) = \varepsilon_{ij}\frac{\exp(-r/\lambda)}{r}. \tag{3.1}$$

For like particle interaction, $\varepsilon_{SS/BB}$ is the product of the effective charge and the real charge $Z_{S/B}$ [72] (subscripts S and B denote small and big particles respectively). According to the Lorentz-Berthelot mixing rules [6], the interaction magnitude between unlike particles is written as

$$\varepsilon_{LS} = \varepsilon_{SL} = (1+\Delta)\sqrt{\varepsilon_{SS}\varepsilon_{BB}}, \tag{3.2}$$

where Δ is the *non-additivity parameter* [72], representing the asymmetry in the mutual interaction between unlike particles. Δ is always positive in binary complex plasmas [72]. When $\Delta = 0$, it reduces to a typical additive Yukawa potential, which is exactly the interaction model used in Ref. [161].

3.3 Results

3.3.1 Results of phase separation simulation

10^5 of two different sized dust particles with off-critical composition are employed in a cubic simulation domain of length 1.1 cm with periodic boundaries. The particle sizes in this study are 3.4 μm and 10.2 μm in diameter. All our simulations started from randomly distributed configurations of particles. The demixing dynamics from the numerical simulations is shown in Fig. 3.1, which shows snapshots at four different time stages demonstrating the typical sequence. Starting from a random mixture as shown in Fig. 3.1a, the system firstly coarsens and form small clusters where there are no clear boundaries between two species, as shown in Fig. 3.1b. Next, sharp interfaces build up while small clusters merge into big ones, as shown in Fig. 3.1c and Fig. 3.1d. In Fig. 3.1d the small particles tend to form big droplets of nearly spherical shape, indicating that the non-additivity induced interfacial tension starts to play a role.

Special attention is placed on the initial stages during the phase separation and dependence of the domain growth rate on the coupling strength, interaction non-additivity and neutral damping rate. It is found that the domain growth following a power law with an exponent α of around 1/3, which is well in accordance with the Lifshitz-Slyozov growth law for the initial diffusion-driven stage of phase separation. We observe that the exponent α is almost independent of coupling strength unless the coupling strength is so high that

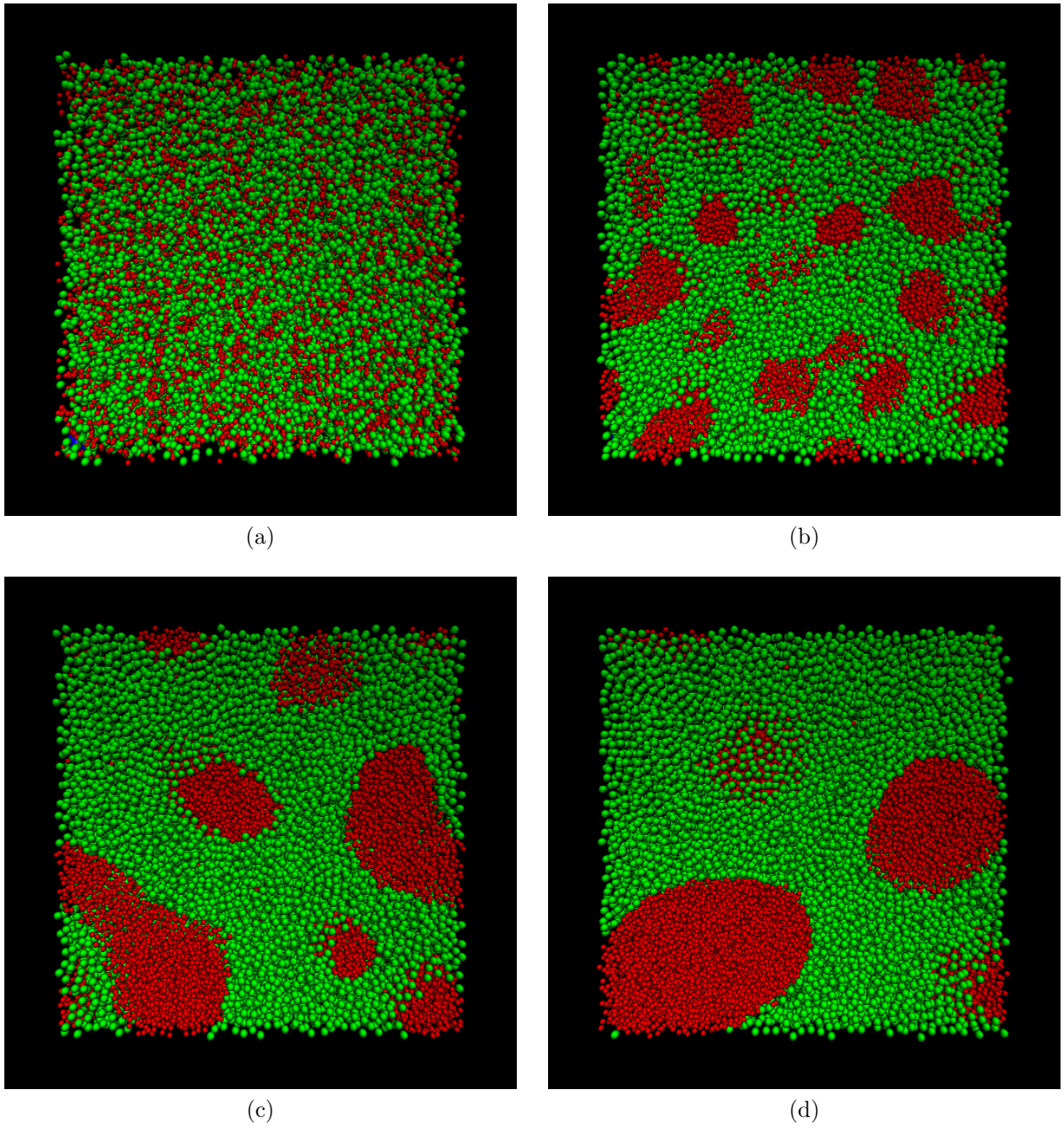

(a) (b)

(c) (d)

Figure 3.1: Demixing in binary complex plasmas. Typical snapshots at four different stages: (a) at $t = 0$ particles are randomly distributed; (b) at $t = 2$ s small particles gathered locally; (c) at $t = 4$ s the initial domains start to coarse; (d) at $t = 20$ s sharp interfaces build up while small red domains merge into big ones. Small (3.4 μm) particles are colored in red and big (10.2 μm) particles are in green.

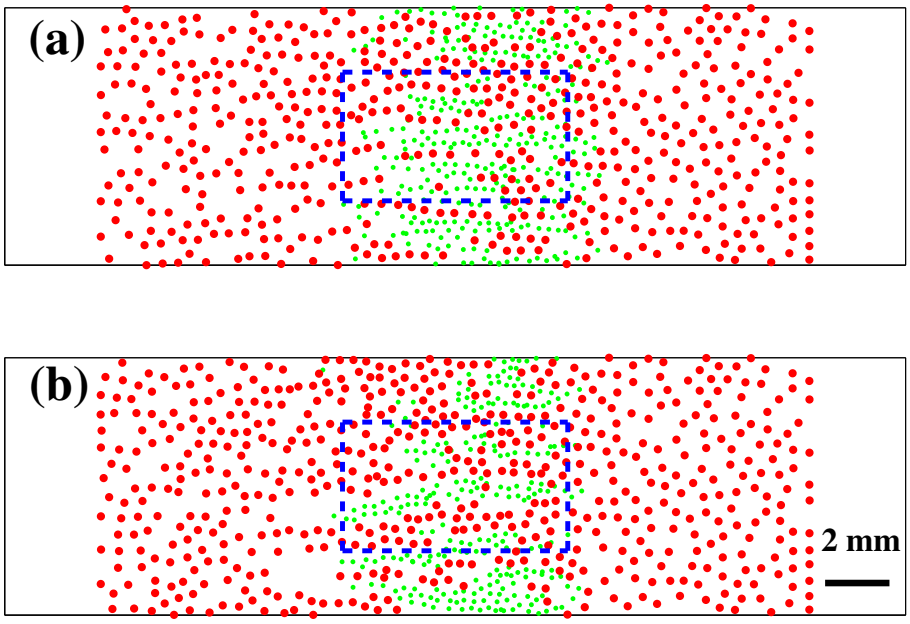

Figure 3.2: Comparison of two snapshots of lane formation in LD simulation for $\Delta = 0$ (a) and $\Delta = 0.5$ (b) taken at the same time step. Small particles (green) are driven from the left to the right through the cloud of big (red) particles. Interestingly enough, small particles are able to penetrate faster for $\Delta = 0$. Also the lanes formed by both species are wider for larger Δ. The blue dashed box in each picture indicates the ROI in which we apply our analysis method.

big particles crystallize and the motions of small particles/droplets are dissipated and/or even caged. Although the demixing process is driven by the interaction non-additivity, it is found that the domain growth rate α is not dependent on Δ in the regimes we observed. The neutral gas damping, besides the viscous dissipation from big-particle phase, can also slow down the phase separation by slowing down the diffusion of particles/clusters, while has no big influence on the growth rate α.

3.3.2 Results of lane formation simulation

We show two snapshots of laning with non-additivity parameter $\Delta = 0$ and $\Delta = 0.5$ in Fig. 3.2. Fig. 3.2a shows the normal laning phenomenon, where narrow lanes—at most 2 particles across—can be observed for both small and big particles. Whereas in Fig. 3.2b, the demixing stimulated laning mode, where like particles try to cluster due to the non-additivity and a demixing stimulated laning mode is achieved.

We show that there is a non-additivity stimulated crossover from normal laning mode to a demixing dominated laning mode. To analyze this crossover on the individual particle level we applied a very sensitive order parameter for lane formation based on anisotropic scaling indices [132, 161, 162]. Extensive numerical simulations enabled us to identify a critical value of the non-additivity parameter Δ for the crossover. In addition the simulations

revealed that the dynamics of lane formation is strongly influenced by the exact spatial configurations at the very moment of contact between two different complex plasmas.

Chapter 4

Mach cones in a three-dimensional complex plasma

The results of this chapter have been published in the following paper which is attached to this thesis.

- K. Jiang, V. Nosenko, Y.-F. Li, M. Schwabe, U. Konopka, A. V. Ivlev, V. E. Fortov, V. I. Molotkov, A. M. Lipaev, O. F. Petrov, M. V. Turin, H. M. Thomas and G. E. Morfill, *Mach cones in a three dimensional complex plasma*, Europhysics Letters, 85, 45002 (2009).

The objective, methods, and results of the paper listed above are summarized in sections 4.1 to 4.3, respectively.

4.1 Objectives

It is common to see a moving disturbance producing waves and wakes in a variety of physical systems. Under certain circumstances, they can form a wake pattern, which is stationary as viewed in the moving frame. The structure of this wake depends mainly on the wave dispersion of the medium and the speed and size/shape of the moving disturbance. A ship moving in deep water consisting of multiple lateral and transverse wakes [121] as in Fig. 4.1a. Some examples of waves and wakes in nature have been showed in Fig. 4.1.

A Mach cone is a type of wake, which has a V-shaped structure in a two-dimensional (2D) case. The existence of Mach cones in complex plasmas was first predicted in theory by Havnes *et al.* [57] and later observed in a 2D plasma crystal as in Fig. 4.1d by Samsonov *et al.* [137, 138] and Melzer *et al.* [107]. Mach cones can either be excited by the electrostatic force from a charged particle moving spontaneously beneath a 2D lattice as in Samsonov's experiment [137, 138], or by the radiation pressure force from a spot of focused laser beam scanning across the 2D complex plasma as in Melzer's experiment [107]. In both experiments, the observed Mach cones were composed of compressional waves. Shortly afterwards, with similar laser beam scanning technique, Nosenko *et al.*

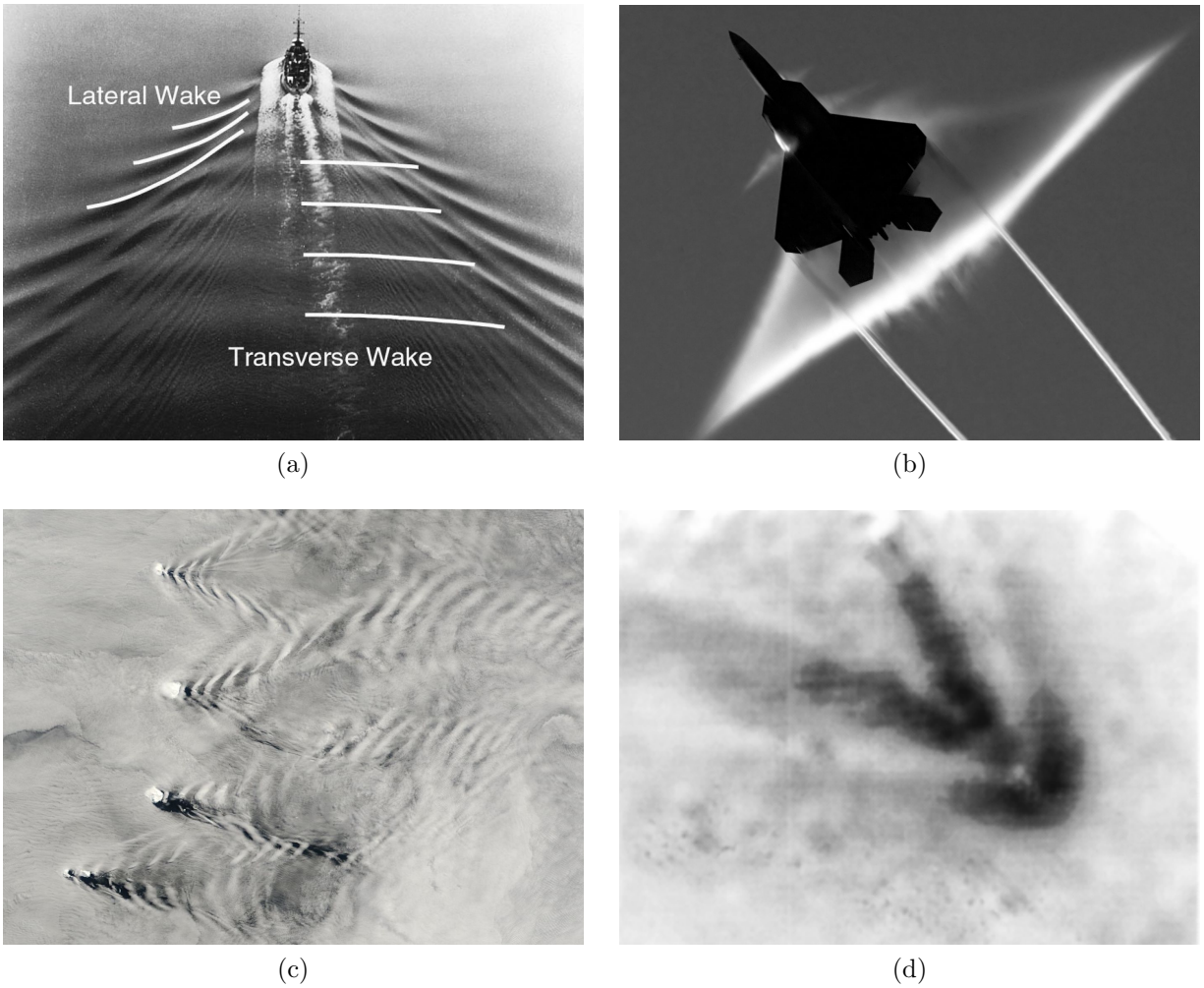

(a) (b)

(c) (d)

Figure 4.1: Examples of wakes in nature: (a) Wake pattern behind a ship moving in deep water consists of multiple lateral and transverse wakes. Photo adapted from Ref. [121]; (b) An F-22 raptor executes a transonic flyby over the aircraft carrier by John C. Stennis; (c) Waves and wakes in a large scale by islands. From *NASA Earth Observatory*; and, (d) Mach cone observed in a 2D complex plasma. Photo adapted from Ref. [137].

observed shear-wave Mach cones in a 2D dust lattice [125, 126]. Inspired by the above-mentioned experiments, various theoretical models [32, 58, 65, 76, 104, 173, 180] have been proposed to interpret Mach cones in 2D complex plasma.

However, experimental observations of Mach cones in three-dimensional (3D) complex plasmas have not yet been reported due to the difficulties of generating 3D homogenous complex plasma in laboratory on the earth. This issue has been addressed by conducting microgravity experiments on board the ISS, where the dust particles are not confined in the sheath region, but rather in the bulk plasma [166]. Here we report the first observation of a 3D Mach cone in complex plasmas from PK-3 Plus project on board ISS under microgravity conditions [166]. A hydrodynamic model is used to compare with the experiments.

4.2 Methods

A hydrodynamic model is developed to provide a simple physical picture of this phenomenon. The details of the model are presented in the attached published paper [75].

4.3 Results

This work presents a hydrodynamic model and the first observation of Mach cones in a three-dimensional complex plasma under microgravity conditions in the PK-3 Plus facility on board the ISS. Numerical results showed different structures of Mach cone. Special attention was paid to the effect of the disturbance velocity and neutral gas damping. Multiple-cone structures of compressional wakes have been found and the damping effect may reduce the number of multiple wakes down to a single cone as shown in Fig. 4.2. The dispersion relation for the dust acoustic wave derived in our hydrodynamic model is in a good agreement with other theories. A single compressional-wave Mach cone in 3D complex plasma was observed in experiments and numerical results in the case of rather strong damping.

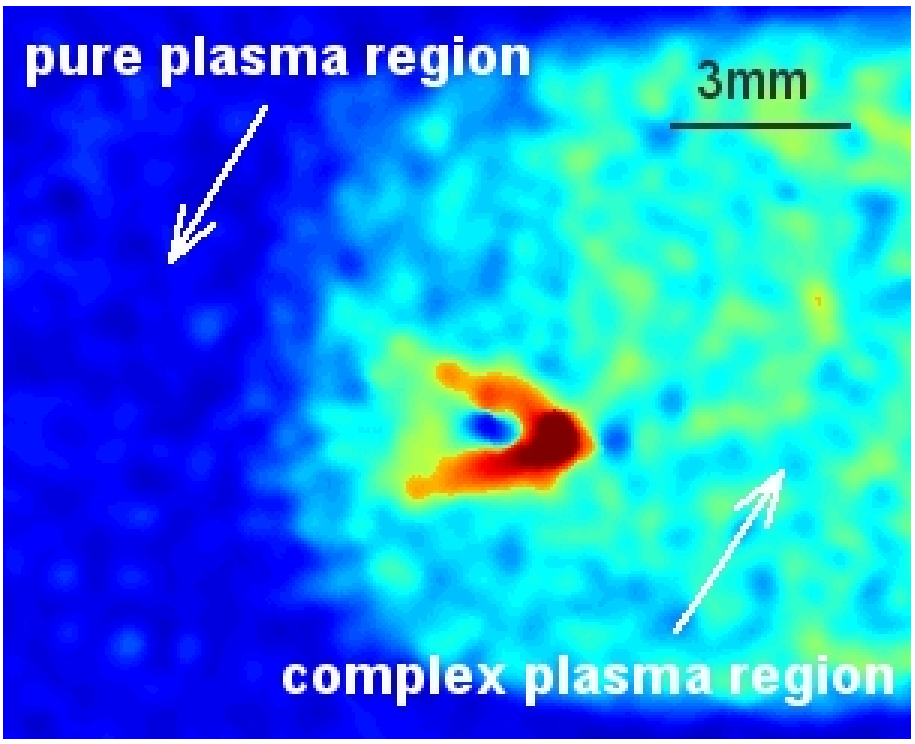

Figure 4.2: Mach cone in a 3D complex plasma. This figure shows a superposition of three consecutive frames shifted so that the cone structures in different frames coincide. Reproduced from Ref. [75]

Chapter 5

Summary

In summary, the contributions of this PhD thesis are listed as follows:

- A method for dust particle manipulation/removal has been tested in newly developed "striped electrode" system. Particle manipulation over ~ 0.5 m with speed up to ~ 10 cm/s has been achieved by controlling the traveling plasma distortions with 100 independent stainless steel stripes. This provides a setup for investigating large 2D complex plasma systems and poses a potential technique for providing clean environments in plasma processing reactors.

- A Langevin dynamics simulation package named *Complex Plasma Langevin Dynamics* (CPLD) has been developed and tested. Linked-list cell method has been implemented to improve the efficiency of the code. Parallelization of the kernel has been accomplished based on spatial decomposition method with OpenMP on a shared memory architecture. CPLD has been tested on IBM Power6 supercomputer installed at the Rechenzentrum Garching (RZG) and on the XGRID cluster at the theory group of Max-Planck-Institute for extraterrestrial physics.

- Dynamics of laning and demixing of binary complex plasma at individual particle level have been studied by using CPLD. The scaling phenomenon of demixing in the initial stage has been studied and the domain growth with an exponent of $\alpha \sim 1/3$ (diffusive regime) has been observed. Effects of neutral gas damping and coupling strength on demixing of binary complex plasma have been discussed. The role of initial configuration and non-additivity in laning phenomenon has also been studied.

- A hydrodynamic model has been developed to investigate Mach cones in complex plasmas. Numerical results have been shown to reproduce a compressional-wave Mach cone observed onboard the International Space Station under microgravity condition with PK-3 Plus setup.

Appendix A

Charging mechanisms and charge fluctuation

The charge on the dust particle is one of the most important parameters in complex plasma physics. It determines the magnitude of dust particles interactions with electrons/ions, electromagnetic fields, and the other dust particles. Thus it is important to study the charging mechanism of dust particles in complex plasma. Dust particles in plasma can be charged due to various mechanism [176], such as electron/ion current collection from the plasma [13], photoelectric effect in the presence of a flux of sufficiently energetic ultraviolet (UV) photons [44], thermionic emission when the grain is heated [157], or secondary electron emission in the presence of high energy electrons beams [24]. For microparticles in most laboratory or industrial plasmas, the dominant charging mechanism is collecting electrons and ions from the background plasma. Dust particles behave like small isolated probes immersed in plasma at floating potential. Because of the higher mobility of the electrons compared to the ions, dust particles are negatively charged. However when other mechanisms start to dominate the charging process, dust particles can be positively charged as well. In this Appendix, a few important charging mechanisms as shown in Fig. A.1 are described in detail.

Electrons and ions Collection

In this subsection charging due to collection of ambient electrons and ions will be discussed, which is the most important charging mechanism for ground-based experiments. As one can see in Fig. A.1a, when a particle is immersed in plasma, it will be charged by ion flux and electron flux until the particle surface reaches floating potential ϕ_f, which ensures the net current to the surface of dust particle being zero in the equilibrium state as

$$\frac{dQ_d}{dt} = I_i + I_e = 0, \tag{A.1}$$

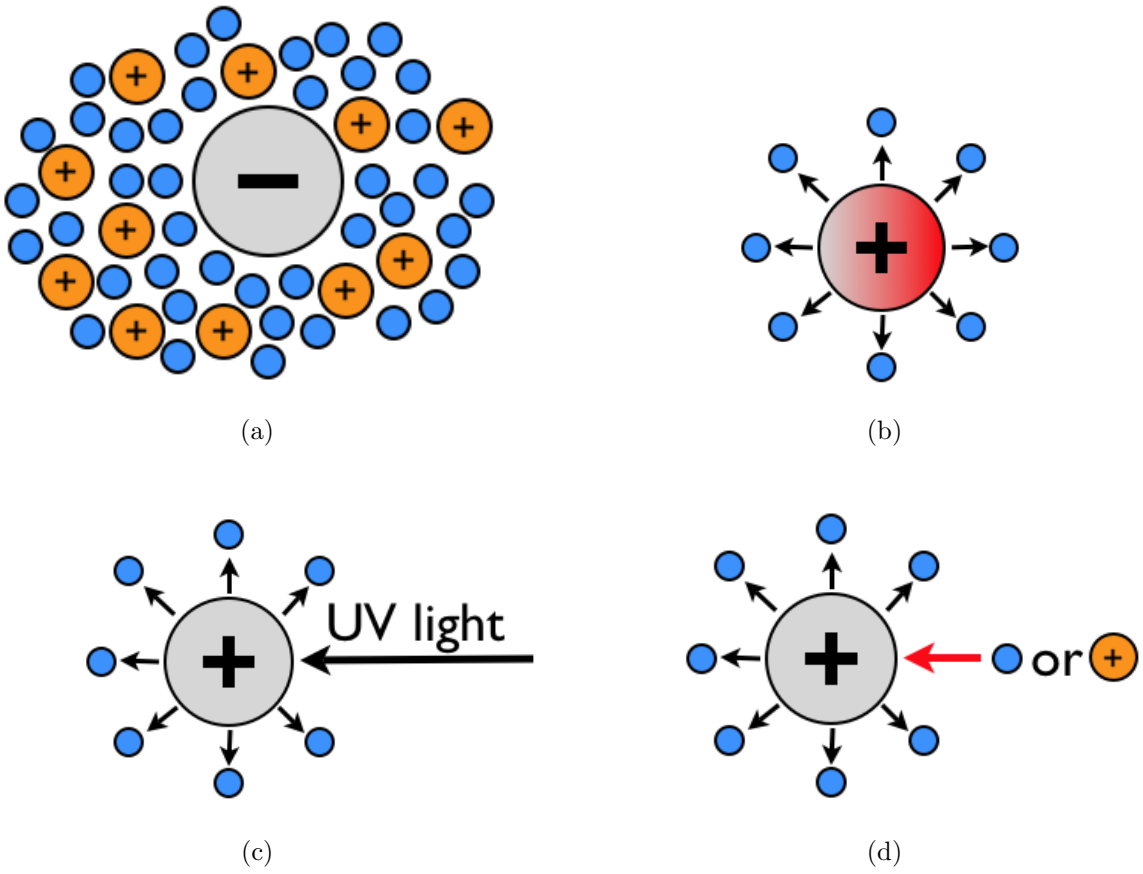

(a) (b)

(c) (d)

Figure A.1: Examples of different charging mechanics: (a) Electrons and ions collection; (b) Thermionic emission; (c) Photoelectric effect; and, (d) Secondary ion and electron emission.

where $Q_d = -eZ_d$ is the charge on the particle surface provided the particle is negatively charged. The charge on the particle then determined by

$$Q_d = C\phi_f, \tag{A.2}$$

where the capacitance C of spherical microparticle is

$$C = r_d\left(1 + \frac{r_d}{\lambda_D}\right) \approx r_d. \tag{A.3}$$

For a typical complex plasma condition, the capacitance is $C = r_d$[1] in the case of $r_d \ll \lambda_D$. In the limiting case of collisionless complex plasmas, generally one has $r_d \ll \lambda_D \ll l_{e(i)}$, where λ_D is the Debye length and $l_{i(e)}$ is the collisional mean free path of ions (electrons). In this case, the floating potential and particle charge can be calculated using *Orbital Motion Limited (OML) theory* [3, 90, 120]. Based on the the energy conservation law and angular momentum, the cross section for ion collection σ_i and electron collection σ_i are respectively as follows

$$\sigma_i = \pi b_c^2 = \pi r_d^2\left(1 - \frac{2e\phi_f}{m_i v_{i0}^2}\right), \tag{A.4}$$

$$\sigma_e = \pi b_c^2 = \pi r_d^2\left(1 + \frac{2e\phi_f}{m_e v_{e0}^2}\right). \tag{A.5}$$

Here $v_{i0(e0)}$ is the ion (electron) velocity very far from the grain. b_c denotes the critical impact parameter when the ions (electrons) just graze the surface of dust particle. The electron and ion current is determined by the integral over the corresponding velocity distribution function and is given by

$$I_i = \pi r_d^2 n_i e\sqrt{\frac{8T_i}{\pi m_i}}\left(1 - \frac{e\phi_f}{T_i}\right), \tag{A.6}$$

$$I_e = -\pi r_d^2 n_e e\sqrt{\frac{8T_e}{\pi m_e}}\exp\left(\frac{e\phi_f}{T_e}\right). \tag{A.7}$$

The above equation is valid for velocity distribution of the plasma species is Maxwellian and the streaming speed of plasma species is much smaller than the thermal speed [152]. For the case of ions with finite streaming speed, the ion current was discussed by Shukla [152]. The charge on the dust particle can therefore be described approximately as [105]

$$Z_d = C_0 T_e r_d \ln\left[\frac{n_i}{n_e}\left(\frac{m_e T_e}{m_i T_i}\right)^{1/2}\right], \tag{A.8}$$

where $C_0 \approx 0.73$ for a wide range of electron temperature in argon plasma [105].

The OML model presumes an isolated particle immersed in a plasma and the validation limit of OML theory has been discussed by Lampe [91] and Khrapak [79]. In a dense complex plasma region, the dust charge is substantially reduced comparing to the charge calculated from OML model [13]. Thus, OML is often used in complex plasma experiments for charge estimation of an upper limit.

[1]Gaussian units [69] are used in this thesis unless otherwise declared.

Thermionic emission

As illustrated in Fig. A.1b, when a dust particle is heated up, the ions and electrons on the surface gain thermal energy and starts to escape from the surface of particle. This occurs when the thermal energy given to the carrier overcomes the forces restraining it. This is called thermionic emission. The charge carriers can either be electrons or ions, and are sometimes referred to as *thermions*. The release of electrons from a hot metal surface is described by *Richardson's law* as

$$J(T) = A_R T_s^2 \exp(-\frac{\varphi}{k_B T_s}), \tag{A.9}$$

where T_s is dust surface temperature, A_R is coefficient used to describe thermionic emission and φ is the work function of the particle material (see more details about φ in the next subsection) and k_B is Boltzmann constant. The particle temperature in a typical complex plasma condition is on the order of room temperature [1], which is too small to serve as a substantial charging mechanism. On the other hand, plastic particles, which are the particles we commonly use will be melt before thermionic emission becomes important [39].

Photoelectric effect

Photoelectric effect, observed by Heinrich Hertz in 1887, descries the phenomenon that electrons are emitted from matter as a consequence of their absorption of energy from electromagnetic radiation of very short wavelength and electrons emitted in this manner are referred to as *photoelectrons* [37]. The physical picture can be seen in Fig. A.1c, when a photon impacts a microparticle, an electron will be liberated from the surface of the particle if the the energy of a photon is larger than the work function, φ, of the dust particle, which is the minimum energy required to liberate electron from the surface of any given matter. The maximum kinetic energy K_{max} of an ejected electron is given by $K_{max} = h\nu - \varphi$, where h is the Planck constant, ν is the frequency of the incident photon. After photoelectrons ejected from the surface of the microparticle, the particle is positively charged correspondingly. For most materials, φ does not exceed 6 eV [122] as seen in table A.1. UV light in most cases carries the energy of $3.10 - 124$ eV ($400 - 10$ nm in wavelength), which makes itself a good candidate to conduct the photoelectric effect and positively charge the dust particles. It is also noteworthy that photoelectric emission is the most important charging mechanism for cosmic dusts charging in many astrophysical environments. Fortov and co-workers has tried to expose the complex plasma experimental system to solar radiation [38], which leads to positively charged particles attaining a potential of W_{pot}. The potential is high enough that the next escaped photoelectron cannot run away from the attractive potential well of the dust particles. The potential $W_{pot} = -e\phi_{pot} = -(h\nu - \varphi)$ determines the dust charge. The photoelectron current under solar irradiation can be $\sim 10^{-9}$ A/cm^2 depending on the material [36].

The situation for dust particles in space can be more complex when Photoelectric effect becomes competitive with electron and ion collection. The *flip-flop effect*—two different

Element	Work function φ/eV
Cu	4.53-5.10
Al	4.06-4.26
Si	4.60-4.91
C	5.0

Table A.1: Electron work function of selected elements. This table contains selected values for the electron work function of the elements which may be regarded as typical values for a reasonably clean surface. φ is a measure of the minimum energy required to extract an electron from the surface of a solid. Adapted from [98].

equilibria with positive and negative charge coexist—starts to dominant and leads to dust agglomeration [109].

Secondary emission

As in Fig. A.1d, when an incident energetic ion or electron hits and penetrates the surface of a solid, it liberates electrons along its path by ionization of atoms in the solid. This process is called secondary emission. The yield of secondary electrons is defined as the ratio of the emitted electron current to the current of incident ions or electrons. For electron impact, it is described by $\delta_e = I_{se}/I_e$, namely, the average number of released electrons per incident electron. Secondary electron emission by ion impact is described by a coefficient γ_i, the average number of released electrons per incident ion. For most materials, we have $\gamma_i \ll 1$, and γ_i depends only weakly on ion energy.

In a small spherical dust particle, a diffusing electron finds a surface in any direction rather than only in one direction for bulk matter. This increases the secondary emission yield. However, on the other hand, small dust particles become transparent for energetic projectiles, which decreases the secondary emission yield [130].

Charging time and charge fluctuations

The charging process for ion current and electron current balancing and establishing an equilibrium stage takes place in the timescale of μs [19]. The charging time τ for dust particle reaching its equilibrium charge can be expressed as [29]

$$\tau = K_\tau \frac{\sqrt{T_e}}{r_d n}, \tag{A.10}$$

where K_τ is a function of T_i/T_e and m_i/m_e, $n = n_i = n_e$ is the plasma density. Note in Eq. (A.10), τ is inversely proportional to the particle radius and plasma density. The charging time coefficient $K_\tau \sim 2.05 \times 10^3$ in the unit of [s μm cm^{-3} eV$^{-1/2}$] for $T_i/T_e = 0.05$ in argon plasma as given by Ref. [29]. For example, a dust particle with radius $r_d = 1$ μm in a typical laboratory plasma with electron temperature $T_e = 3$ eV and density $n = 10^9$ cm^{-3} has a charging time of $\tau \approx 3.6$ μs. The charge of dust particles is actually not a continuous

regular variable in experimental situation, where the charging process due to electron and ion current toward the grain surface is discrete. As a result, the particle charge can fluctuate around its average value. Analysis of charge fluctuations due to charging discreteness was performed by Cui [29] and Matsoukas [105]. For typical conditions of complex plasmas in gas discharges, the magnitude of the charge fluctuations δZ_d is given by Cui [29] as

$$\delta Z_d \sim 0.5\sqrt{Z_{d0}}, \tag{A.11}$$

where Z_{d0} is the equilibrium charge on dust particles. Therefore, if we define a relative fluctuation of particle charge $\xi = \delta Z_d / Z_{d0}$, then it is evident that ξ scales with $r_d^{-1/2}$ since $Z_d \propto r_d$ by taking Eq. (A.3) into account. Clearly that, big particles have relatively small charge fluctuation, and for typical complex plasma conditions with about μm particles, the fluctuations is not very important, but for nanometer sized dust, fluctuations of the charge due to the discrete steps of collecting an ion or electron become important [115].

List of Figures

List of Tables

Bibliography

[1] M. R. Akdim and W. J. Goedheer. Modeling the effect of dust on the plasma parameters in a dusty argon discharge under microgravity. *Phys. Rev. E*, 67, 2003. 066407.

[2] E. Allahyarov and H. Löwen. Nonadditivity in the effective interactions of binary charged colloidal suspensions. *Journal of Physics: Condensed Matter*, 21(42):424117, 2009.

[3] J. E. Allen. Probe theory - the orbital motion approach. *Phys. Scripta*, 45:497 – 503, 1992.

[4] M. P. Allen. Brownian dynamics simulation of a chemical reaction in solution. *Molecular Physics*, 40:1073 – 1087, 1980.

[5] M. P. Allen. Algorithms for brownian dynamics. *Molecular Physics*, 47:599 – 601, 1982.

[6] M. P. Allen and D. J. Tildesley. *Computer Simulation of Liquids*. Clarendon Press, Oxford, 1987.

[7] B. M. Annaratone, M. Glier, T. Stuffler, M. Raif, H. M. Thomas, and G. E. Morfill. The plasma-sheath boundary near the adaptive electrode as traced by particles. *New Journal of Physics*, 5:92, 2003.

[8] Tetyana Antonova. *Interaction of particles with complex electrostatic structures and 3D clusters*. PhD thesis, Ludwig-Maximilians-Universität, 2007.

[9] O. Arp, D. Block, A. Piel, and A. Melzer. Dust coulomb balls: Three-dimensional plasma crystals. *Phys. Rev. Lett.*, 93(16):165004, Oct 2004.

[10] O. Arp, D. Block, M. Klindworth, and A. Piel. Confinement of coulomb balls. *Phys. Plasmas*, 12:122102, 2005.

[11] K. Avinash, A. Bhattacharjee, and S. Hu. Nonlinear theory of void formation in colloidal plasmas. *Phys. Rev. Lett.*, 90, 2003. 075001.

[12] M. J. Baines, I. P. Williams, and A. S. Asebiomo. Resistance to the motion of a small sphere moving through a gas. *Mon. Not. R. Astron. Soc.*, 130:63–74, 1965.

[13] A. Barkan, N. D'Angelo, and R. L. Merlino. Charging of dust grains in a plasma. *Phys. Rev. Lett.*, 73(23):3093–3096, Dec 1994.

[14] Michael S. Barnes, John H. Keller, John C. Forster, James A. O'Neill, and D. Keith Coultas. Transport of dust particles in glow-discharge plasmas. *Phys. Rev. Lett.*, 68 (3):313–316, Jan 1992.

[15] S. E. Beck, S. M. Collins, and J. F. O'Hanlon. A study of methods for moving particles in rf processing plasmas. *Plasma Science, IEEE Transactions on*, 22(2):128 –135, apr. 1994. ISSN 0093-3813.

[16] G. J. Bendo, B. A. Buckalew, D. A. Dale, B. T. Draine, R. D. Joseph, R. C. Kennicutt, Jr., K. Sheth, J.-D. T. Smith, F. Walter, D. Calzetti, J. M. Cannon, C. W. Engelbracht, K. D. Gordon, G. Helou, D. Hollenbach, E. J. Murphy, and H. Roussel. Spitzer and jcmt observations of the active galactic nucleus in the sombrero galaxy (ngc 4594). *apj*, 645:134–147, July 2006.

[17] Herman J. C. Berendsen. *Simulating the Physical World, Hierarchical Modeling from Quantum Mechanics to Fluid Dynamics*. Cambridge University Press, 2007.

[18] A. Bose and M. S. Janaki. Shear-wave mach cones in a strongly coupled dusty plasma. *Phys. Plasmas*, 13:012104, 2006.

[19] A. Bouchoule, J.-P. Boeuf, C. Punset, J. Perrin, and L. Boufendi et al. *Dusty Plasmas*. John Wiley & Sons Ltd., 1999.

[20] G. E. P. Box and Mervin E. Muller. A note on the generation of random normal deviates. *Ann. Math. Statist.*, 29(2):610–611, 1958.

[21] Manis Chaudhuri. *Electric potential and ion drag force in highly collisional complex plasma*. PhD thesis, Ludwig-Maximilians-Universität, 2008.

[22] F. F. Chen. *Introduction to Plasma Physics and Controlled Fusion, Second Edition*. Plenum Press, New York, 1984.

[23] F. Cheung. *Dust Clusters in Magnetized Plasma*. PhD thesis, The University of Sydney, March 2005.

[24] V. W. Chow, D. A. Mendis, and M. Rosenberg. Role of grain size and particle velocity distribution in secondary electron emission in space plasma. *J. Geophys. Res.*, 98: 19065–19076, 1993.

[25] J. H. Chu and Lin I. Direct observation of coulomb crystals and liquids in strongly coupled rf dusty plasmas. *Phys. Rev. Lett.*, 72(25):4009–4012, Jun 1994.

[26] J. E. Colwell, S. Batiste, M. Horányi, S. Robertson, and S. Sture. Lunar surface: Dust dynamics and regolith mechanics. *Reviews of Geophysics*, 45:26, 2007.

[27] I. D. Couzin and N. R. Franks. Self-organized lane formation and optimized traffic flow in army ants. *Proc. R. Soc. Lond. B*, 270:139–146, 2003.

[28] William Crookes. *Radiant Matter*. The British Association for the Advancement of Science, 1879.

[29] C. Cui and J. Goree. Fluctuations of the charge on a dust grain in a plasma. *IEEE*

Trans. Plasma Sci., 22:151, 1994.

[30] J. E. Daugherty and D. B. Graves. Derivation and experimental verification of a particulate transport model for a glow discharge. *J. Appl. Phys.*, 78:2279–2287, 1993.

[31] E. H. A. de Hoog, W. K. Kegel, A. van Blaaderen, and H. N. W. Lekkerkerker. Direct observation of crystallization and aggregation in a phase-separating colloid-polymer suspension. *Phys. Rev. E*, 64(2):021407, Jul 2001.

[32] D. Dubin. The phonon wake behind a charge moving relative to a two-dimensional plasma crystal. *Phys. Plasmas*, 7:3895, 2000.

[33] J. Dzubiella, G. P. Hoffmann, and H. Löwen. Lane formation in colloidal mixtures driven by an external field. *Phys. Rev. E*, 65(2):021402, Jan 2002.

[34] Paul S. Epstein. On the resistance experienced by spheres in their motion through gases. *Phys. Rev.*, 23(6):710–733, Jun 1924.

[35] Donald L. Ermak and Helen Buckholz. Numerical integration of the langevin equation: Monte carlo simulation. *Journal of Computational Physics*, 35(2):169 – 182, 1980. ISSN 0021-9991.

[36] B. Feuerbacher and B. Fitton. Photoemission from surface states on tungsten. *Phys. Rev. Lett.*, 29(12):786–789, Sep 1972.

[37] Richard Feynman. *The Feynman Lectures on Physics*. Addison-Wesley, 1963.

[38] V. E. Fortov, A. P. Nefedov, O. S. Vaulina, A. M. Lipaev, V. I. Molotkov, A. A. Samaryan, V. P. Nikitskii, A. I. Ivanov, S. F. Savin, A. V. Kalmykov, A. Ya. Solovev, and P. V. Vinogradov. Dusty plasma induced by solar radiation under microgravitational conditions: An experiment on board the mir orbiting space station. *J. Exp. Theo. Phys.*, 87(6):1087 – 1097, 12 1998.

[39] V. E. Fortov, A. V. Ivlev, S. A. Khrapak, and G. E. Morfill. Complex (dust) plasma: current status, open issues, perspectives. *Phys. Rep.*, 421:1–103, 2005.

[40] Vladimir E. Fortov and Gregor E. Morfill. *Complex and Dusty Plasmas: From Laboratory to Space*. CRC Press Taylor & Francis Group, 2009.

[41] D. A. Frank-Kamenezki. *Plasma–der vierte Aggregatzustand*. Verlag Progress, Moskau, 1963.

[42] Daan Frenkel and Berend Smit. *Understanding Molecular Simulation: From Algorithms to Applications*. Academic Press, second edition, 2001.

[43] W. J. Goedheer, V. Land, and J. Venema. Hydrodynamic and kinetic modelling of complex radio-frequency plasmas. *J. Phys. D: Appl. Phys.*, 42:194015, 2009.

[44] C. K. Goertz. Dusty plasmas in the solar system. *Rev. Geophys.*, 27:271–292, 1989.

[45] C. K. Goertz and G. E. Morfill. A model for the formation of spokes in saturn's ring. *Icarus*, 53:219 – 229, 1983.

[46] J. Goree, G. E. Morfill, V. N. Tsytovich, and S. V. Vladimirov. Theory of dust voids in plasmas. *Phys. Rev. E*, 59(6):7055–7067, 1999.

[47] A. Groisman and V. Steinberg. Elastic turbulence in a polymer solution flow. *Nature*, 405(6):53–55, May 2000.

[48] E. Grün and M. Landgraf. Fast dust in the heliosphere. *Space Science Reviews*, 99: 151–164, 2001. ISSN 0038-6308. 10.1023/A:1013888830386.

[49] E. Grün, C. K. Goertz, G. E. Morfill, and O. Havnes. Statistics of saturn's spokes. *Icarus*, 99:191–201, 1992.

[50] E. Grün, B. A. S. Gustafson, S. F. Dermott, and H. Fechtig, editors. *Interplanetary Dust*. Berlin: Springer, 2001.

[51] S. Hamaguchi and R. T. Farouki. Plasmaparticulate interactions in nonuniform plasmas with finite flows. *Phys. Rev. E*, 49(5):4430–4441, May 1994.

[52] S. Hamaguchi and R. T. Farouki. Polarization force on a charged particulate in a nonuniform plasma. *Phys. Plasmas*, 1(5):2110, May 1994.

[53] P. Hartmann, Z. Donkó, G. J. Kalman, S. Kyrkos, K. I. Golden, and M. Rosenberg. Collective dynamics of complex plasma bilayers. *Phys. Rev. Lett.*, 103(24):245002, Dec 2009.

[54] Peter Hartmann, Angela Douglass, Jorge C. Reyes, Lorin S. Matthews, Truell W. Hyde, Anikó Kovács, and Zoltán Donkó. Crystallization dynamics of a single layer complex plasma. *Phys. Rev. Lett.*, 105(11):115004, Sep 2010.

[55] O. Havnes, G. E. Morfill, and C. K. Goertz. Plasma potential and grain charges in a dust cloud embedded in a plasma. *J. Geophys. Res*, 89:10999, 1984.

[56] O. Havnes, T. Nitter, V. Tsytovich, G. E. Morfill, and T. Hartquist. On the thermophoretic force close to walls in dusty plasma experiments. *Plasma Sources Sci. Technol.*, 3:448–451, August 1994.

[57] O. Havnes, T. Aslaksen, T. W. Hartquist, F. Li, F. Melandsø, Morfill G. E., and Nitter T. Probing the properties of planetary ring dust by the observation of mach cones. *J. Geophys. Res.*, 100:1731, 1995.

[58] O. Havnes, F. Li, T. W. Hartquist, T. Aslaksen, and A. Brattli. Mach cones in dusty plasmas in planetary rings and in laboratory experiments. *Planet. Space Sci.*, 49: 223–229, 2001.

[59] Y. Hayashi and K. Tachibana. Observation of coulomb-crystal formation from carbon particles grown in a methane plasma. *Jpn. J. Appl. Phys.*, 33, 1994. L804-L8003.

[60] Dirk Helbing, Illés J. Farkas, and Tamás Vicsek. Freezing by heating in a driven mesoscopic system. *Phys. Rev. Lett.*, 84(6):1240–1243, Feb 2000.

[61] William G. Hoover. *Molecular Dynamics (Lecture Notes in Physics)*. Springer, 1986.

[62] M. Horányi. Charged dust dynamics in the solar system. *Ann. Rev. Astron. Astrophys.*,

34:383–418, September 1996.

[63] W. Hörmann and G. Derflinger. The acr method for generating normal random variables. *OR Spectrum*, 12:181–185, 1990. ISSN 0171-6468. 10.1007/BF01719718.

[64] L. J. Hou, Z. L. Mišković, A. Piel, and P. K. Shukla. Brownian dynamics of charged particles in a constant magnetic field. *Phys. Plasmas*, 16:053705, 2009.

[65] L.J. Hou, You-Nian Wang, and Z. L. Mišković. Theoretical study of laser-excited mach cones in dusty plasmas. *Phys. Rev. E*, 70(5):056406, Nov 2004.

[66] L.J. Hou, Y. N. Wang, and Z. L. Mišković. Formation and rotation of two-dimensional coulomb crystals in magnetized complex plasmas. *Phys. Plasmas*, 12, 2005.

[67] L.J. Hou, Z. L. Mišković, Alexander Piel, and Michael S. Murillo. Wave spectra of two-dimensional dusty plasma solids and liquids. *Phys. Rev. E*, 79(4):046412, Apr 2009.

[68] L.J. Hou, Alexander Piel, and P. K. Shukla. Self-diffusion in 2d dusty-plasma liquids: Numerical results. *Phys. Rev. Lett.*, 102:085002, 2009.

[69] J. D. Huba. NRL plasma formulary. Washington, 2009.

[70] I. H. Hutchinson. Ion collection by a sphere in a flowing plasma: 3. floating potential and drag force. *Plasma Physics and Controlled Fusion*, 47(1):71, 2005.

[71] A. V. Ivlev, S. K. Zhdanov, S. A. Khrapak, and G. E. Morfill. Ion drag force in dusty plasmas. *Plasma Phys. Control. Fusion*, 46(12B):B267–B279, 2004.

[72] A. V. Ivlev, S. K. Zhdanov, H. M. Thomas, and G. E. Morfill. Fluid phase separation in binary complex plasmas. *EPL (Europhysics Letters)*, 85(4):45001, 2009.

[73] G. M. Jellum and D. B. Graves. Particulates in aluminum sputtering discharges. *Journal of Applied Physics*, 67(10):6490 –6496, may 1990. ISSN 0021-8979.

[74] G. M. Jellum, J. E. Daugherty, and D. B. Graves. Particle thermophoresis in low pressure glow discharges. *J. Appl. Phys.*, 69(10):6923–6934, May 1991.

[75] K. Jiang, V. Nosenko, Y. F. Li, M. Schwabe, U. Konopka, A. V. Ivlev, V. E. Fortov, V. I. Molotkov, A. M. Lipaev, O. F. Petrov, M. V. Turin, H. M. Thomas, and G. E. Morfill. Mach cones in a three-dimensional complex plasma. *EPL*, 85:45002, 2009.

[76] Ke Jiang, L.J. Hou, You-Nian Wang, and Z. L. Mišković. Excitation of mach cones and energy dissipation by charged particles moving over two-dimensional strongly coupled dusty plasmas. *Phys. Rev. E*, 73(1):016404, Jan 2006.

[77] S. Katano and M. Iizumi. Crossover phenomenon in dynamical scaling of phase separation in fe-cr alloy. *Phys. Rev. Lett.*, 52(10):835–838, Mar 1984.

[78] V. M. Kendon, J-C. Desplat, P. Bladon, and M. E. Cates. 3d spinodal decomposition in the inertial regime. *Phys. Rev. Lett.*, 83(3):576–579, Jul 1999.

[79] S. Khrapak and G. E. Morfill. Basic processes in complex (dusty) plasmas: Charging, interactions, and ion drag force. *Contrib. Plasma Phys.*, 49:3:148 168, 2009.

[80] S. A. Khrapak, A. V. Ivlev, G. E. Morfill, and H. M. Thomas. Ion drag force in complex plasmas. *Phys. Rev. E*, 66(4):046414, Oct 2002.

[81] S. A. Khrapak, A. V. Ivlev, V. V. Yaroshenko, and G. E. Morfill. Influence of a polarization force on dust acoustic waves. *Phys. Rev. Lett.*, 102(24):245004, Jun 2009.

[82] B. Klumov, M. Rubin-Zuzic, and G. Morfill. Crystallization waves in a dusty plasma. *JETP Letters*, 84:542–546, 2007. ISSN 0021-3640. 10.1134/S0021364006220036.

[83] H. Kobayashi, K. Maeda, and M. Izawa. Behavior of particles reflected by turbo molecular pump in plasma etching apparatus. *Semiconductor Manufacturing, IEEE Transactions on*, 22(4):462–467, Nov. 2009. ISSN 0894-6507.

[84] R. Koningsveld, W. H. Stockmayer, J. W. Kennedy, and L. A. Kleintjens. Liquid-liquid phase separation in multicomponent polymer systems. xi. dilute and concentrated polymer solutions in equilibrium. *Macromolecules*, 7(1):73–79, 1974.

[85] U. Konopka. *Wechselwirkungen geladener Staubteilchen in Hochfrequenzplasmen*. PhD thesis, Ruhr-Universitt-Bochum, 7 2000.

[86] U. Konopka, G.E. Morfill, and L. Ratke. Measurement of the interaction potential of microspheres in the sheath of a rf discharge. *Phys. rev. Lett.*, 84(5):891–894, 2000.

[87] U. Konopka, D. Samsonov, A. V. Ivlev, J. Goree, V. Steinberg, and G. E. Morfill. Rigid and differential plasma crystal rotation induced by magnetic fields. *Phys. Rev. E*, 61(2):1890–1898, 2000.

[88] V.F. Kovalev, K.I. Popov, V.Y. Bychenkov, and W. Rozmus. Laser triggered coulomb explosion of nanoscale symmetric targets. *Phys. Plasma*, 14:053103, 2007.

[89] Y. Kurimoto, N. Matsuda, G. Uchida, S. Iizuka, M. Suemitsu, and N. Sato. Fine particle removal by a negatively-charged fine particle collector in silane plasma. *Thin Solid Films*, 457:285, 2004.

[90] J. G. Lafromboise and L. W. Parker. Probe design for orbit-limited current collection. *Phys. Fluids*, 16:629, 1973.

[91] M. Lampe. Limits of validity for orbital-motion-limited theory for a small floating collector. *Journal of Plasma Physics*, 65:3:171–180, 2001.

[92] M. Lampe, G. Joyce, and G. Ganguli. Interactions between dust grains in a dusty plasma. *Phys. Plasmas*, 7(10):3851–3861, 2000.

[93] Victor Land, Lorin S. Matthews, Truell W. Hyde, and Diana Bolser. Fluid modeling of void closure in microgravity noble gas complex plasmas. *Phys. Rev. E*, 81(5): 056402, May 2010.

[94] Irving Langmuir. Positive ion currents from the positive column of mercury arcs. *Science*, 58:290–291, 1923.

[95] Don Stephen Lemons. *An Introduction to Stochastic Processes*. John Hopkins Uni-

versity Press, 2002.

[96] Mirjam E. Leunissen, Christina G. Christova, Antti-Pekka Hynninen, C. Patrick Royall, Andrew I. Campbell, Arnout Imhof, Marjolein Dijkstra, René van Roij, and Alfons van Blaaderen. Ionic colloidal crystals of oppositely charged particles. *Nature*, 437:235, 2005.

[97] Y. Li, U. Konopka, Ke Jiang, T. Shimizu, H. Höfner, H. M. Thomas, and G. E. Morfill. Removing dust particles from a large area discharge. *Appl. Phys. Lett.*, 94: 081502, 2009.

[98] David R. Lide, editor. *CRC Handbook on Chemistry and Physics*. Taylor and Francis Group, LLC, 90th (internet version 2010) edition, 2010.

[99] I. M. Lifshitz and V. V. Slyozov. The kinetics of precipitation from supersaturated solid solutions. *Journal of Physics and Chemistry of Solids*, 19(1-2):35 – 50, 1961. ISSN 0022-3697.

[100] B. Liu, J. Goree, and V. Nosenko. Radiation pressure and gas drag forces on a melamine-formaldehyde microsphere in a dusty plasma. *Phys. Plasmas*, 10(1):9–20, 2003.

[101] Hartmut Löwen. Particle-resolved instabilities in colloidal dispersions. *Soft Matter*, 6:3133 – 3142, 2010.

[102] Z. W. Ma and A. Bhattacharjee. Molecular dynamics simulations of mach cones in two-dimensional yukawa crystals. *Phys. Plasmas*, 9:3349, 2002.

[103] A. A. Mamun, P. K. Shukla, and R. Bingham. Plasma voids (holes) in a dusty plasma. *Phys. Lett. A*, 298:179–184, 2002.

[104] A. A. Mamun, P. K. Shukla, and G. E. Morfill. Theory of mach cones in magnetized dusty plasmas with strongly correlated charged dust grains. *Phys. Rev. Lett.*, 92(9): 095005, Mar 2004.

[105] T. Matsoukas and M. Russell. Fokker-planck description of particle charging in ionized gases. *Phys. Rev. E*, 55(1):991–994, Jan 1997.

[106] A. Melzer, T. Trottenberg, and A. Piel. Experimental determination of the charges on dust particles forming coulomb lattices. *Phys. Lett. A*, 191:301–308, 1994.

[107] A. Melzer, S. Nunomura, D. Samsonov, Z. W. Ma, and J. Goree. Laser-excited mach cones in a dusty plasma crystal. *Phys. Rev. E*, 62:4162 – 4176, 2000.

[108] R. L. Merlino and J. A. Goree. Dusty plasmas in the laboratory, industry, and space. *Phys. Today*, 57:32–39, 2004.

[109] N. Meyer-Vernet. The flip-flop of electric potential of dust grains in space. *Astronomy and Astrophysics*, 105:98, 1982.

[110] M. Mikikian and L. Boufendi. Experimental investigations of void dynamics in a dusty discharge. *Phys. Plasmas*, 11(8):3733–3737, 2004.

[111] W. J. Miloch, J. Trulsen, and H. L. Pcseli. Numerical studies of ion focusing behind macroscopic obstacles in a supersonic plasma flow. *Phys. Rev. E*, 77:056408, 2008.

[112] W. J. Miloch, S. V. Vladimirov, H. L. Pcseli, and J. Trulsen. Numerical simulations of potential distribution for elongated insulating dust being charged by drifting plasmas. *Phys. Rev. E*, 78:036411, 2008.

[113] C. J. Mitchell, M. Horányi, O. Havnes, and C. C. Porco. Saturn's spokes: Lost and found. *Science*, 311:1587, 2006.

[114] Yoshinori Momonoi, Kenetsu Yokogawa, and Masaru Izawa. Dry cleaning technique for particle removal based on gas-flow and down-flow plasma. *Journal of Vacuum Science Technology B: Microelectronics and Nanometer Structures*, 22(1):268 –274, jan. 2004. ISSN 1071-1023.

[115] G. E. Morfill, A. V. Ivlev, and J. R. Jokipii. Charge fluctuation instability of the dust lattice wave. *Phys. Rev. Lett.*, 83(5):971–974, Aug 1999.

[116] G. E. Morfill, H. M. Thomas, U. Konopka, H. Rothermel, M. Zuzic, A. Ivlev, and J. Goree. Condensed plasmas under microgravity. *Phys. Rev. Lett.*, 83:1598–1601, 8 1999.

[117] G. E. Morfill, C. Räth, Y-F. Li, J. S. Hu, B. L. Ling, X. Gao, and M. Horányi. Dust capture experiment in ht-7. *New Journal of Physics*, 11(11):113041, 2009.

[118] Gregor E. Morfill and Alexei V. Ivlev. Complex plasmas: An interdisciplinary research field. *Rev. Mod. Phys.*, 81(4):1353–1404, Oct 2009.

[119] Gregor E Morfill, Uwe Konopka, Michael Kretschmer, Milenko Rubin-Zuzic, Hubertus M. Thomas, Sergej K. Zhdanov, and Vadim Tsytovich. The classical tunnelling effect?- observations and theory. *New J. Phys.*, 8:7, 2006.

[120] H. Mott-Smith and I. Langmuir. The theory of collectors in gaseous discharges. *Phys. Rev.*, 28:727–763, 1926.

[121] W. H. Munk, P. Scully-Power, and F. Zachariasen. Ships from space. *Proceedings of The Royal Society of London, Series A: Mathematical and Physical Sciences*, 412(1843):231–254, 1987.

[122] A. P. Nefedov, O. F. Petrov, V. I. Molotkov, and V. E. Fortov. Formation of liquidlike and crystalline structures in dusty plasmas. *JETP Letters*, 72:218–226, 2000.

[123] R. R. Netz. Conduction and diffusion in two-dimensional electrolytes. *Europhys. Lett.*, 63 (4):616–622, 2003.

[124] T. Nitter. Levitation of dust in rf and dc glow discharges. *Plasma Sources Sci. Technol.*, 5(1):93–111, February 1996.

[125] V. Nosenko, J. Goree, Z. W. Ma, and A. Piel. Observation of shear-wave mach cones in a 2d dusty-plasma crystal. *Phys. Rev. Lett.*, 88(13):135001, Mar 2002.

[126] V. Nosenko, J. Goree, Z. W. Ma, D. H. E. Dubin, and A. Piel. Compressional and

shear wakes in a two-dimensional dusty plasma crystal. *Phys. Rev. E*, 68(5):056409, Nov 2003.

[127] V. Nosenko, J. Goree, and A. Piel. Laser method of heating monolayer dusty plasmas. *Phys. Plasmas*, 13:032106, 2006.

[128] V. Nosenko, S. Zhdanov, A. V. Ivlev, G. E. Morfill, J. Goree, and A. Piel. Heat transport in a two-dimensional complex (dusty) plasma at melting conditions. *Phys. Rev. Lett.*, 100:025003, 2008.

[129] John F. O'Hanlon, J. Kang, L. K. Russell, and L. Hong. The effects of electrostatic, molecular drag and gravitationalforces on the behavior of particle clouds in an rf discharge. *IEEE Trans. Plasma Sci.*, 22:122, 1994.

[130] Alexander Piel. *Plasma Physics-An Introduction to Laboratory, Space and Fusion Plasmas*. Springer, 2010.

[131] Dennis Rapaport. *The Art of Molecular Dynamics Simulation*. Cambridge University Press, second edition, 2004.

[132] Christoph Räth, Wolfram Bunk, Markus B. Huber, Gregor E. Morfill, Jörg Retzlaff, and Peter Schuecker. Analysing large-scale structure -I. Weighted scaling indices and constrained randomization. *Monthly Notices of the Royal Astronomical Society*, 337: 413–421, 2002.

[133] M. Rex and H. Löwen. Influence of hydrodynamic interactionson lane formation in oppositely charged driven colloids. *European Physical Journal E*, 26:143–150, 2008.

[134] S. Rosanvallon, C. Grisolia, P. Delaporte, J. Worms, F. Onofri, S.H. Hong, G. Counsell, and J. Winter. Dust in iter: Diagnostics and removal techniques. *Journal of Nuclear Materials*, 386-388:882 – 883, 2009. ISSN 0022-3115. Fusion Reactor Materials, Proceedings of the Thirteenth International Conference on Fusion Reactor Materials.

[135] M. Rosenberg and D. A. Mendis. Use of UV to reduce particle trapping in process plasmas. *IEEE transactions on plasma science*, 24:1133, 1996.

[136] H. Rothermel, T. Hagl, G. E. Morfill, M. H. Thoma, and H. M. Thomas. Gravity compensation in complex plasmas by application of a temperature gradient. *Phys. Rev. Lett.*, 89(17):175001, 2002.

[137] D. Samsonov, J. Goree, Z. W. Ma, A. Bhattacharjee, H. M. Thomas, and G. E. Morfill. Mach cones in a coulomb lattice and a dusty plasma. *Phys. Rev. Lett.*, 83 (18):3649–3652, Nov 1999.

[138] D. Samsonov, J. Goree, H. M. Thomas, and G. E. Morfill. Mach cone shocks in a two-dimensional yukawa solid using a complex plasma. *Phys. Rev. E*, 61(5):5557–5572, May 2000.

[139] N. Sato, G. Uchida, and S. Iizuka. Ivth european workshop on dusty and colloidal plasmas, portugal. 2000.

[140] N. Sato, G. Uchida, T. Kaneko, S. Shimizu, and S. Iizuka. Dynamics of fine particles in magnetized plasmas. *Physics of Plasmas*, 8:1786, 2001.

[141] B. Schmittmann and R. K. P. Zia. Driven diffusive systems. an introduction and recent developments. *Physics Reports*, 301(1-3):45 – 64, 1998. ISSN 0370-1573.

[142] Wilfried Schröder. Otto jesse and the investigation of noctilucent clouds 115 years ago. *Bulletin of the American Meteorological Society*, 82(11):2457–2468, 2001.

[143] G. S. Selwyn, J. Singh, and R. S. Bennett. In situ laser diagnostic studies of plasma-generated particulate contamination. *J. Vac. Sci. Technol. A*, 7:2758 – 2765, 1989.

[144] Gary S. Selwyn, J. S. McKillop, Kurt L. Haller, and J. J. Wu. In situ contamination measurements by hene laser light scattering: A case study. *J. Vac. Sci. Technol. A*, 8:1726, 1990.

[145] Gary S. Selwyn, John E. Heidenreich, and Kurt L. Haller. Rastered laser light scattering studies during plasma processing: Particle contamination trapping phenomena. *J. Vac. Sci. Technol. A*, 9:2817–2824, 1991.

[146] Heru Setyawan, Manabu Shimada, Yutaka Hayashi, and Kikuo Okuyama. Removal of particles during plasma processes using a collector based on the properties of particles suspended in the plasma. *Journal of Vacuum Science Technology A: Vacuum, Surfaces, and Films*, 23(3):388 –393, may. 2005. ISSN 0734-2101.

[147] T. E. Sheridan. Monte carlo study of melting in a finite two-dimensional dusty plasma. *Phys. Plasmas*, 16:083705, 2009.

[148] S. Shimizu, B. Klumov, T. Shimizu, H. Rothermel, O. Havnes, H. M. Thomas, and G. E. Morfill. Synthesis of water ice particles in a plasma chamber. *Journal of Geophysical Research*, 115, 2010.

[149] T. Shimizu, W. Jacob, H. Thomas, G. E. Morfill, T. Abe, Y. Watanabe, and N. Sato. Particle growth in hydrogenmethane plasmas. *Thin Solid Films*, 506-507:652–655, 2006.

[150] P. K. Shukla. Shielding of a slowly moving test charge in dusty plasmas. *Phys. Plasmas*, 1:1362, 1994.

[151] P. K. Shukla and B. Eliasson. Colloquium: Fundamentals of dust-plasma interactions. *Rev. Mod. Phys.*, 81:25, 2009.

[152] P. K. Shukla and A. A. Mamun. *Introduction to Dusty Plasma Physics*. Institute of Physics Publishing, Bristol and Philadelphia, 2002.

[153] Eric D. Siggia. Late stages of spinodal decomposition in binary mixtures. *Phys. Rev. A*, 20(2):595–605, Aug 1979.

[154] R. D. Smirnov, S. I. Krasheninnikov, J. H. Yu, A. Yu Pigarov, M. Rosenberg, and J. L. Terry. On visibility of carbon dust particles in fusion plasmas with fast framing cameras. *Plasma Phys. Control. Fusion*, 51:055017, 2009.

[155] Bradford A. Smith, Laurence Soderblom, Reta Beebe, Joseph Boyce, Geoffery Briggs, Anne Bunker, Stewart A. Collins, Candice J. Hansen, Torrence V. Johnson, Jim L. Mitchell, Richard J. Terrile, Michael Carr, Allen F. Cook, Jeffrey Cuzzi, James B. Pollack, G. Edward Danielson, Andrew Ingersoll, Merton E. Davies, Garry E. Hunt, Harold Masursky, Eugene Shoemaker, David Morrison, Tobias Owen, Carl Sagan, Joseph Veverka, Robert Strom, and Verner E. Suomi. Encounter with saturn: Voyager 1 imaging science results. *Science, New Series*, 212:163 – 191, 1981.

[156] Bradford A. Smith, Laurence Soderblom, Raymond Batson, Patricia Bridges, Jay Inge, Harold Masursky, Eugene Shoemaker, Reta Beebe, Joseph Boyce, Geoffrey Briggs, Anne Bunker, Stewart A. Collins, Candice J. Hansen, Torrence V. Johnson, Jim L. Mitchell, Richard J. Terrile, Allan F. Cook, Jeffrey Cuzzi, James B. Pollack, G. Edward Danielson, Andrew P. Ingersoll, Merton E. Davies, Garry E. Hunt, David Morrison, Tobias Owen, Carl Sagan, Joseph Veverka, Robert Strom, and Verner E. Suomi. A new look at the saturn system: The voyager 2 images. *Science, New Series*, 215:504–537, 1982.

[157] A. Sodha and S. Guha. Physics of colloidal plasmas. *Advances in Plasma Physics*, 4:219, 1971.

[158] Kenneth G. Spears, Timothy J. Robinson, and Richard M. Roth. Particle distributions and laser-particle interactions in an rf discharge of silane. *Plasma Science, IEEE Transactions on*, 14(2):179 –187, april 1986. ISSN 0093-3813.

[159] L. Spitzer. *Diffuse Matter in Space*. Wiley, 1968.

[160] K. R. Sütterlin. *Physics of Complex Plasmas: Some fundamental problems*. PhD thesis, Ludwig-Maximilians-Universität, 2010.

[161] K. R. Sütterlin, A. Wysocki, A. V. Ivlev, C. Räth, H. M. Thomas, M. Rubin-Zuzic, W. J. Goedheer, V. E. Fortov, A. M. Lipaev, V. I. Molotkov, O. F. Petrov, G. E. Morfill, and H. Löwen. Dynamics of lane formation in driven binary complex plasmas. *Phys. Rev. Lett.*, 102(8):085003, Feb 2009.

[162] K. R. Sütterlin, H. M. Thomas, A. V. Ivlev, G. E. Morfill, V. E. Fortov, A. M. Lipaev, V. I. Molotkov, O. F. Petrov, A. Wysocki, and H. Löwen. Lane formation in driven binary complex plasmas on the international space station. *IEEE Transactions on Plasma Science*, 38(4):861–868, apr. 2010. ISSN 0093-3813.

[163] L. Talbot, R. K. Cheng, R. W. Schefer, and D. R. Willis. Thermophoresis of particles in a heated boundary layer. *J. Fluid Mech.*, 101:737–758, 1980.

[164] H. Thomas, G. E. Morfill, V. Demmel, J. Goree, B. Feuerbacher, and D. Möhlmann. Plasma crystal: Coulomb crystallization in a dusty plasma. *Phys. Rev. Lett.*, 73(5): 652–655, Aug 1994.

[165] H. M. Thomas and G. E. Morfill. Melting dynamics of a plasma crystal. *Nature*, 379:806–809, 1996.

[166] H. M. Thomas, G. E. Morfill, V. E. Fortov, A. V. Ivlev, V. I. Molotkov, A. M.

Lipaev, T. Hagl, H. Rothermel, S. A. Khrapak, K. R. Sütterlin, M. Rubin-Zuzic, O. F. Petrov, V. I. Tokarev, and S. K. Krikalev. Complex plasma laboratory pk-3 plus on the international space station. *New J. Phys.*, 10:033036, 2008.

[167] Lewi Tonks and Irving Langmuir. Oscillations in ionized gases. *Phys. Rev.*, 33(2): 195–210, Feb 1929.

[168] V. Tsytovich, G. E. Morfill, S. Vladimirov, and H. Thomas. *Elementary Physics of Complex Plasmas*. Springer, New York, 2008.

[169] Vadim N. Tsytovich. Dust plasma crystals, drops, and clouds. *Phys.-Usp.*, 40:53 – 94, 1997.

[170] Vadim N. Tsytovich and J. Winter. On the role of dust in fusion devices. *Phys.-Usp.*, 41:815–822, 1998.

[171] W. F. van Gunsteren and H. J. C. Berendsen. Algorithms for brownian dynamics. *Molecular Physics*, 45:637 – 647, 1982.

[172] Frank Verheest. *Waves In Dusty Space Plasmas*. Dordrecht: Kluwer Academic, 2000.

[173] Xiaogang Wang, A. Bhattacharjee, and S. Hu. Longitudinal and transverse waves in yukawa crystals. *Phys. Rev. Lett.*, 86(12):2569–2572, Mar 2001.

[174] Y. Watanabe, M. Shiratani, Y. Kubo, I. Ogawa, and S. Ogi. Effects of low-frequency modulation on rf discharge chemical vapor deposition. *Appl. Phys. Lett.*, 53:1263, 1988.

[175] S. J. Weidenschilling. *Protostars and Planets III*. Univ. Arizona Press, Tucson, 1993.

[176] E. C. Whipple. Potentials of surfaces in space. *Reports on Progress in Physics*, 44 (11):1197, 1981.

[177] Henry Smith William. *A History of Science*. Kessinger, 2004.

[178] J. Winter. Dust in fusion devices - experimental evidence, possible sources and consequences. *Plasma Phys. Control. Fusion*, 40:1201–1210, 1998.

[179] A. Wysocki, C. Räth, A. V. Ivlev, K. R. Sütterlin, H. M. Thomas, S. Khrapak, S. Zhdanov, V. E. Fortov, A. M. Lipaev, V. I. Molotkov, O. F. Petrov, H. Löwen, and G. E. Morfill. Kinetics of fluid demixing in complex plasmas: Role of two-scale interactions. *Phys. Rev. Lett.*, 105(4):045001, Jul 2010.

[180] S. K. Zhdanov, G. E. Morfill, D. Samsonov, M. Zuzic, and O. Havnes. Origin of the curved nature of mach cone wings in complex plasmas. *Phys. Rev. E*, 69(2):026407, Feb 2004.

[181] X. H. Zheng and J. C. Earnshaw. Plasma-dust crystals and brownian motion. *Phys. Rev. Lett.*, 75(23):4214–4217, Dec 1995.

Publication list

Publications on refereed journals. Nr.1-7 are the research done during PhD study in Max-Planck-Institute for Extraterrestrial Physics. Nr.8-12 are the research done before PhD study.

1. **Ke Jiang**, L.-J. Hou, A. V. Ivlev, Y.-F. Li, C.-R. Du, H. M. Thomas, G. E. Morfill, and K. R. Sütterlin, *Initial stages in phase separation of binary complex plasmas: Numerical experiments*, Europhysics Letters 93, 55001 (2011).

2. **Ke Jiang**, C.-R. Du, K. R. Sütterlin, A. V. Ivlev, and G. E. Morfill, *Lane formation in binary complex plasmas: Role of non-additive interactions and initial configurations*, Europhysics Letters 92, 65002 (2010).

3. **Ke Jiang**, L.-J. Hou, A. V. Ivlev, Y.-F. Li, K. R. Sütterlin, H. M. Thomas, and G. E. Morfill, *Demixing in Binary Complex Plasma: Computer Simulation*, accepted by IEEE at May 1, 2011.

4. Yangfang Li, Wen-gui Zhang, J. X. Ma, **Ke Jiang**, H. M. Thomas, and G. E. Morfill, *Traveling electric field probed by a fine particle above voltage-modulated strips in a striped electrode device*, Phys. Plasmas 17, 033705 (2010).

5. **Ke Jiang**, V. Nosenko, Y.-F. Li, M. Schwabe, U. Konopka, A. V. Ivlev, V. E. Fortov, V. I. Molotkov, A. M. Lipaev, O. F. Petrov, M. V. Turin, H. M. Thomas and G. E. Morfill, *Mach cones in a Three Dimensional Complex Plasma*, Europhysics Letters, 85, 45002 (2009).

6. **Ke Jiang**, Y.-F. Li, T. Shimizu, U. Konopka, H. M. Thomas, and G. E. Morfill, *Controlled particle transport in a plasma chamber with striped electrode*, Phys. Plasmas 16, 123702 (2009).

7. Y.-F. Li, U. Konokpa, **Ke Jiang**, T. Shimizu, H. Höfner, H. M. Thomas, and G. E. Morfill, *Removing dust particles from a large area discharge*, Applied Physics Letters 94, 081502 (2009).

8. **Ke Jiang**, Yuan-Hong Song, and You-Nian Wang, *Theoretical study of the wave dispersion relation for a two-dimensional strongly coupled Yukawa system in a magnetic field*, Phys. Plasmas 14, 103708 (2007).

9. **Ke Jiang**, Lu-Jing Hou, Xiang Xu, and You-Nian Wang, *Waves and wakes excited by a moving disturbance in a 2D magnetized dusty plasma*, New Journal of Physics 9, 57, (2007).

10. Lu-Jing Hou, Z. L. Miskŏvić, **Ke Jiang**, and You-Nian Wang, *Energy Loss of a Charged Particle Moving over a 2D Strongly Coupled Dusty Plasma*, Phys. Rev. Lett. 96, 255005 (2006).

11. **Ke Jiang**, Lu-Jing Hou, You-Nian Wang and Z. L. Miskŏvić, *Excitation of Mach cones and energy dissipation by charged particles moving over two-dimensional strongly coupled dusty plasmas*, Phys. Rev. E 73, 016404 (2006).

12. **Ke Jiang**, Lu-Jing Hou, and You-Nian Wang, *Interactions of a Projectile Charge with Two-Dimensional Dusty Plasmas*, Chinese Phys. Lett. 22, 1713 (2005).

Curriculum Vitae

Ke Jiang

Gender: male
Birthday: 23. June 1981
Birthplace: Dalian, China
Home address: Gerhart-Hauptmann-Ring 3, 81737 Munich, Germany
Telephone: +49-89-300003011
Email(work): jiang@mpe.mpg.de
Email(personal): dustyplasma@gmail.com

Education

07/2007 - 08-2011	Theory and Complex Plasma group Max-Planck-Institute for Extraterrestrial Physics, Germany Ludwig-Maximilians-University (LMU), Germany **PhD in Physics** Majoring in Physics (Supervisor: Prof. Gregor Morfill)
09/2004 - 01/2007	Department of Physics Dalian University of Technology, P. R. China **Master of Science** Majoring in Plasma Physics (Supervisor: Prof. Younian Wang)
09/2000 - 08/2004	Department of Physics Dalian University of Technology, P. R. China **Bachelor of Engineering** Majoring in Electronic Science and Technology

Enclosed papers

This cumulative thesis consists of six papers, which are reprinted below with permission from American Institute of Physics (AIP), Institute of Physics (IOP), and Institute of Electrical and Electronic Engineers (IEEE).

1. K. Jiang, Y.-F. Li, T. Shimizu, U. Konopka, H. M. Thomas, and G. E. Morfill, *Controlled particle transport in a plasma chamber with striped electrode*, Phys. Plasmas 16, 123702 (2009).
   Reprinted with permission from [K. Jiang et al Phys. Plasmas 16, 123702 (2009)]. Copyright [2009], American Institute of Physics.

2. Y.-F. Li, U. Konokpa, K. Jiang, T. Shimizu, H. Höfner, H. M. Thomas, and G. E. Morfill, *Removing dust particles from a large area discharge*, Applied Physics Letters 94, 081502 (2009).
   Reprinted with permission from [Y.-F. Li *et al.* Applied Physics Letters 94, 081502 (2009)]. Copyright [2009], American Institute of Physics.

3. Ke Jiang, L.-J. Hou, A. V. Ivlev, Y.-F. Li, C.-R. Du, H. M. Thomas, G. E. Morfill, and K. R. Sütterlin, *Initial stages in phase separation of binary complex plasmas: Numerical experiments*, Europhysics Letters 93, 55001 (2011). Copyright: IOP.

4. K. Jiang, L.-J. Hou, A. V. Ivlev, Y.-F. Li, K. R. Sütterlin, H. M. Thomas, and G. E. Morfill, *Demixing in Binary Complex Plasma: Computer Simulation*, accepted by IEEE Transactions on Plasma Science (2011). Copyright: IEEE.

5. K. Jiang, C.-R. Du, K. R. Sütterlin, A. V. Ivlev, and G. E. Morfill, *Lane formation in binary complex plasmas: Role of non-additive interactions and initial configurations*, Europhysics Letters 92, 65002 (2010). Copyright: IOP.

6. K. Jiang, V. Nosenko, Y.-F. Li, M. Schwabe, U. Konopka, A. V. Ivlev, V. E. Fortov, V. I. Molotkov, A. M. Lipaev, O. F. Petrov, M. V. Turin, H. M. Thomas and G. E. Morfill, *Mach cones in a three dimensional complex plasma*, Europhysics Letters, 85, 45002 (2009). Copyright: IOP.

Controlled particle transport in a plasma chamber with striped electrode

Ke Jiang, Yang-fang Li, T. Shimizu, U. Konopka, H. M. Thomas, and G. E. Morfill
Max-Planck-Institute for Extraterrestrial Physics, 85748 Garching, Germany

(Received 16 September 2009; accepted 19 November 2009; published online 9 December 2009)

The controlled transport of micrometer size dust particles in a parallel-plate radio frequency discharge has been investigated. The lower stainless steel electrode consisted of 100 independently controllable electrical metal stripes. The voltage signals on these stripes were modulated, causing traveling plasma sheath distortions. Because the particles trapped in local potential wells moved according to the direction of the distortion, the transport velocity could be actively controlled by adjusting frequencies and phase shifts of the applied periodic voltage signals. To investigate the detailed principle of this transport, molecular dynamic simulations was performed to reproduce the observations with the plasma background conditions calculated by separated particle-in-cell simulations for the experimental parameters. The findings will help develop novel technologies for investigating large-scale complex plasma systems and techniques for achieving clean environments in plasma processing reactors. © *2009 American Institute of Physics*. [doi:10.1063/1.3273074]

I. INTRODUCTION

Dust particles are notorious in plasma-assisted material processing because they introduce defects into the final products. The formation of the dust particles was observed in several plasma processes, such as etching, sputtering, or thin film deposition.[1–7] Spears *et al.*[1] found that a silane plasma was contaminated by micron-sized particles visualized using laser light scattering. Subsequently it was reported by Watanabe[2] that in plasma enhanced chemical vapor deposition dust particles grown *in situ* may increase the deposition time and decrease the quality of the silicon film. Particles were also observed in etching[3,4] and sputtering processes,[5,6] as well as in nuclear fusion devices.[7] In general the dust particles immersed in a laboratory plasma are usually negatively charged and therefore trapped typically in the plasma sheath. The removal of these particles is a major technological challenge.[8]

There are several methods for removing dust particles from processing plasmas:[6,9–13] by manipulating various forces acting on them, such as gravitational force, Coulomb force, ion drag force, neutral drag force, thermophoretic force, as well as laser radiation pressure force.[8] In Ref. 10, for example, it is shown that fine particles with a diameter more than 10 nm in a silane plasma can be dramatically reduced by using a so-called negatively charged fine particle collector, which influences the local static electric fields by a hollow cathode secondary plasma. O'Hanlon and co-workers[11] showed theoretically and experimentally that the neutral drag force induced by a directed gas flow can be strong enough to remove particles from their trap locations. Other approaches are also based on localized secondary plasmas[12] or the thermopheretic force[6] to drive the dust particles. Large scale electrodes—those with an area exceeding a square meter—pose a technological challenge, however, because of the difficulty in moving dust particles from the center of the device to the edges.

In a recent experiment,[13] we demonstrated the use of "traveling plasma distortions"—a plasma potential profile that propagates in space—to transport fine particles over large distances. In this paper, we discuss detailed follow up experiments and related simulations of dust transport based on traveling plasma potential traps produced by a striped electrode (SE) in a capacitively coupled rf plasma chamber. We applied oscillating signals to all stripes with individual phase shifts to establish a wavelike plasma distortion in the lower sheath region. As a result, particles were transported individually or in clouds according to the wave direction. To investigate the detailed principal aspects of the transport, we compare the observation with molecular dynamic (MD) simulations supported by particle-in-cell (PIC) simulations with a background plasma description.

II. EXPERIMENTS ON CONTROLLED PARTICLE TRANSPORT

The experiments were carried out in a modified parallel-plate plasma chamber with an inner diameter of 80 cm and a height of 40 cm (a sketch for the device is provided in Fig. 1). The chamber contains two square shaped horizontal electrodes of 52×52 cm^2. The upper powered electrode, which we refer to as "PE", connected to a 13.56 MHz rf generator through a matching unit, has a frame shape structure with three 48×16 cm^2 openings to allow access from the top. The lower electrode, which we refer to as the "SE," consists of 100 electrically insulated stainless steel stripes of 0.5×50 cm^2. The stripes of the lower electrode are connected individually to a 100 channel function generator, which enables us to choose waveforms, frequencies, dc biases, amplitudes, and phase angles for each stripe independently. The two electrodes are separated by 5 cm. A capacitively coupled plasma is generated in argon at constant gas flow rate and working gas pressure maintained by a mass flow and a pressure controller, respectively. For plasma diagnostic purpose, we introduced a rf compensated Langmuir probe (LP) (Hiden ESPion Advanced Langmuir Probe). Microsized particles were dropped into the plasma from a dust dispenser mounted above the top electrode. A laser sheet

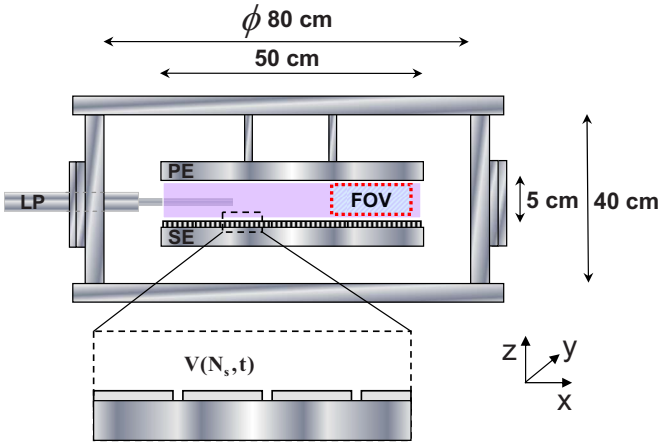

FIG. 1. (Color online) Sketch of our experimental setup. The modified parallel-plate chamber has an upper PE and a lower SE. The stainless steel stripes are connected independently to a multichannel function generator with signal $V(N_s,t)$. The plasma parameters were diagnosed by LP.

(central wavelength 680 nm, power 200 mW) is aligned perpendicular to the electrode. The laser light is scattered by particles between the electrodes. To obtain particle positions, a camera (Basler A404 k) equipped with an interference filter and macrolens (Nikon AF 85 mm f/1.4 D IF) is connected to a digital video capture card (DVR Express CLFC) which is used to record this scattered light so that the particle positions could be revealed at up to 96 frames/s in a field of view (FOV) of 10.1×7.4 cm^2 within the laser sheet. For further reference we define the camera's pointing position vector to be the y axis and the directions horizontal and vertical within the FOV to be x and z, respectively (see Fig. 1).

In this experiment, we use an argon gas flow of 2 SCCM (SCCM denotes cubic centimeter per minute at STP) at a working pressure of 28 Pa. The plasma is sustained by adjusting the output power of the rf generator at 30 W corresponding to the measured peak-to-peak voltage of 52 V at the upper electrode. The plasma parameters were measured to be $T_e\approx3$ eV for the electron temperature and $n_0\approx6\times10^8$ cm^{-3} for the plasma density. The plasma potential was measured to be 22 V at the center of the discharge, 2 cm above the SE. Monodisperse spheres with a diameter of 17 μm and a mass of $m_d=3.06\times10^{-9}$ g were used as particles. Sinusoidal signals, described by

$$V(N_s,t) = V_{\text{bias}} + V_a \sin(2\pi f \times t + N_s \times \delta\phi), \tag{1}$$

were applied to the stripes, where N_s is the stripe number, f is the frequency, V_{bias} is the bias voltage (fixed at -15 V for this study), V_a is the amplitude of the sinusoidal signal, and $\delta\phi$ is the fixed phase shift between neighboring stripes.

Controlled particle transport was achieved by adjusting different parameters of the signals. We first investigated the positions of particles in 400 consecutive frames (8 s with 50 frames/s recording). Here only the particle positions along the x axis are discussed because we found that the vertical movement along z was negligibly small. Note that two parallel insulated plates separated by a distance of 5 cm in the y direction were placed along x for particle confinement. A morphological image processing was performed to determine particle positions. Repeating this procedure for all the recorded frames, a set of particle positions versus time was obtained from each event.

In Figs. 2(a)–2(c), particle transport with different V_a are shown. In Fig. 2(a), when V_a is 1 V, the horizontal electric field is not strong enough to move particles, resulting in local particle oscillation. When V_a is increased to 2 V, we found three different behaviors of the particles, as shown in Fig. 2(b). One is the constant particle transport along x due to the increase in the horizontal electric driving force. The second is the particle oscillation, similar to that in Fig. 2(a). The third is a combination of the constant transport and local oscillation. The transport is achieved by creating local potential distortions as in Ref. 13. With V_a increased to 5 V, the horizontal electric field is strong enough to trap all the particles and transport them with a constant velocity, as shown in Fig. 2(c). In these experiments $\delta\phi=\pi/3$, $f=0.2$ Hz were kept constant.

Next, the dependencies of the particle transport on f and $\delta\phi$ were examined with V_a fixed at 13 V (well above the 5 V necessary to "trap" particles according to Fig. 2). The particle behavior with different f are shown in Figs. 3(a)–3(c). In this series, $\delta\phi$ was kept constant at $\pi/6$. In Fig. 3(a), the particles are well confined and follow the moving distortion. As f increases, the particles cannot respond (f has to be much less than dust plasma frequency) and consequently are partially trapped. However, the speed of particle transport increases, as shown in Figs. 3(b) and 3(c). Still higher f results in less trapping efficiency of the particles and oscillations as expected. A similar phenomenon is seen when $\delta\phi$ is changed with fixed f at 0.5 Hz, as shown in Figs. 3(d)–3(f). In this case, as $\delta\phi$ increases, the transport velocity decreases but more particles are trapped in the potential wells. In summary, for a given particle size, higher transport velocity requires higher f and smaller $\delta\phi$. However, the trapping of the particles is disturbed if f becomes too large and $\delta\phi$ too small. In order to transport particles efficiently, the velocity of the plasma distortions must be high and the particles must be trapped in the potential wells. To achieve this, three parameters—V_a, f, and $\delta\phi$—can be "designed." In "normal industry" situation, we have to deal with grown particles of a size distribution. By selecting a particular f, we can remove smaller grown particles effectively. The "design criterion" is therefore to affect transport in a short time compared to the growth time.

III. SIMULATIONS

In this part, we aim to reproduce the experimental findings by a numerical simulation. The challenge for a numerical reproduction of the dust transport in the plasma sheath lies in the particle transport model as well as the plasma sheath modification by the external applied voltages. Therefore, first the potential structure modified by the external applied voltages was investigated by a PIC simulation. Next, with the results from the PIC, MD simulations were performed for the motion of particles.

The local modification of the plasma sheath was investigated by the PIC method. As we mentioned in the experi-

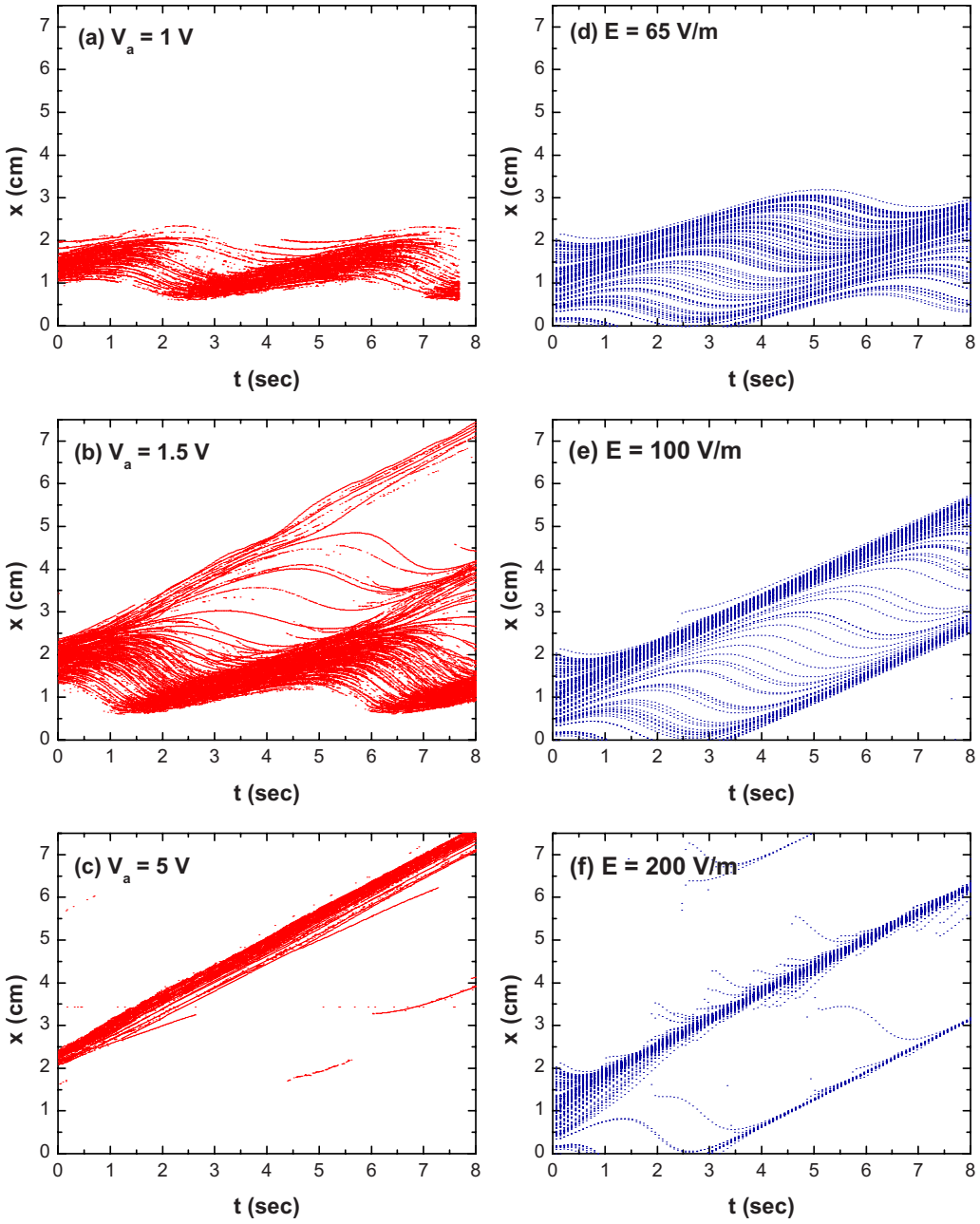

FIG. 2. (Color online) Dependence of the particle positions along the x axis (during the transportation) on the horizontal electric field strength (which in turn strongly depends on the amplitude of the applied voltage, V_a): (a) $V_a=1$ V, (b) $V_a=2$ V, and (c) $V_a=5$ V from experiments and (d) $E=65$ V/m, (e) $E=100$ V/m, and (f) $E=200$ V/m from simulations for comparison. In all the cases, $\delta\phi=\pi/3$ and $f=0.2$ Hz were kept constant.

mental part, the frequency for the particle transport is usually 0.1–10 Hz, which is enough for the sheath to reach equilibrium; therefore we only apply static dc-bias signals on each stripe to investigate the modification of the sheath. We started from XOOPIC (Object Oriented Particle in Cell code for X11–based Unix computers) (Ref. 14) as a basis and developed it based on our requirements. For our simulation, we consider a two-dimensional rectangular calculation domain in the x-z plane with 3.12×3 cm^2 above the SE. Static dc-bias signals were applied on each stripe with $V_{\text{bias}}=-15$ V, $V_a=13$ V, and $\delta\phi=\pi/3$ in Eq. (1). A periodic boundary condition was used along the x direction in the simulation. Figure 4 shows the potential profile above the SE at different heights. The potential structure is modulated according to the applied voltages on the stripes. For a sinusoidal modulation on the stripes, the potential distribution, the horizontal and vertical electric fields at a height of several millimeters, are all in a sinusoidal shape. The dashed dotted line in Fig. 4 represents the average height (of 4.9 mm) where the particles were observed in the experiments. The sheath works as a low pass filter resulting in a sinusoidal potential profile even if we use a rectangular potential input on the stripes. We emphasize the significance of this finding because we use a sinusoidal potential profile as the input external force for our MD simulation.

We estimated the particle charge from $eZ_dE=m_dg$ (the balance of electric and gravitational forces). Z_d was calculated to be 38 000 and there is good agreement with the

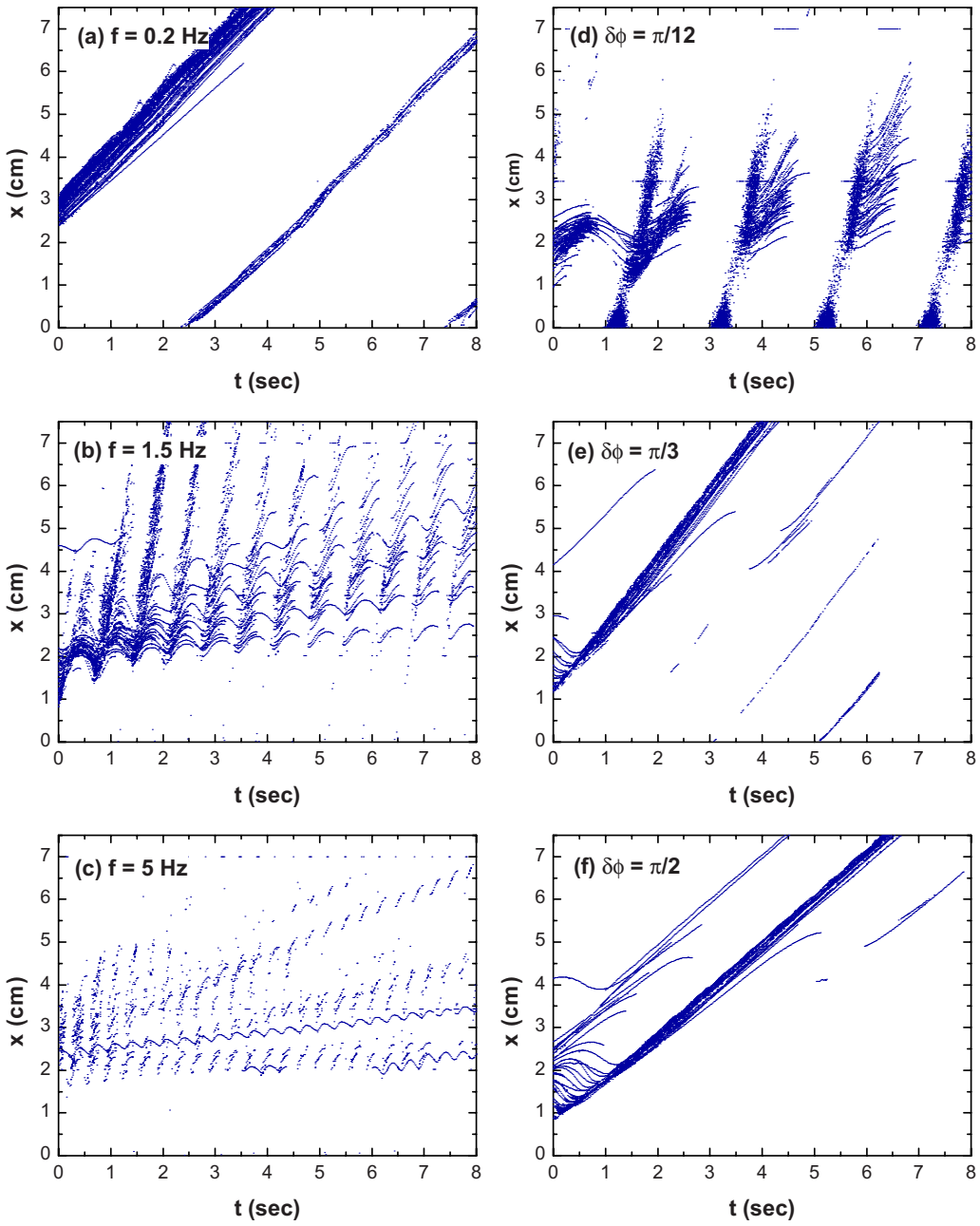

FIG. 3. (Color online) Dependence of the particle positions along the x axis (during the transportation) on the frequency of the external vibration and the phase shift between every pair of neighboring stripes for (a) $f=0.2$ Hz, (b) $f=1.5$ Hz, and (c) $f=5$ Hz with $V_a=13$ V, $\delta\phi=\pi/6$ and (d) $\delta\phi=\pi/12$, (e) $\delta\phi=\pi/3$, and (f) $\delta\phi=\pi/2$ with $V_a=13$ V, $f=0.5$ Hz.

experimental estimation by the vertical resonance method ($Z_d \approx 26\,500$).[15]

Typically all the particles are well confined vertically due to the balance of electric and gravitational forces, although externally applied low-frequency voltages could result in small vertical oscillations. These small oscillations in vertical direction are neither our major concern nor comparable with the horizontal motions. Hence, two-dimensional MD simulations in the x-y plane were performed on the Langevin level. The many-particle Langevin equation is a stochastic differential equation in which two force terms have been added to Newton's second law to approximate the effects of the background (gas) medium,

$$\dot{\mathbf{r}}_i = \mathbf{v}_i, \tag{2}$$

$$m_d \dot{\mathbf{v}}_i = \mathbf{F}_i + \mathbf{F}_{\text{ext}} + \mathbf{F}_{Ep} + \mathbf{R}_i, \quad i = 1,2,\ldots,N. \tag{3}$$

Here $\mathbf{r}_i=(x,y)$ and $\mathbf{v}_i=(v_x,v_y)$ are the position and velocity of dust particle i, respectively. m_d is the particle mass and $\mathbf{F}_i$ is the sum of all forces exerted on particle i by the other $N-1$ particles. In our simulation, the forces in this equation are derived from a screened Coulomb potential (Yukawa potential) $\phi(r_{ij})=(eZ_d/r_{ij})\exp[-r_{ij}/\lambda_D]$,[16] where λ_D is the Debye screening length and r_{ij} is the distance between particles i and j; we then have $\mathbf{F}_i=-eZ_d\Sigma\nabla\phi$. The second term $\mathbf{F}_{\text{ext}}$ represents the external force,

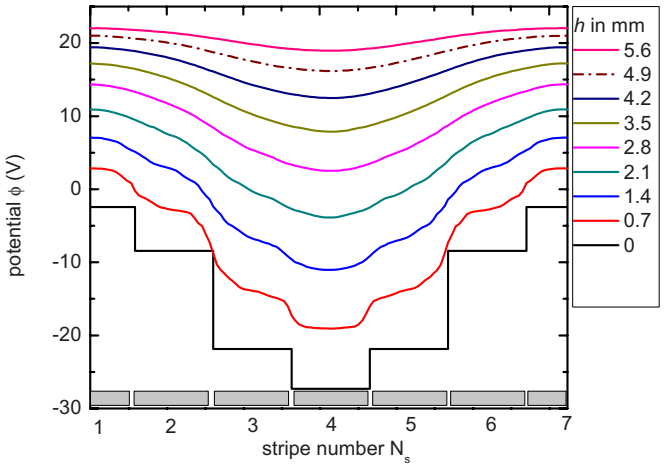

FIG. 4. (Color online) Potential profile at different heights (h=0 to h=5.6 mm in steps of 0.7 mm from the surface of the SE) is plotted, with $V_{\text{bias}}=-15$ V, $V_a=13$ V, $f=0.5$ Hz, and $\delta\phi=\pi/3$. The black solid line is the potential on the stripes (h=0) and the dashed dotted line is the potential profile at the average dust particle levitating height ($h\approx 4.9$ mm). The shadowed rectangles represent seven stripes with N_s being the stripe number.

$$\mathbf{F}_{\text{ext}}(x,t) = eZ_d\mathbf{E}(x,t) = eZ_dE_x \sin(kx+\omega t)\mathbf{e}_x,$$

where $\mathbf{E}(x,t)$ is the horizontal electric field, E_x is the amplitude, $k=2\pi/\lambda$ is the wave number, $\omega=2\pi f$ is the angular frequency, $\lambda=l_s\times 2\pi/\delta\phi$ is the wavelength, and $l_s=5.2$ mm is the width of the single stripe and the insulating space. E_x was obtained from the PIC simulation. The remaining terms on the right hand side of Eq. (3) represent the effect of the surrounding medium. The damping force term, $\mathbf{F}_{Ep}=-\gamma m_d\mathbf{v}_i$, represents the average effect of collisions between the dust particles and the neutral gas. For simplicity we assume the friction coefficient γ to be isotropic and constant. Adopting the model from Epstein,[17] the friction coefficient is given as $\gamma=\delta_{Ep}(4\pi/3)N_n m_n v_n r_d^2/m_d$, where N_n, m_n, and v_n are the neutral gas density, mass, and thermal velocity of the neutral gas, and r_d is the radius of the particles, the coefficient δ_{Ep} depends on how gas molecules scatter from the microparticle's surface. In our calculation, we used $\delta_{Ep}=1.48$—the value given by Konopka[18] for analyzing the horizontal oscillation of melamine formaldehyde particles in argon and krypton. This is slightly higher than 1.44—the theoretical maximum predicted by Epstein[17]—and 1.26—the experimental value measured using a single-particle laser acceleration method by Liu.[19] Finally in Eq. (3), the other random force term $\mathbf{R}_i(t)$ represents a stochastic process satisfying

$$\langle \mathbf{R}_i(t)\rangle = 0, \tag{4}$$

$$\langle \mathbf{R}_i(0)\mathbf{R}_i(t)\rangle = 2m_d\gamma k_B T\delta(t), \quad i=1,2,\ldots,N. \tag{5}$$

The stochastic force represents fluctuations due to the discreteness of collisions with the neutral gas, and is conveniently represented by a Gaussian process, as suggested by Allen[20] for computational purpose. The random force actually plays the role to randomly kick particles locally in time and drive the system to the expected temperature T. When the system is in thermal equilibrium, the friction and the stochastic acceleration are related to the ambient temperature via the fluctuation-dissipation theorem.[21] Such a Brownian description has been used for MD simulations in complex plasma studies.[22–26] Although not included in this paper, other heating mechanisms such as ion-dust streaming instability and charge fluctuations could also lead to dust particle heating.[27,28]

Taking the advantage of the linearity of the friction term, we then follow the algorithm from Ref. 20 to integrate Eq. (3) over a time interval Δt. We drop the subscript i for simplicity, $\mathbf{v}$ and $\mathbf{r}$ are given by

$$\mathbf{r}(t+\Delta t) = \mathbf{r}(t) + c_a\mathbf{v}(t)\Delta t + c_b\mathbf{a}(t)\Delta t^2 + c_c\mathbf{a}(t-\Delta t)\Delta t^2 + \mathbf{B}_r, \tag{6}$$

$$\mathbf{v}(t+\Delta t) = c_d\mathbf{v}(t) + c_e\mathbf{a}(t+\Delta t)\Delta t + c_f\mathbf{a}(t)\Delta t + c_g\mathbf{a}(t-\Delta t)\Delta t + \mathbf{B}_v, \tag{7}$$

with $c_a=c_1$, $c_b=c_2+c_3$, $c_c=-c_3$, $c_d=c_0$, $c_e=c_2-c_0c_3/c_1$, $c_f=c_1-c_2+2c_0c_3/c_1$, and $cg=-c_0c_3/c_1$, where $c_0=\exp(-\gamma\Delta t)$, $c_1=(\gamma\Delta t)^{-1}(1-c_0)$, $c_2=(\gamma\Delta t)^{-1}(1-c_1)$, and $c_3=(\gamma\Delta t)^{-1}(\frac{1}{2}-c_2)$. The integrals over the random force $\mathbf{R}_i$ have been rewritten as $\mathbf{B}_r$ and $\mathbf{B}_v$. It was showed by Chandrasekhar[29] and Hou[24] that $\mathbf{B}_r$ and $\mathbf{B}_v$ are simply random numbers correlated with variances and covariance of $\mathbf{r}$ and $\mathbf{v}$, and they are independent of $\mathbf{r}$ and $\mathbf{v}$. Following the technique from Refs. 23, 24, and 30, we obtain

$$\mathbf{B}_r = B_1\mathbf{N}_1(0,1) + B_2\mathbf{N}_2(0,1), \tag{8}$$

$$\mathbf{B}_v = \sigma_v\mathbf{N}_3(0,1), \tag{9}$$

where $B_1=\sigma_{vr}/\sigma_v$ and $B_2=\sqrt{\sigma_r^2-B_1^2}$. $\mathbf{N}_1(0,1)$, $\mathbf{N}_2(0,1)$, and $\mathbf{N}_3(0,1)$ are standard normal distributions (i.e., having mean 0 and variance 1) and are statistically independent of each other. σ_v and σ_r are the variances of $\mathbf{v}(t)$ and $\mathbf{r}(t)$, respectively, and σ_{vr} is the covariance between $\mathbf{v}(t)$ and $\mathbf{r}(t)$. For variances and covariance, we have[20,31]

$$\sigma_v = \sqrt{\frac{k_BT}{m_d}(1-e^{-2\gamma\Delta t})}, \tag{10}$$

$$\sigma_r = \sqrt{\frac{2k_BT}{m_d\gamma\Delta t}\left(1-2\frac{1-e^{-\gamma\Delta t}}{\gamma\Delta t}+\frac{1-e^{-2\gamma\Delta t}}{2\gamma\Delta t}\right)}, \tag{11}$$

$$\sigma_{vr} = \Delta t\frac{k_BT}{m_d\gamma\Delta t}(1-2e^{-\gamma\Delta t}+e^{-2\gamma\Delta t}), \tag{12}$$

where k_B is the Boltzmann constant and T is the expected dust temperature. The algorithm described here reduces to the well-known MD algorithm of Beeman[32] when γ=0. The coefficients in Eqs. (6) and (7) only need to be calculated once at the beginning of the simulation for each run, so do variances and covariance if a desired temperature is given before running the code. Therefore, this method is as efficient as a conventional frictionless MD method algorithm, where the system is only governed by the pair interaction force without taking into account external forces and stochastic effects of the background.

The length scale is characterized by $\lambda_D=103$ μm and time scales of interest are related to the inverse of a nominal dust plasma frequency, $\omega_0^{-1}=(e^2Z_d^2/m_d\lambda_D^3)^{-1/2}=1/220$ s with $Z_d=26\,500$ and $m_d=3.06\times10^{-9}$ g. The input parameters for the simulation include normalized friction coefficient $\gamma/\omega_0=0.1$, the expected dust temperature $T=0.024$ eV. The horizontal electric field strength at the particle height is $\sim10^2$ V/m. We performed our MD simulation for 1000 particles with periodic boundary conditions in a rectangular domain of 7.5 cm in the x direction and 4 cm in the y direction. Initially, the particles are randomly distributed in a small region (in a width of 1 cm). Then $\mathbf{F}_{\text{ext}}$ was instantaneously applied, leading to transportation of dust particles along the x direction. The time step for the simulation was $\delta t=0.02\omega_0^{-1}$. The time distance for the output data was $800\delta t$ which was kept within the same order as experimental recording speed (50 frames/s). Simulation results with different V_a are shown in Figs. 2(d)–2(f), showing a qualitative agreement with the experiment. From the PIC simulation, E_x is 65 V/m (d), 100 V/m (e), and 200 V/m (f) when V_a on the SE are 1, 2, and 5 V, respectively. By increasing V_a, E_x is increased. The comparison between the experimental and simulation results in Fig. 2 shows that the experimental results are well reproduced and the local oscillation and continuous transport of particles are also observed. If particles are fully trapped as in Figs. 2(c) and 2(f), they are transported with the sheath distortion at the velocity of $v_p=\omega/k=l_s\times2\pi f/\delta\phi$.

IV. CONCLUDING REMARKS

Plasmas are an indispensable tool in the field of material processing. However, dust particles are commonly produced in the plasma processing chambers as an undesirable by-product. Utilization of the SE enables us to generate a moving distortion or potential traps in front of the electrode, thus it provides a method to transport/remove dust particles over large distances without generating significant disturbances in the plasma region.

The dependence of the particle transport in the electric field generated by the SE was studied experimentally and numerically. The experimental results show that there are three typical regimes, namely, local oscillation, partially trapped and fully trapped regimes by changing the amplitude, the frequency, and the phase shift of the signals on each stripe.

Using PIC simulation, the sheath structure was studied and the electric field at the particle trapping position was determined to be around a few 10^3 V/m vertically and $\sim10^2$ V/m horizontally. Using the results from PIC as the input for the basic background plasma information, particle-resolved MD simulations were carried out. It was found that the transport efficiency of the dust particles is strongly dependent on the amplitude, dc bias, frequency, and phase shift of the applied signals on the stripes—as observed in the experiments. Three distinct transport regimes were also found in the simulation. The dust particles exhibited only a local oscillation when the potential profile was slightly modulated. At a very strong modulations, all the dust particles were fully trapped and transported with the velocity of the traveling potential distortions. In an intermediate case, both transport and local oscillations were observed. The simulation results show a qualitative agreement with our experimental findings.

The present method is independent of the reactor size and thus has the potential to work for very large area discharges. The SE is fit for use in a parallel-plate reactor, in which the upper and lower electrodes function as a PE and a counterelectrode, respectively, or the lower electrode is used as striped PE and the upper one as a counterelectrode. Although we only showed the results in this paper by using a low-frequency modulation, the similar potential distortion can be also produced by applying an amplitude-modulated high-frequency signal. In the latter case, placing a dielectric substrate, such as a silicon wafer, on top of the SE should not affect generating the sheath distortion.

ACKNOWLEDGMENTS

We are grateful to the help from B. Steffes, H. Rothermel, G. Stadler, M. Pustylnik, and F. Huber. K.J. would like to thank L. J. Hou and B. Klumov for helpful discussions about MD simulation.

This work was supported by the Deutschen Zentrums für Luft-und Raumfahrt (DLR) under Contract No. 50WP0700.

[1] K. G. Spears, T. J. Robinson, and R. M. Roth, IEEE Trans. Plasma Sci. **14**, 179 (1986).
[2] Y. Watanabe, M. Shiratani, Y. Kubo, I. Ogawa, and S. Ogi, Appl. Phys. Lett. **53**, 1263 (1988).
[3] G. S. Selwyn, J. Singh, and R. S. Bennett, J. Vac. Sci. Technol. A **7**, 2758 (1989).
[4] G. S. Selwyn, Proceedings of IEEE International Conference on Plasma Science, 1989, Paper No. 89CH2760-7, p. 154.
[5] G. S. Selwyn, J. S. McKillop, K. L. Haller, and J. J. Wu, J. Vac. Sci. Technol. A **8**, 1726 (1990).
[6] G. M. Jellum, J. E. Daugherty, and D. B. Graves, J. Appl. Phys. **69**, 6923 (1991).
[7] V. N. Tsytovich and J. Winter, Phys. Usp. **41**, 815 (1998).
[8] P. K. Shukla and A. A. Mamun, *Introduction to Dusty Plasma Physics* (Institute of Physics, Bristol, 2002).
[9] S. E. Beck, S. M. Collins, and J. F. O'Hanlon, IEEE Trans. Plasma Sci. **22**, 128 (1994).
[10] Y. Kurimoto, N. Matsuda, G. Uchida, S. Iizuka, M. Suemitsu, and N. Sato, Thin Solid Films **457**, 285 (2004).
[11] J. F. O'Hanlon, J. Kang, L. K. Russell, and L. Hong, IEEE Trans. Plasma Sci. **22**, 122 (1994).
[12] B. M. Annaratone, M. Glier, T. Stuffler, M. Raif, H. M. Thomas, and G. E. Morfill, New J. Phys. **5**, 92 (2003).
[13] Y.-F. Li, U. Konopka, K. Jiang, T. Shimizu, H. Höner, H. M. Thomas, and G. E. Morfill, Appl. Phys. Lett. **94**, 081502 (2009).
[14] J. Verboncoeur, A. Langdon, and N. Gladd, Comput. Phys. Commun. **87**, 199 (1995).
[15] T. Trottenberg, A. Melzer, and A. Piel, Plasma Sources Sci. Technol. **4**, 450 (1995).
[16] U. Konopka, G. Morfill, and L. Ratke, Phys. Rev. Lett. **84**, 891 (2000).
[17] P. Epstein, Phys. Rev. **23**, 710 (1924).
[18] U. Konopka, "Wechselwirkungen geladener Staubteilchen in Hochfrequenzplasmen," Ph.D. thesis, Ruhr-Universität-Bochum, 2000.
[19] B. Liu, J. Goree, V. Nosenko, and L. Boufendi, Phys. Plasmas **10**, 9 (2003).
[20] M. P. Allen, Mol. Phys. **40**, 1073 (1980); **47**, 599 (1982).
[21] D. S. Lemons, *An Introduction to Stochastic Processes in Physics* (The Johns Hopkins University Press, Baltimore, 2002).
[22] Y. Feng, B. Liu, and J. Goree, Phys. Rev. E **78**, 026415 (2008).
[23] L. J. Hou and A. Piel, Phys. Plasmas **15**, 073707 (2008).
[24] L. J. Hou, A. Piel, and P. K. Shukla, Phys. Rev. Lett. **102**, 085002 (2009).

[25]B. A. Klumov, M. Rubin-Zuzic, and G. E. Morfill, JETP Lett. **84**, 542 (2006).
[26]K. R. Sütterlin, A. Wysocki, A. V. Ivlev, C. Räth, H. M. Thomas, M. Rubin-Zuzic, W. J. Goedheer, V. E. Fortov, A. M. Lipaev, V. I. Molotkov, O. F. Petrov, G. E. Morfill, and H. Löwen, Phys. Rev. Lett. **102**, 085003 (2009).
[27]J. D. Williams and E. Thomas, Jr., IEEE Trans. Plasma Sci. **35**, 303 (2007).
[28]G. Joyce, M. Lampe, and G. Ganguli, Phys. Rev. Lett. **88**, 095006 (2002).
[29]S. Chandrasekhar, Rev. Mod. Phys. **15**, 1 (1943).
[30]L. J. Hou, Z. L. Mišković, A. Piel, and P. K. Shukla, Phys. Plasmas **16**, 053705 (2009).
[31]M. P. Allen and D. J. Tildesley, *Computer Simulation of Liquids* (Oxford University Press, New York, 1989).
[32]D. Beeman, J. Comput. Phys. **20**, 130 (1976).

Removing dust particles from a large area discharge

Yang-fang Li,[a] U. Konopka, K. Jiang, T. Shimizu, H. Höfner, H. M. Thomas, and G. E. Morfill
Max-Planck-Institute for Extraterrestrial Physics, 85748 Garching, Germany

(Received 16 December 2008; accepted 9 February 2009; published online 27 February 2009)

Introducing a striped electrode in a large area discharge allows us to transport microparticles in the discharge in a user defined way. A directed and continuous dust transport is established by modulating the voltage signals on all individual electrodes to cause a traveling plasma sheath distortion. Particles, trapped in the potential wells and thus following the distortions, are finally removed from the central discharge region. Transport efficiency and velocity can be controlled by changing amplitude and traveling velocity of the plasma distortions. © *2009 American Institute of Physics*. [DOI: 10.1063/1.3089873]

Particle contamination in processing plasma reactors that are designed for deposition, etching, and sputtering applications (e.g., for solar cells, flat panel displays, and chip production) often plays a crucial role in the quality and the yield of the processed products.[1] In these situations, the main contamination sources are particles grown through chemical reactions in the processing plasma[2] or direct sputtering of dust particles from the electrodes. For example, in capacitatively coupled radio-frequency (rf) discharges in silane gas,[3] nanometer sized precursors grow within fractions of a second, reaching density of 10^{10} cm^{-3}. These precursors coagulate within seconds to form hundred nanometer sized agglomerates. The final dust cloud then consists of 10^8 particles/cm^3.[3,4] Particles and precursors are in general highly negatively charged due to plasma particle bombardment. Only the very small particles might get slightly positively charged as a result of statistical fluctuations of the charging process, secondary or photoelectron emission.[5]

The negatively charged particles are well confined. They do not impact on the processed substrate since the sum of gravity, ion drag, and thermophoresis acting on them is in general well compensated by the sheath electric confinement force. Still, after some growth time, the sheath confinement might be too weak to levitate the largest particles. This problem might in principle be handled by a suitable orientation of the processing device, however, vertical mounting of very large (several m^2) thin glass plates (or other substrates) is not feasible mechanically in many situations. In any case, the main problems arise from positively charged nanoparticles that are strongly attracted to the surfaces during the discharge process and those particles that, after the discharge is switched off, keep a significant residual positive/negative charge[6] so that they are attracted to the surfaces by static electric fields. Because of their high density, dust particles also collect a significant amount of the free electrons in the plasma. As a result, the repetitive process of precursor growth, coagulation, continuous growth. and sedimentation can cause local inhomogeneities and fluctuations in the plasma conditions that might reduce the quality of the plasma process.

To avoid dust contamination effects, either the growth of fine particles has to be suppressed or the contaminating particles efficiently have to be removed from the discharge. Suppressing particle growth could be realized, for example, in *a*-Si:H processes using H_2 dilution in SiH_4 (Ref. 7) or using a sine-wave modulated rf plasma in a plasma-enhanced chemical vapor deposition of silicon dioxide thin film using the mixture of tetraethoxysilane and oxygen ($TEOS/O_2$) without significantly decreasing the film growth rate.[8] Removing particles from a discharge has been demonstrated, for example, by Uchida and co-workers[9,10] using their "negatively charged fine particle collector" that is based on the influence of static electric fields and hollow cathode secondary plasmas on the particles. Other approaches use localized secondary plasmas or the influence of temperature gradients on the particles.[11] In spite of all these efforts, the "question of scale" remains, i.e., how to remove unwanted nano- and microparticles from several meter-sized electrode assemblies. In contrast to the more localized already investigated particle removal methods, the technique proposed here is based on traveling plasma distortions in front of a multisegmented electrode and thus is reactor size independent.

To demonstrate the proposed method of dust removal by traveling plasma distortions, we used a large area capacitively coupled rf plasma reactor with an inner diameter of 80 cm and a height of 40 cm. As sketched in Fig. 1, the plasma is generated by the rf-driven 50×50 cm^2 square electrode that mainly consists of a frame structure. The striped electrode, separated 5 cm from the driven electrode, consists of 100 electrical insulated stainless steel narrow strips of 0.5×50 cm^2 (for simplicity, we only sketched ten individual strips in Fig. 1).

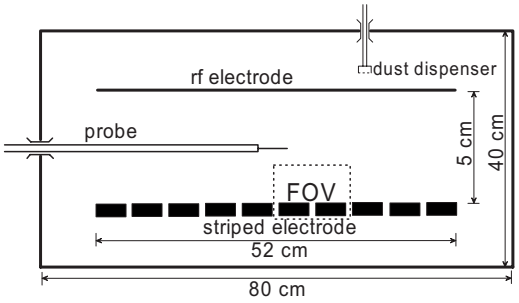

FIG. 1. The sketch of the striped electrode device. FOV denotes field of view.

[a]Electronic mail: yfli@mpe.mpg.de.

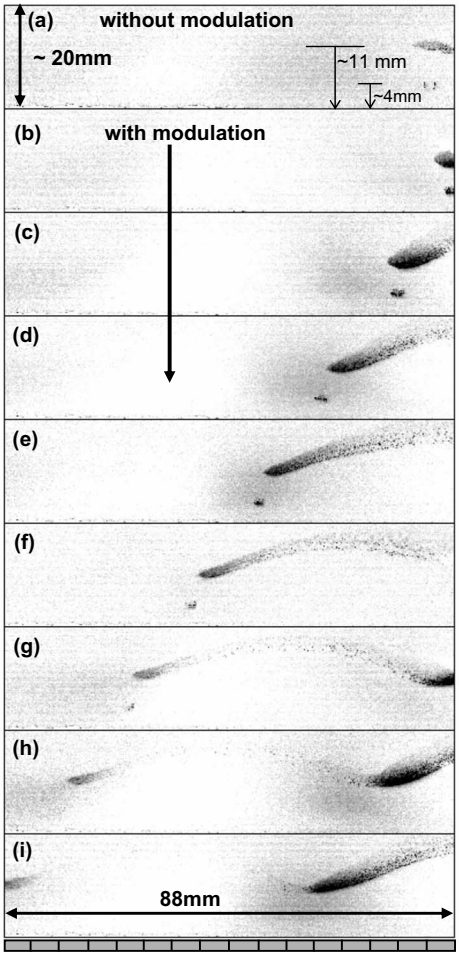

FIG. 2. (a) The suspending positions of the injected and grown particles with all the strips floating. [(b)–(i)] The profile of the particles during transportation is shown for every second after the sinusoidal modulation signals are applied to the strips. Only interested region extracted from the original images is presented. The scale of the stripe electrode is shown at the bottom of the images. Note that when the modulation is on, all the injected and most grown particles are attracted to the trapping point of the potential profile so that we see the significant increase of the particle density in trapping point in (b)–(i). And also the particle number decreases from (b) to (i) because a lot of particles move outside of the camera's focus area during the long-distance transportation.

Each strip is driven independently by one channel of a multichannel voltage function generator. For each generator channel, different waveform, frequency, dc-bias, amplitude, and phase angle can be chosen separately. For the present experiments, a voltage signal, which is described by

$$V(N_s,t) = V_{\mathrm{dc}} + V_a \sin(2\pi f \times t + N_s \times \delta\Phi), \qquad (1)$$

was applied to each strip with N_s being the strip number. The bias voltage was set to $V_{\mathrm{dc}}=-15$ V, the amplitude to $V_a=20$ V, and the frequency to $f=0.2$ Hz. A fixed phase shift of $\delta\Phi=\pi/6$ was chosen between every pair of neighboring strips. The plasma was generated in argon at a pressure of 28 Pa with an rf-power of 30 W. Plasma parameters measured by an rf compensated Langmuir probe (Hiden ESPion Advanced Langmuir Probe) gave an electron temperature of ~2–3 eV, plasma density of $\sim 1\times 10^9$ cm^{-3}, and a plasma potential of ~22 V in the center of the discharge area, 2 cm above the striped electrode.

Two kinds of particles were used in the present experiments. Al_2O_3 spherical particles with an average diameter of 3 μm were injected into the plasma region by a dust dispenser mounted on the top flange of the chamber. The other very small particles ($\lesssim 1$ μm) were grown inside the chamber. The particles were illuminated by a laser sheet (with wavelength 680 nm, cw mode) perpendicular to the electrode and the observing direction of a camera (Basler A404k). The camera was aligned with the longer side of the strips. The particle motion across strips was captured by this side view camera at 49 frames per second. Using a camera lens with focal length of 85 mm (Nikon AF 85 mm f/1.4D IF), the camera with $2352\times 1726(W\times H)$ pixels sensor imaged a field of view of 8.8×6.5 cm^2. An interference filter with center wavelength 680 nm and bandwidth 12 nm was added between the lens and camera sensor.

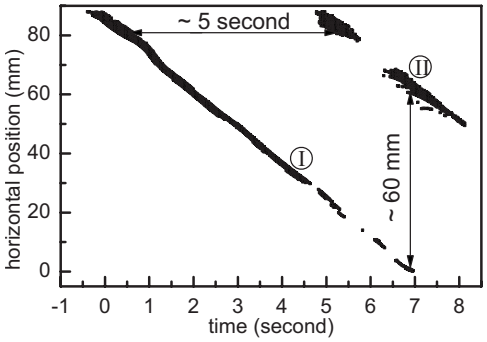

FIG. 3. The horizontal position of the injected particles with respect to the recording time. I and II correspond to two separate dust clouds trapped in different potential wells. Their time and space duration (~5 s and ~60 mm, respectively) are approximately equal to the $1/f$ and λ of the applied signals on strips.

The camera showed that applying different voltage signals on strips modified the sheath structure, i.e., the potential profile, above the striped electrode. As the previous work has shown using an adaptive electrode device.[12] The injected and grown, negatively charged particles then found their equilibrium (trapping) points with lowest energy (highest electric potential) in the sheath, presheath, or bulk plasmas region determined by the force balance on the particles. By producing the time varying, traveling potential profile above the striped electrode, we succeeded in manipulating/transporting the dust particles by attracting the particles to a new-generated trapping point.

Figure 2 shows how the particles were transported by the traveling plasma sheath distortion. The top image (a) shows the position of the levitated particles without modulating signals on the strips (the strips were electrically floating with the floating voltage ~−3 V). The injected particles were levitated at the height of ~4 mm from the striped electrode and the grown particles located at the height of ~11 mm. When the modulation was switched on ($t=0$), all the injected particles and most of the grown particles were first attracted to the nearest trapping points. Then the directed transportation, from right-to-left, of the injected particles as well as the trapped grown particles was achieved by the continuous modulation on the strips. However, a small part of the grown particles were pushed out of the trapping region as a result of the interparticle repulsion in the cloud. Those particles, levitated at larger distance from the electrode, are only weakly trapped and thus perform mainly a horizontal and vertical oscillation overlayed by a slow horizontal drift.

Figure 3 visualizes the horizontal time depending posi-

tion of the injected particles. The particles were transported from right to left with almost a constant velocity $v_p \sim 12$ mm/s, which was approximately the traveling velocity v_{pT} of the plasma distortion. For the sinusoidal modulation in present experiments, v_{pT} was determined by the applied signals on the strips and was calculated as $v_{pT}=\lambda f$, where $\lambda = W \times 2\pi/\delta\Phi$ is the spatial period of the traveling potential distortion and W is the width of each strip (including the insulating space of ~0.2 mm). With the selected parameters $\delta\Phi=\pi/6$ and $f=0.2$ Hz, we expected the traveling velocity of $v_{pT} \sim 12.5$ mm/s. It was found that the particle transport velocity was equal to v_{pT} as long as the particles could be trapped in the potential well during the transportation. Therefore, the transport efficiency relies on the trapping of the particles in the distorted potential profile. If the particles were trapped by the potential wells, they were transported directly by the traveling sheath distortion and their velocity was approximately the phase velocity of the modulating signals on strips. Otherwise, if the particles were not full trapped by the potential well, they oscillated during the transportation and then the transport efficiency was low. The trapping of the particles can be improved by choosing appropriate parameters for the modulating signal on strips by producing stronger potential gradient (increasing V_a) or/and slower traveling velocity, namely, decreasing f and/or increasing $\delta\Phi$.

The transport velocity v_p of the particles are proportional to the frequency f and inversely proportional to $\delta\Phi$. In principle, the particles can gain a very high velocity during the transportation, which means high removal efficiency. However, to transport the particles with higher speed, it is necessary to produce stronger potential well (with larger V_a and also appropriate change of V_{dc}) for the efficient trapping of the particles. Then the higher transport speed of the particles results in more disturbance to the plasma. For the application of this device in reactive plasmas, it is necessary to find a proper set of parameters from the viewpoint of the particle-removal rate, related to the particle growth rate, and processing quality. We expect that the homogeneity of the plasma is still be given in time average for a process time $T_P \gg 1/f$. However, process parameters have to be readjusted accordingly to compensate for the effects of the plasma modulation.

As an advantage to other particle removal methods, the here demonstrated one is reactor size independent and thus has the potential to work for very large area discharges. Although not tested here, an efficient dust removal can be also expected in case of a dielectric barrier on top of the striped electrode since modifying the applied signals on the electrode by an ac-modulation would still lead to the required plasma sheath distortions. Also a setup with the manipulation electrode to be the upper electrode might be considered for future applications.

This work was supported by DLR under Contract Nos. 50JR0582 and 50WP0700. We are grateful to the help from B. Steffes, H. Rothermel, G. Stadler, and M. Pustylnik.

[1] *Physics, Chemistry and Technological Impacts in Plasma Processing*, edited by A. Bouchoule (Wiley, New York, 1999).
[2] R. P. Donovan, *Particle Control for Semiconductor Manufacture* (Dekker, New York, 1990).
[3] Y. Watanabe, J. Phys. D **39**, R329 (2006).
[4] G. S. Selwyn, J. E. Heidenreich, and K. L. Haller, J. Vac. Sci. Technol. A **9**, 2817 (1991).
[5] P. K. Shukla and A. A. Mamun, *Introduction to Dusty Plasma Physics* (CRC, Boca Raton, 2001), Chap. 2.
[6] A. V. Ivlev, M. Kretschmer, M. Zuzic, G. E. Morfill, H. Rothermel, H. M. Thomas, V. E. Fortov, V. I. Molotkov, A. P. Nefedov, A. M. Lipaev, O. F. Petrov, Yu. M. Baturin, A. I. Ivanov, and J. Goree, Phys. Rev. Lett. **90**, 055003 (2003).
[7] M. Shiratani, S. Maeda, K. Koga, and Y. Watanabe, Jpn. J. Appl. Phys., Part 1 **39**, 287 (2000).
[8] N. Kashihara, H. Setyawan, M. Shimada, Y. Hayashi, C. S. Kim, K. Okuyama, and S. Winardi, J. Nanopart. Res. **8**, 395 (2006).
[9] Y. Kurimoto, N. Matsuda, G. Uchida, S. Iizuka, M. Suemitsu, and N. Sato, Thin Solid Films **457**, 285 (2004).
[10] N. Sato, S. Iizuka, and G. Uchida, World Patent No. WO 01/01467 A1, (1 April 2001).
[11] G. M. Jellum, J. E. Daugherty, and D. B. Graves, J. Appl. Phys. **69**, 6923 (1991).
[12] B. M. Annaratone, M. Glier, T. Stuffler, M. Raif, H. M. Thomas, and G. E. Morfill, New J. Phys. **5**, 92 (2003).

epl A Letters Journal Exploring the Frontiers of Physics

March 2011

EPL, **93** (2011) 55001
doi: 10.1209/0295-5075/93/55001

www.epljournal.org

Initial stages in phase separation of binary complex plasmas: Numerical experiments

K. Jiang[a], L.-J. Hou, A. V. Ivlev, Y.-F. Li, C.-R. Du, H. M. Thomas, G. E. Morfill and K. R. Sütterlin

Max Planck Institute for Extraterrestrial Physics - 85748 Garching, Germany, EU

received 5 January 2011; accepted in final form 8 February 2011
published online 11 March 2011

PACS 52.27.Lw – Dusty or complex plasmas; plasma crystals
PACS 64.75.Cd – Phase equilibria of fluid mixtures, including gases, hydrates, etc.
PACS 64.75.Gh – Phase separation and segregation in model systems (hard spheres, Lennard-Jones, etc.)

Abstract – Numerical experiments are performed to investigate the initial stages in phase separation induced by interaction non-additivity Δ in binary complex plasmas. A characteristic length scale obtained from time-dependent pair correlation functions is used to monitor the domain growth. It is found that the domain growth follows a power law with an exponent α of around 1/3, which is in a good agreement with the Lifshitz-Slyozov growth law for the initial diffusive regime of phase separation. It is also found that α is almost independent of Δ as long as the system is within the spinodal region. The coupling strength is also found to have almost no influence on α, unless the coupling is so large that the background large-particle phase starts crystallizing.

Introduction. – A complex plasma is a suspension of micron-sized particles immersed in a usual plasma with ions, electrons and neutral gas. Dust particles acquire a few thousands of electron charges by absorbing the surrounding electrons and ions, and consequently interact with each other via a screened Coulomb potential $\propto r^{-1}\exp(-r/\lambda)$, where r is the inter-particle distance, and λ the screening length, while undergoing Langevin dynamics due to frequent collisions with neutrals [1,2]. When the interaction potential energy between charged dust particles significantly exceeds their kinetic energy, they become strongly coupled and, consequently, can form ordered structures of a liquid or solid state. Complex plasmas have been regarded as an ideal model system to study various phenomena in liquids, solids as well as strongly coupled Coulomb systems at the kinetic level [1–4]. Recently, complex plasmas with different types of dust-particles (or multi-component complex plasmas) have gained more and more attention [5–12], as these systems could have much richer phase diagram, structures and dynamics properties than the single-component ones. And recent experiments with binary complex plasmas (complex plasmas with two different types of dust particles) under microgravity conditions [5,6,8,10,11] have demonstrated their promising prospect, as so many interesting phenomena have been observed, such as "classic tunneling" [5], lane formation [6–9] and in particular phase separation [10,11], which is the subject of this letter.

Phase separation, in which different types of particles tend to separate from each other, is a ubiquitous phenomenon in many different systems of multi-component mixtures, such as molecular fluids and colloidal suspensions [13–15], and has been a long-standing research topic in physics, because of its both fundamental and practical importance. It can be stimulated by either the interplay between individual particles, such as the so-called interaction non-additivity or external perturbations, such as shear flow, temperature gradient and electric field [16–18]. Phase separation is a scaling phenomenon like the fluid-solid phase transition [19,20]: The average domain size $L(t)$ follows a simple power law as $L(t) \propto t^{\alpha}$, sequenced to three consecutive regimes (diffusive, viscous and inertial regimes) with different growth exponents α [14] peculiar to each regime. The growth law for the diffusive regime was given by [21,22],

$$L(t) \propto (\gamma_T D t)^{1/3}, \tag{1}$$

where γ_T is the interfacial tension of domain boundaries and D is the diffusive transport coefficient. The viscous regime was then studied by considering the viscous effect

[a] E-mail: jiang@mpe.mpg.de

and a linear growth regime was obtained [23], with $L(t) \propto (\gamma_T t/\mu)$, where μ is the viscosity of the liquid. There have been many numerical simulations studying different regimes and the crossover between them. For example, the hydrodynamical viscous regime has been numerically studied with "model H" [24–26]. The viscous regime and inertial regime are also studied with lattice-based methods [27,28]. Molecular dynamics simulations have also been used to resolve the dynamics on an atomistic level, mainly for Lenard-Jones mixtures [29–31].

In complex plasmas, phase separation was first observed in experiments by Morfill *et al.* [5] and later on by Sütterlin *et al.* [6], both under microgravity conditions. Ivlev *et al.* [10] have recently shown theoretically for binary complex plasmas that the inter-species interaction always has positive non-additivity, *i.e.*, for point particles of type "1" and "2", the 1-2 is always more repulsive than the geometric mean of 1-1 and 2-2 interactions. This non-additivity leads to a spinodal region (where the fluid mixture is unstable and starts demixing) which overlaps with typical experimental conditions of complex plasmas in laboratory [10]. This explains well the phase separation phenomena observed in recent experiments and also makes binary complex plasmas a promising model system for studying the kinetics of the phase separation [11].

In this letter, we perform Langevin dynamics simulations to study the phase separation in binary complex plasmas for a wide range of system states, as a complementary of both theory and experiment. Our simulation differs from the recent simulation of Wysocki *et al.* [11] in two aspects. Firstly, ref. [11] focused on critical role of two-scale interaction in driving the phase separation, whereas here we focus on non-additive single Yukawa interaction. Secondly, we additionally study the influence of coupling strength and damping due to dust-neutral collisions on the phase separation of binary complex plasmas.

Simulation. – Our simulation is based on the so-called Langevin dynamics method [32,33], in which the dynamics of dust particles are described by the Langevin equation:

$$\begin{aligned} \dot{\mathbf{r}} &= \mathbf{v}, \\ \dot{\mathbf{v}} &= -\xi\mathbf{v} + \frac{1}{m}\mathbf{F}(\mathbf{r}) + \mathbf{A}(t). \end{aligned} \tag{2}$$

Here as usual, m, $\mathbf{v}$ and $\mathbf{r}$ are, respectively, the mass, velocity, and position of a dust particle, ξ is the frictional damping rate (in our case it represents Epstein damping), $\mathbf{A}(t)$ is a random acceleration representing Brownian motion of dust particles, $\mathbf{F} = -\sum \nabla\phi$ is the deterministic force coming from the inter-particle interactions within the system. In our system there are two different particle species (small and large) with the relative size and consequently charge ratio $r_L/r_S = Z_L/Z_S \equiv \eta$, and mass ratio $m_L/m_S = \eta^3$ (hereafter, subscript "S" and "L" denote small and large particles). The pairwise potential is then characterized by six parameters: three interaction magnitudes ε_{ij} and three screening lengths λ_{ij}. We assume both species experience the same screening, $\lambda_{ij} = \lambda$, determined by the background plasma, but different interaction magnitudes ε_{ij}. The general form of the pairwise interaction potential (energy) now reads

$$\phi_{ij}(r) = \varepsilon_{ij}\frac{\exp(-r/\lambda)}{r}. \tag{3}$$

For like-particle interaction, $\varepsilon_{ij} = \varepsilon_{SS(LL)}$ is the product of the asymptotic (far-field) charge, $Z^*_{S(L)}$ and the actual (surface) charge $Z_{S(L)}$ [10], whereas for interaction between unlike particles one has

$$\varepsilon_{ij} = \varepsilon_{LS} = \varepsilon_{SL} = (1+\Delta)\sqrt{\varepsilon_{SS}\varepsilon_{LL}}, \tag{4}$$

according to the Lorentz-Berthelot mixing rules [32]. Here Δ is the so-called non-additivity parameter, which represents the asymmetry in the mutual interaction between unlike particles and is always positive in binary complex plasmas [10]. When the nonlinear screening effect dominates, Δ is given by [10]

$$\Delta = \frac{(\sqrt{\nu_L/\nu_S} - 1)^2}{2\sqrt{\nu_L/\nu_S}}, \tag{5}$$

where $\nu_{S(L)}(Z) = Z^*_{S(L)}/Z_{S(L)}$ is renormalizing charge ratio. For $\Delta = 0$, ϕ_{ij} reduces to the usual (additive) Yukawa potential.

In the simulation, eq. (2) is integrated numerically by using a Beeman-like method [32,33], for $N = N_S + N_L$ particles in a cubic box with periodic boundary condition. Here $N_{S(L)}$ is number of small (large) particles and we choose $N = 10^5$ in all the simulations with a fixed composition ratio of $x_S = x_L = 0.5$. In this case the large particles represent the background, while the small particles form the growing domains.

The system is characterized by the following dimensionless parameters [2]: the coupling parameter Γ, the screening parameter κ and the damping rate γ, defined, respectively, as

$$\Gamma = \frac{Z^2}{ak_BT}, \qquad \kappa = \frac{a}{\lambda}, \qquad \gamma = \xi/\omega_p \tag{6}$$

for each species, where k_B is the Boltzmann constant, T is the temperature used in the Langevin thermostat and $a = (4\pi n/3)^{-1/3}$ is the Wigner-Seitz radius with n being the number density of each species, and $\omega_p = \sqrt{Z^2/ma^3}$ the nominal dust plasma frequency. Initially we have $a_S = a_L$, $\Gamma_L/\Gamma_S = \eta^2$, $\kappa_L = \kappa_S$, $\gamma_L/\gamma_S = \eta^{-1}$. We use a_S for the normalization of spatial scale and ω_{pS} for the temporal scale. The system size in all our simulations is $\bar{L} = 76a_S$.

Results and discussions. – The system states in our simulation are chosen according to typical complex plasma parameters with PK-3 Plus chamber on board the International Space Station [34]. All our simulations started from uniformly and randomly mixed configurations of large and

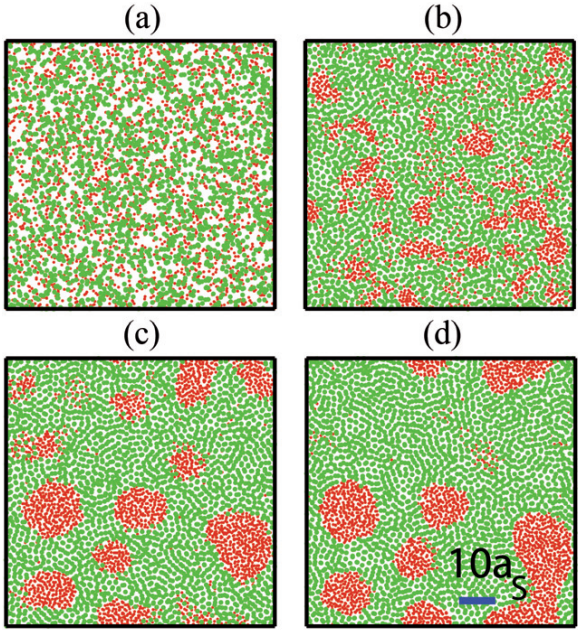

Fig. 1: (Color online) Snapshots of the binary system for $\Gamma_S = 20$, $\kappa_S = \kappa_L = 1$, $\eta = 3$, $\Delta = 0.03$ and $\gamma_S = 0.05$ at four different time stages: (a) $t = 0$, (b) $t = 400\omega_{pS}^{-1}$, (c) $t = 800\omega_{pS}^{-1}$, and (d) $t = 4000\omega_{pS}^{-1}$, respectively. Red represents small particles and green is for large ones.

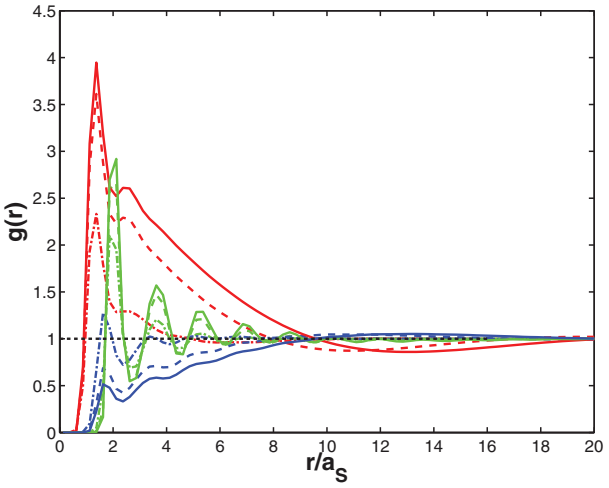

Fig. 2: (Color online) The radial distribution functions $g_{SS}(r)$ (red), g_{LL} (green) and g_{SL} (blue) for the same case as in fig. 1 at different time stages where the dash-dotted lines depict $t = 400\omega_{pS}^{-1}$, the dashed lines depict $t = 800\omega_{pS}^{-1}$, and the solid lines depict $t = 4000\omega_{pS}^{-1}$, respectively, corresponding to snapshots in figs. 1(b), (c), and (d).

small particles. While the systems evolved towards their thermodynamic stable states, the structure transition of the system was monitored. Figure 1 shows snapshots of a cross-section in the system for $\Gamma_S = 20$, $\eta = 3$ (which gives $\Delta \approx 0.03$ according to eq. (5)) and $\gamma_S = 0.05$, demonstrating the typical sequence: One can see that starting from a random mixture, the system coarsens with no clear boundaries between two species, as shown in fig. 1(b). Next, sharp interfaces build up while small clusters merge into large droplets, as shown in fig. 1(c) and fig. 1(d). One can also observe that in fig. 1(d) most droplets are convex, indicating that the non-additivity–induced interfacial tension starts playing an important role.

Figure 2 shows the evolution of the binary radial distribution functions (denoted as $g_{SS}(r)$, $g_{SL}(r)$, $g_{LL}(r)$ or simply $g(r)$) for the corresponding snapshots in fig. 1. We can see that the phase separation occurs along with the structure evolution of each phase: As the two types of particles separate from each other, local structures start developing. One notes that during demixing, peaks of $g_{SL}(r)$ decrease in magnitude, whereas peaks of $g_{SS}(r)$ are more and more pronounced. This is merely a consequence of demixing, during which it is getting more and more difficult to find a small particle near a large one, while small particles are gathering and forming clusters. Meanwhile, peaks in $g_{LL}(r)$ grow not only in magnitude but also in number, which indicates that a long-range order is being built up in the large-particle phase.

It should be stressed that the coupling strengths given in all the figures are initial values, which are derived from initial density of each species. The actual coupling strengths vary during the demixing due to the change of the density. For instance, in the case of fig. 1(d), the coupling strength of large particles is estimated to be about 195 based on the density calculated from the first peak positions of $g_{LL}(r)$.

In order to study the demixing process, we monitor the growth rate of domains in our system. The zero crossing of $g_{SS}(r) - 1$ at large distances ($r/a_S > 2$) is used as a characteristic length, $L(t)$ [35–37]. It should be noted that $L(t)$ used in this letter is proportional to the characteristic length scale based on the structure factor [36].

Figure 3 depicts the evolution of $L(t)$ during the phase separation of binary systems at different coupling strengths and fixed η and γ. Note here that the non-additivity is determined by η through eq. (5) according to the theory in ref. [10]. One observes that the growth curves for lower Γ_S are always above those of higher Γ_S, which can be easily understood: For higher coupling strength, the kinetic energy is lower, which leads to the decrease of particle diffusion and consequently the demixing process is slowed down. Meanwhile, we observe that the exponent of L is almost independent of the coupling strength unless the coupling strength becomes too high. For example, the linear fit for $\Gamma_S = 50$ in fig. 3 yields $\alpha = 0.31$ (typical statistical error in the fitting is about a few percent of α according to the chi-square minimization method), while the other four cases give $\alpha = 0.36$. This is probably due to the approaching crystallization of large particles ($\Gamma_L = \eta^2\Gamma_S = 450$), which inhibits coalescence of droplets

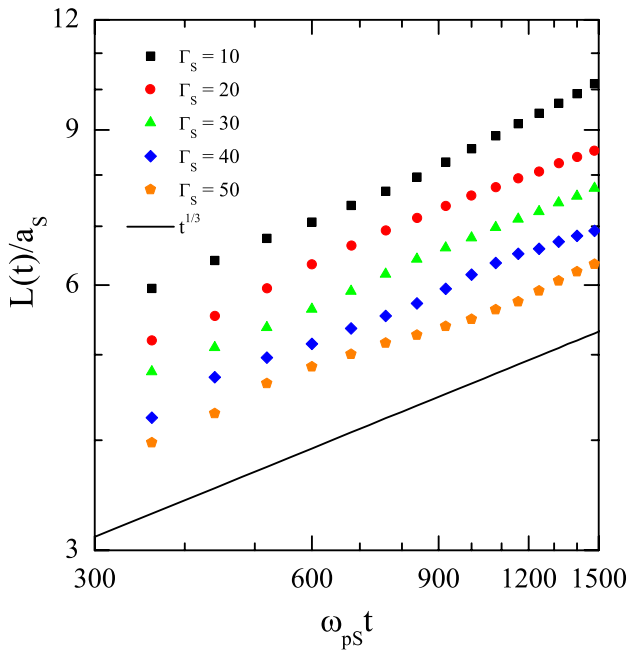

Fig. 3: (Color online) Influence of the coupling strength on domain growth. Evolution of L is shown for $\kappa_S = \kappa_L = 1$, $\eta = 3$, $\gamma_S = 0.05$ and different coupling strengths, namely $\Gamma_S = 10$ (black square), $\Gamma_S = 20$ (red dot), $\Gamma_S = 30$ (green triangle), $\Gamma_S = 40$ (blue diamond) and $\Gamma_S = 50$ (orange pentagon). The black line $t^{1/3}$ is shown for comparison.

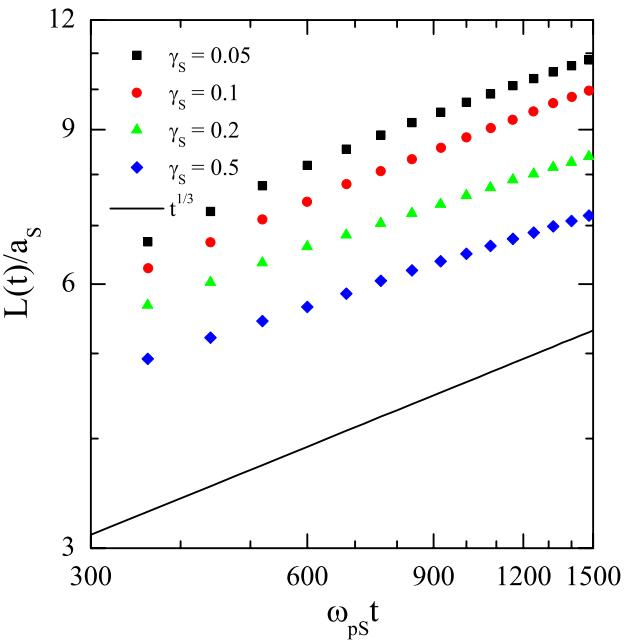

Fig. 4: (Color online) Influence of the neutral gas damping on domain growth. Evolution of L is shown for $\Gamma_S = 20$, $\kappa_S = \kappa_L = 1$, $\eta = 3$, $\Delta = 0.07$ for different γ_S, namely $\gamma_S = 0.05$ (black square), $\gamma_S = 0.1$ (red dot), $\gamma_S = 0.2$ (green triangle), $\gamma_S = 0.5$ (blue diamond). The black line $t^{1/3}$ is shown for comparison.

formed by small particles. This also explains why a relative small growth rate $\alpha \lesssim 0.17$ was observed in ref. [11] (as shown in figs. 4(b) and (c) therein), where the coupling strength was an order of magnitude larger.

Figure 4 shows $L(t)$ for different damping rates to study the effects of neutral gas damping on the growth rate. Firstly one observe that the curve of strong damping rate is always lower than those with weaker damping because the diffusive transport coefficient D is lower at higher damping rates, which results in smaller absolute initial value according to eq. (1). Secondly α decreases slightly with the increase of damping rate: as $\alpha|_{\gamma_S=0.05} = 0.34$ and $\alpha|_{\gamma_S=0.5} = 0.27$. A possible explanation could be the nontrivial prolonged effect of dissipation on transient kinetics, as described in ref. [38], which exactly matches the observation time of our simulation (fig. 3 therein).

The values of α deduced from our simulations are within [0.27, 0.37], which is in good agreement with the diffusive regime with $\alpha = 1/3$. The crossover from the diffusive to viscous regime has not been observed. This may be due to the late occurrence of viscous regime (which has been mentioned in [31]) or due to the finite-size effect in our system [29]. The demixing dynamics will be strongly impeded when the domain size L is comparable to the system size (in our case $\bar{L} = 76 a_S$). According to ref. [29], the finite-size effect starts to play a role when L goes beyond 1/3 of the system size. Therefore we have confined all our discussions in the very initial stage of demixing, $t\omega_{pS} < 1500$, when the domain size is still significantly smaller than this limit. However one should have a sufficiently large system when trying to resolve later stages of demixing, *e.g.*, for the viscous regime the system size should be at least one order of magnitude bigger.

Conclusions. – We have studied the interaction non-additivity–induced phase separation phenomenon in a binary complex plasma by using Langevin dynamics simulation. Special attention was payed to the initial stages of the phase separation and to the dependence of the domain growth exponent on the coupling strength, interaction non-additivity, and neutral damping rate. We found that the domain growth follows a power law with an exponent α of around 1/3, which is well in accordance with the Lifshitz-Slyozov growth law for the initial diffusion-driven stage of phase separation. We observe that the exponent of L is almost independent of the coupling strength unless the coupling is so high that large particles crystallize.

* * *

The authors would like to thank Dr V. Nosenko and Dr T. Shimizu for helpful discussions. KJ would like to thank I. Weidl for the technical support in running all our simulations on the IBM Power6 supercomputer installed at Rechenzentrum Garching.

REFERENCES

[1] Shukla P. K. and Eliasson B., *Rev. Mod. Phys.*, **81** (2009) 25.
[2] Morfill G. E. and Ivlev A. V., *Rev. Mod. Phys.*, **81** (2009) 1353.
[3] Fortov V., Ivlev A., Khrapak S. and Morfill G., *Phys. Rep.*, **421** (2005) 1.
[4] Fortov V. E. and Morfill G. E., *Complex and Dusty Plasmas: From Laboratory to Space* (CRC Press Taylor & Francis Group) 2009.
[5] Morfill G. E., Konopka U., Kretschmer M., Rubin-Zuzic M., Thomas H. M., Zhdanov S. K. and Tsytovich V., *New J. Phys.*, **8** (2006) 7.
[6] Sütterlin K. R., Wysocki A., Ivlev A. V., Räth C., Thomas H. M., Rubin-Zuzic M., Goedheer W. J., Fortov V. E., Lipaev A. M., Molotkov V. I., Petrov O. F., Morfill G. E. and Löwen H., *Phys. Rev. Lett.*, **102** (2009) 085003.
[7] Jiang K., Du C.-R., Sütterlin K. R., Ivlev A. V. and Morfill G. E., *EPL*, **92** (2010) 65002.
[8] Sütterlin K., Thomas H., Ivlev A., Morfill G., Fortov V., Lipaev A., Molotkov V., Petrov O., Wysocki A. and Löwen H., *IEEE Trans. Plasma Sci.*, **38** (2010) 861.
[9] Sütterlin K. R., Wysocki A., Räth C., Ivlev A. V., Thomas H. M., Khrapak S., Zhdanov S., Rubin-Zuzic M., Goedheer W. J., Fortov V. E., Lipaev A. M., Molotkov V. I., Petrov O. F., Morfill G. E. and Löwen H., *Plasma Phys. Control. Fusion*, **52** (2010) 124042.
[10] Ivlev A. V., Zhdanov S. K., Thomas H. M. and Morfill G. E., *EPL*, **85** (2009) 45001.
[11] Wysocki A., Räth C., Ivlev A. V., Sütterlin K. R., Thomas H. M., Khrapak S., Zhdanov S., Fortov V. E., Lipaev A. M., Molotkov V. I., Petrov O. F., Löwen H. and Morfill G. E., *Phys. Rev. Lett.*, **105** (2010) 045001.
[12] Hartmann P., Donkó Z., Kalman G. J., Kyrkos S., Golden K. I. and Rosenberg M., *Phys. Rev. Lett.*, **103** (2009) 245002.
[13] de Hoog E. H. A., Kegel W. K., van Blaaderen A. and Lekkerkerker H. N. W., *Phys. Rev. E*, **64** (2001) 021407.
[14] Aarts D. G. A. L., Dullens R. P. A. and Lekkerkerker H. N. W., *New J. Phys.*, **7** (2005) 40.
[15] Löwen H., *Soft Matter*, **6** (2010) 3133.
[16] Debye P. and Kleboth K., *J. Chem. Phys.*, **42** (1965) 3155.
[17] Tsori Y., *Rev. Mod. Phys.*, **81** (2009) 1471.
[18] Tsori Y., Tournilhac F. and Leibler L., *Nature*, **430** (2004) 544.
[19] Vaulina O. S. and Khrapak S. A., *JETP*, **90** (2000) 287.
[20] Hartmann P., Douglass A., Reyes J. C., Matthews L. S., Hyde T. W., Kovács A. and Donkó Z., *Phys. Rev. Lett.*, **105** (2010) 115004.
[21] Lifshitz I. and Slyozov V., *J. Phys. Chem. Solids*, **19** (1961) 35.
[22] Huse D. A., *Phys. Rev.B*, **34** (1986) 7845.
[23] Siggia E. D., *Phys. Rev. A*, **20** (1979) 595.
[24] Shinozaki A. and Oono Y., *Phys. Rev. E*, **48** (1993) 2622.
[25] Hohenberg P. C. and Halperin B. I., *Rev. Mod. Phys.*, **49** (1977) 435.
[26] Tanaka H., *J. Phys.: Condens. Matter*, **12** (2000) R207.
[27] Kendon V. M., Desplat J.-C., Bladon P. and Cates M. E., *Phys. Rev. Lett.*, **83** (1999) 576.
[28] Puri S. and Wadhawan V., *Kinetics of Phase Transitions* (CRC Press) 2009.
[29] Ma W.-J., Maritan A., Banavar J. R. and Koplik J., *Phys. Rev. A*, **45** (1992) R5347.
[30] Laradji M., Toxvaerd S. and Mouritsen O. G., *Phys. Rev. Lett.*, **77** (1996) 2253.
[31] Thakre A. K., den Otter W. K. and Briels W. J., *Phys. Rev. E*, **77** (2008) 011503.
[32] Allen M. P. and Tildesley D. J., *Computer Simulation of Liquids* (Clarendon Press, Oxford) 1987.
[33] Hou L. J., Mišković Z. L., Piel A. and Shukla P. K., *Phys. Plasmas*, **16** (2009) 053705.
[34] Thomas H. M., Morfill G. E., Fortov V. E., Ivlev A. V., Molotkov V. I., Lipaev A. M., Hagl T., Rothermel H., Khrapak S. A., Sütterlin R. K., Rubin-Zuzic M., Petrov O. F., Tokarev V. I. and Krikalev S. K., *New J. Phys.*, **10** (2008) 033036.
[35] Amar J. G., Sullivan F. E. and Mountain R. D., *Phys. Rev. B*, **37** (1988) 196.
[36] Yelash L., Virnau P., Paul W., Binder K. and Müller M., *Phys. Rev. E*, **78** (2008) 031801.
[37] Bucior K., Yelash L. and Binder K., *Phys. Rev. E*, **77** (2008) 051602.
[38] Ott T. and Bonitz M., *Phys. Rev. Lett.*, **103** (2009) 195001.

Demixing in Binary Complex Plasma: Computer Simulation

Ke Jiang, Lu-Jing Hou, Alexei V. Ivlev, Yang-Fang Li, K. Robert Sütterlin, Hubertus M. Thomas, and Gregor E. Morfill

***Abstract*—Computer simulations are employed to investigate the phase separation (demixing) phenomenon induced by interaction nonadditivity in binary complex plasmas with two different sized microparticles. The system firstly coarsens, and small particles start gathering and forming small clusters inside the large-particle phase, while there are no clear boundaries between two species. Next, sharp interfaces build up while the small-particle clusters merge into droplets and small droplets continue to merge into big ones. Finally, the two species completely separate from each other, and the small particles tend to form big droplets of nearly spherical shape, due to the surface tension.**

***Index Terms*—Author, please supply index terms/keywords for your paper. To download the IEEE Taxonomy, go to http://www.ieee.org/documents/2009Taxonomy_v101.pdf.**

A COMPLEX plasma is a suspension of micrometer-sized particles immersed in a plasma with ions, electrons, and neutral gas. Dust particles acquire a few thousands of electron charges by absorbing the surrounding electrons and ions and consequently interact with each other via a Debye–Hückel potential, while undergoing Brownian motion due to frequent collisions with neutrals. When the interaction potential energy between charged dust particles significantly goes beyond their kinetic energy, they become strongly coupled and form ordered structures of a liquid and/or solid state. The complex plasma has been regarded as an ideal model system to study various phenomena in liquids and solids as well as strongly coupled Coulomb systems at kinetic level. Recently, complex plasmas with different types of dust particles are gaining more and more attentions as these systems could have much richer phase diagram, structures, and dynamic properties than the single component ones. Moreover, recent experiments [1], [2] with binary complex plasmas (complex plasmas with two different types of dust particles) under microgravity conditions have demonstrated their promising prospect, as so many interesting phenomena have been observed, such as lane formation [1] and phase separation [2].

Phase separation, in which different types of particles tend to separate from each other, is a ubiquitous phenomenon in many different systems of multicomponent mixtures, such as molecular fluids and colloidal suspensions, and has been a long-standing research topic in physics because of both its fundamental and practical importance. It can be stimulated by either the interplay between individual particles, such as the interaction nonadditivity (which will be explained shortly), or external perturbations, such as shear flow, temperature gradient, and electric field. The phase separation is a scaling phenomenon with the average domain size following a power law and is sequenced to a series of domain growth regimes with different growth exponents peculiar to each regime. The diffusive regime obeys the power law with a growth exponent of 1/3, where diffusion is the dominant mechanism driving like particles to accumulate in the formation of tiny clusters. After the formation of clear interfaces between unlike particles, the minimization of interfacial energy becomes the dominant mechanism. This regime is termed as the viscous regime with domain growth following a linear scaling law. The last regime with a growth exponent of 2/3 is known as the inertial regime, where the segregation is dominated by inertia due to the increase of the Reynolds number. There have been many numerical simulations studying different regimes and the crossover between them. For example, the hydrodynamic viscous regime has been numerically studied with "model H." The viscous regime and inertial regime are also studied with lattice-based methods. Molecular dynamics simulations have also been used to resolve the dynamics on an atomistic level, mainly on Lenard–Jones fluid mixtures.

In complex plasmas, phase separation was reported by Sütterlin *et al.* [1] from microgravity experiments on board the ISS. Ivlev *et al.* [3] have recently shown in theory that, in a binary complex plasma, the interspecies interaction is always asymmetrical, i.e., for point particles of types "1" and "2," the 1–2 (interspecies interaction) is always more repulsive than the geometric mean of the 1–1 and 2–2 interactions. This asymmetry in the mutual interaction is called "interaction nonadditivity," and in the case of complex plasma, one has always a positive nonadditivity. According to the theory, such a nonadditivity leads to a spinodal region (where the fluid mixture is unstable and different species turn to demix), which overlaps with typical experimental conditions of complex plasmas in the laboratory. This explains well the phase separation phenomena observed in recent experiments and also makes binary complex plasmas a promising model system for studying the kinetics of phase separation [3].

Our simulation, as a complementary of both theory and experiment, is based on the Langevin dynamics method. All our

Manuscript received November 29, 2010; accepted May 1, 2011.

The authors are with the Max-Planck Institute for Extraterrestrial Physics, 85741 Garching, Germany (e-mail: jiang@mpe.mpg.de; hou@mpe.mpg.de; ivlev@mpe.mpg.de; yfli@mpe.mpg.de; robert@mpe.mpg.de; thomas@mpe.mpg.de; gem@mpe.mpg.de).

Digital Object Identifier 10.1109/TPS.2011.2153878

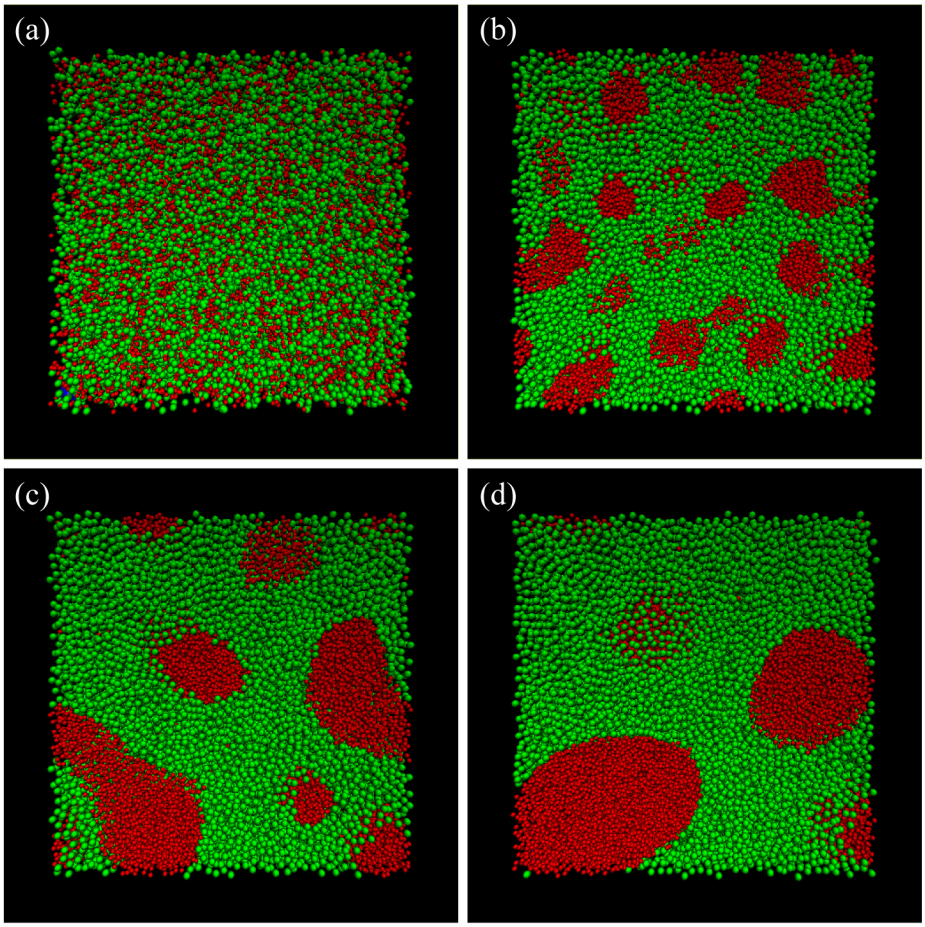

Fig. 1. Demixing in binary complex plasmas. Typical snapshots at four different stages. (a) At $t = 0$, particles are randomly distributed. (b) At $t = 2$ s, small particles gathered locally. (c) At $t = 4$ s, the initial domains start to coarse. (d) At $t = 20$ s, sharp interfaces build up while small red domains merge into big ones. Small (3.4 μm) particles are colored in red, and big (10.2 μm) particles are in green.

simulations started from randomly distributed configurations of particles. 10^5 of two different sized dust particles with off-critical composition are employed in a cubic simulation domain with a length of 1.1 cm and with periodic boundaries. Fig. 1 shows snapshots at four different time stages demonstrating the typical sequence. One sees that, starting from a random mixture as in Fig. 1(a), the system firstly coarsens, and there are no clear boundaries between two species, as shown in Fig. 1(b). Next, sharp interfaces build up while small red domains merge into big ones, as shown in Fig. 1(c) and (d). One can also observe that, in Fig. 1(d), at the final stage, one can observe that the small particles tend to form big droplets of nearly spherical shape, indicating that the nonadditivity-induced interfacial tension starts to play a role.

Thus, we have performed Langevin dynamics simulations to study the phase separation in binary complex plasma with two different sized microparticles. Our simulation vividly shows the dynamics of demixing processes of two species and complements the recent experimental observation of the demixing phenomenon in binary complex plasma. More detailed results will be presented elsewhere.

References

[1] K. R. Sütterlin, A. Wysocki, A. V. Ivlev, C. Räth, H. M. Thomas, M. Rubin-Zuzic, W. J. Goedheer, V. E. Fortov, A. M. Lipaev, V. I. Molotkov, O. F. Petrov, G. E. Morfill, and H. Löwen, "Dynamics of lane formation in driven binary complex plasmas," *Phys. Rev. Lett.*, vol. 102, no. 8, p. 085 003, Feb. 2009.

[2] A. Wysocki, C. Räth, A. V. Ivlev, K. R. Sütterlin, H. M. Thomas, S. Khrapak, S. Zhdanov, V. E. Fortov, A. M. Lipaev, V. I. Molotkov, O. F. Petrov, H. Löwen, and G. E. Morfill, "Kinetics of fluid demixing in complex plasmas: Role of two-scale interactions," *Phys. Rev. Lett.*, vol. 105, no. 4, p. 045 001, Jul. 2010.

[3] A. V. Ivlev, S. K. Zhdanov, H. M. Thomas, and G. E. Morfill, "Fluid phase separation in binary complex plasmas," *Europhys. Lett.*, vol. 85, no. 4, p. 45 001, Feb. 2009.

A Letters Journal Exploring the Frontiers of Physics

December 2010

EPL, **92** (2010) 65002
doi: 10.1209/0295-5075/92/65002

www.epljournal.org

Lane formation in binary complex plasmas: Role of non-additive interactions and initial configurations

K. Jiang[(a)], C.-R. Du, K. R. Sütterlin, A. V. Ivlev and G. E. Morfill

Max Planck Institute for Extraterrestrial Physics - 85741 Garching, Germany, EU

received 27 September 2010; accepted in final form 30 November 2010
published online 12 January 2010

PACS 52.27.Lw – Dusty or complex plasmas; plasma crystals
PACS 64.75.Cd – Phase equilibria of fluid mixtures, including gases, hydrates, etc.
PACS 64.75.Gh – Phase separation and segregation in model systems (hard spheres, Lennard-Jones, etc.)

Abstract – In this letter, we study the influence of non-additive interactions on lane formation, using Langevin dynamics simulations. Lane formation and positive non-additivity have recently been observed in binary complex plasmas on board the International Space Station (ISS). Positive non-additivity of particle interactions is known to stimulate phase separation (demixing), but its effect on lane formation is unknown. We show that there is a non-additivity–stimulated crossover from the normal laning mode to a demixing-dominated laning mode. To analyze this crossover on the individual particle level we applied a very sensitive order parameter for lane formation based on anisotropic scaling indices. Extensive numerical simulations enabled us to identify a critical value of the non-additivity parameter Δ for the crossover. In addition the simulations revealed that the dynamics of lane formation is strongly influenced by the exact spatial configurations at the very moment of contact between two different complex plasmas.

Introduction. – The formation of lanes can be found pervasively in nature when two species are moving toward and penetrating into each other. It is commonly known from pedestrian dynamics in highly populated pedestrian areas [1] that human beings tend to form lanes to maximize the traffic flow. A similar phenomenon was also found in army ants, the formation of distinct traffic lanes is favorable in order to minimize congestion [2]. Lane formation, as an instability on the particle scale, also drew significant attention in different branches of physics, such as colloidal dispersions [3–6], lattice gases [7], molecular ions [8], and recently, in complex plasmas [9,10].

Complex plasmas consist of micron-sized particles immersed in a plasma, where dust particles are normally negatively charged and interact with each other via a screened Coulomb potential [11–13]. The first lane formation experiments in binary complex plasmas [9] were carried out under microgravity conditions with a rf discharge in the PK-3 Plus laboratory [14]. In these experiments, two different sizes of spherical melamine-formaldehyde (MF) microparticles were used. Small microparticles were driven and penetrated into a fairly homogeneous cloud formed by large particles. The penetration featured remarkable streaming lanes, as can be seen in fig. 1. In refs. [9] and [10] this phenomenon was compared to Langevin dynamics (LD) simulations assuming an additive Yukawa interaction between particles to emphasize the physics leading to lane formation. Even though demixing was noticed in the same experiment the influence of it was specifically neglected in these previous publications. In binary complex plasmas the inter-particle interaction exhibits asymmetry, *i.e.*, for point particles of type "1" and "2" with purely repulsive interaction, the 1-2 (inter-species) interaction is always more repulsive than the geometric mean of 1-1 and 2-2 interactions [15]. This asymmetry in the mutual interaction is called "interaction non-additivity", and in the case of complex plasma it is always positive, which will stimulate demixing (phase separation). Numerical simulations of the phase separation in the absence of lane formation have been performed [16,17].

In this letter, we present extensive numerical simulations regarding lane formation in non-additive binary complex plasmas. This complements the previous studies on dynamics of lane formation in two fundamental ways. First, we could confirm the significant effect of initial configurations on both the onset and evolution of lanes, which was believed to be important in

[(a)] E-mail: jiang@mpe.mpg.de

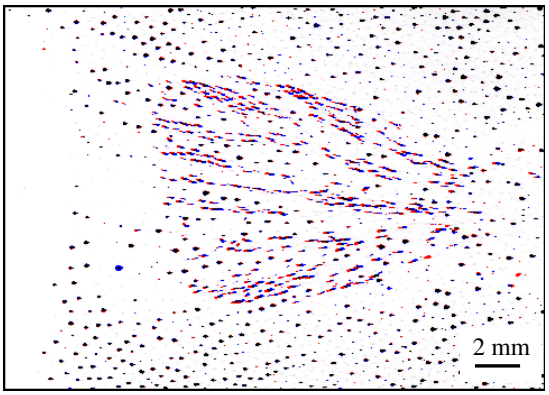

Fig. 1: (Color online) Lane formation in complex plasmas. A short burst of small (3.4 μm) particles —seen as elongated red-blue streaks— is injected into a cloud of large (9.2 μm) background particles —the almost round black spots. Small particles are driven towards the right. Lanes are formed by both small and large particles. The image is an overlay of two consecutive frames recorded in the experiment with a frame rate of 50 Hz, color coded red for first frame and blue for second frame.

the non-equilibrium laning transition [10]. Second, our analysis shows a crossover from normal laning mode to demixing-stimulated laning mode.

Non-additivity in binary complex plasmas. – For both large and small particles in the binary mixture of complex plasmas we assume that they can be treated as point-like and that their electric potential is screened exponentially with the same screening length λ (plasma screening length), but different interaction magnitudes ε_{ij}. The general form of inter-particle interaction can then be written as

$$\phi_{ij}(r) = \varepsilon_{ij}\frac{\exp(-r/\lambda)}{r}. \tag{1}$$

For like-particle interaction, $\varepsilon_{ij} = \varepsilon_{SS/LL}$ is the product of the effective charge and the real charge $Z_{S/L}$ [15] (subscripts S and L denote small and large particles, respectively). According to the Lorentz-Berthelot mixing rules [18] for the interaction between unlike particles one gets

$$\varepsilon_{ij} = \varepsilon_{LS} = \varepsilon_{SL} = (1+\Delta)\sqrt{\varepsilon_{SS}\varepsilon_{LL}}. \tag{2}$$

Δ is the non-additivity parameter [15], which represents the asymmetry in the mutual interaction between unlike particles. Δ is always positive in binary complex plasmas [15]. Our model reduces to a typical Yukawa potential when $\Delta = 0$, which is the exact interaction model adopted in ref. [9].

Simulation. – In complex plasmas, dust particle motion can be described by the Langevin equation, which is a stochastic differential equation involving damping from neutral gas and Brownian motion of the dust particles:

$$\dot{\mathbf{p}}_i = \mathbf{F}_i - \gamma_i \mathbf{p}_i + \mathbf{R}_i, \tag{3}$$

where $\mathbf{p}_i$ is the momentum of dust particle i, γ_i is the dust neutral gas collision frequency, and is given as $\gamma_i = 1.48\frac{4\pi}{3}N_n m_n v_n \sigma_i^2/m_i$ as in [19,20], where N_n, m_n and v_n are the density, mass and thermal velocity of the neutral gas, and σ_i is the diameter of the particles, m_i is the mass of the dust particle. $\mathbf{F}_i = -\sum\nabla\phi + \mathbf{F}_{ext}$ in eq. (3) is the deterministic force comprised of interparticle interactions and external force fields. The last term, $\mathbf{R}_i(t)$, is a stochastic force representing the Brownian motion of dust particles in plasma. It is commonly described by a delta-correlated stationary Gaussian process with zero-mean satisfying

$$\langle \mathbf{R}_i(0)\mathbf{R}_i(t)\rangle = 2\gamma_i k_B T m_i \delta(t). \tag{4}$$

Here, δ is the Dirac delta. The stochastic force and friction are related through the fluctuation-dissipation theorem [21] (the cooling by friction should cancel the heating by noise). The Langevin equation, eq. (3), is numerically integrated using an extended Beeman [22] algorithm as described in refs. [18,23].

All the plasma and particle parameters are chosen according to the experiments established in refs. [9,10]: screening length $\lambda = 150\,\mu$m, charges $Z_S = 4000e$ and $Z_L = 11000e$, particle diameter $\sigma_S = 3.4\,\mu$m and $\sigma_L = 9.2\,\mu$m; mass density of MF particles $\rho_S = \rho_L = 1.5\,\mathrm{g/cm^3}$. This results in friction coefficients $\gamma_S = 250\,\mathrm{s^{-1}}$ and $\gamma_L = 92.4\,\mathrm{s^{-1}}$. The mean inter-particle distances (before the penetration) are $a_S = 464\,\mu$m and $a_L = 493\,\mu$m, respectively. The simulation was performed for a binary mixture of 5759 small and 12287 large particles within a simulation domain of $4.4\,\mathrm{cm}\times 0.8\,\mathrm{cm}\times 0.8\,\mathrm{cm}$ in the x, y and z directions. Periodic boundary conditions are used for the y and z directions and a free boundary is adopted for the x-direction. Large particles are confined with an external parabolic potential at two edges within a region of 2.2 cm width along x at the center of the simulation domain. Small particles are initially confined and equilibrated within a region of 0.7 cm width along x separated by 0.3 cm from the large particles. Then $\mathbf{F}_{ext} = 0.08\mathbf{e}_x$ pN, the force driving small particles into the large-particle cloud, was instantaneously applied. Simulation snapshots are shown in fig. 2.

In order to study the effect of the non-additivity on the laning pattern, a set of 1000 statistically independent initial particle configurations had been prepared. The random seeds for homogeneous distribution of small and big particles had been varied. Both species were equilibrated for a short time to remove the artificial heat. Then the system was evolved with five different values of Δ (0.0, 0.1, 0.2, 0.3, 0.5). This resulted in a total of 5000 different penetration events. In addition to finding a systematic dependance of lane formation on Δ, this enabled us to study the effect of initial configurations on lane formation phenomena.

Analysis. – In order to quantify the lane formation in the LD simulations, we employed an anisotropic scaling

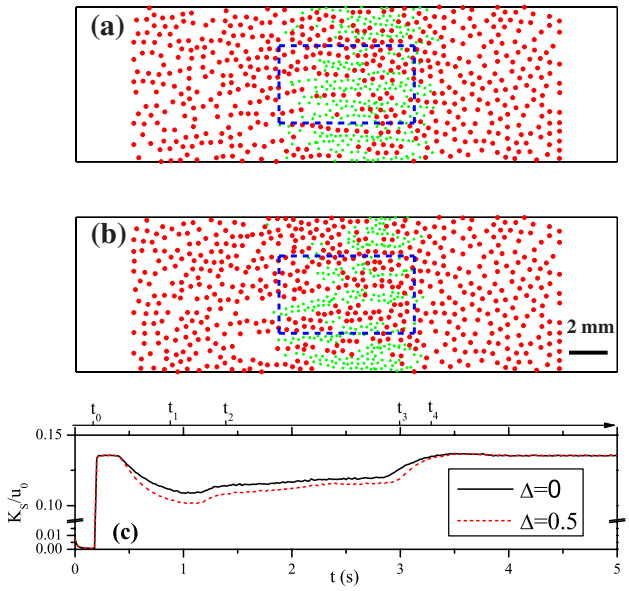

Fig. 2: (Color online) Comparison of two snapshots of lane formation in LD simulation for $\Delta = 0$ (a) and $\Delta = 0.5$ (b) taken at the same time step. Small particles (green) are driven from the left to the right through the cloud of large particles (red). Interestingly enough, small particles are able to penetrate faster for $\Delta = 0$. Also the lanes formed by both species are wider for larger Δ. The blue dashed box in each picture indicates the ROI in which we apply our analysis method. The evolution of the mean kinetic energy K_S of a single small particle during the whole penetration is shown in (c) with solid line representing the case of $\Delta = 0$ and dashed line representing $\Delta = 0.5$.

index method (ASIM) to realize a local nonlinear measure for structure characterization. Based on the weighted scaling index method [24], the anisotropic scaling index α is defined as

$$\alpha(\mathbf{r}_i, \xi, \epsilon, \theta) = \frac{2\sum_{j=1}^{N}(d_{ij}/\xi)^2 e^{-(d_{ij}/\xi)^2}}{\sum_{j=1}^{N} e^{-(d_{ij}/\xi)^2}}, \qquad (5)$$

where $d_{ij} = d(\mathbf{r}_i, \mathbf{r}_j, \epsilon, \theta)$ is the distance between particle i and j in a space stretched by ϵ along direction $\mathbf{u} = \binom{\cos\theta}{\sin\theta}$, $-\pi/2 \leqslant \theta \leqslant \pi/2$. The coordinates in the new space can be expressed by applying a stretch matrix $\Lambda = \left(\begin{smallmatrix} 1 & 0 \\ 0 & \epsilon \end{smallmatrix}\right)$ and rotation matrix $\Omega = \left(\begin{smallmatrix} \cos\theta & \sin\theta \\ \sin\theta & -\cos\theta \end{smallmatrix}\right)$ on the simulation coordinate, *i.e.*, $\mathbf{r}'_i = \Lambda\Omega\mathbf{r}_i$, and thus, $d_{ij} = |\mathbf{r}'_i - \mathbf{r}'_j|$. The parameter ξ defines a spatial scale on which the α index is sensitive. By determining the value of θ that maximizes the difference $\alpha(\mathbf{r}_i, \xi, \epsilon, \theta + \pi/2) - \alpha(\mathbf{r}_i, \xi, \epsilon, \theta)$ we obtained a "preferred" direction $\mathbf{u}_i$ associated with particle i, signifying the local anisotropy. The "length" of this anisotropy is given by ξ and ϵ describes the ratio between its "length" and "width". The ASIM has been applied not only in complex plasma [9,10,25] but also in, *e.g.*, cosmology [24] and medical technology [26].

In order to characterize the global laning, we defined a laning-order parameter S, which is the largest eigenvalue of a second-rank tensor $Q = 2N^{-1}\sum_{i=1}^{N} \mathbf{u}_i \otimes \mathbf{u}_i - I$, where I is identity matrix. $S = 1$ denotes a perfect alignment while $S = 0$ represents a perfectly random phase.

Following ref. [9], we divided the volume of the simulation box into several slabs ($350\,\mu$m wide) in the z-direction (perpendicular to $\mathbf{F}_{ext}$) and analyzed the quasi-2D stringlike structure in the (x,y)-plane. To allow the direct comparison of our results, we used the same spatial scale ξ and anisotropic aspect ratio ϵ, *i.e.*, $\xi = 1200\,\mu$m and $\epsilon = 5$ for large particles. In order to reduce boundary effects in the analysis, we selected a fixed region of interest (ROI) in the center of the large-particle cloud (see fig. 2). For the calculation of S, only large particles inside the ROI were taken into account.

As suggested in ref. [9], we expected lane formation to be very sensitive to the initial spatial configuration of both particle species. A slight topological deviation in the initial encounter of two particle clouds could result in large differences of the laning pattern and penetration speed, introducing a large variance in the evolution of the global laning-order parameter S. To evaluate the influence of initial particle configuration and to separate it from the systematic effect induced by non-additivity we analyzed a large set of statistically independent numerical simulations as described in the simulation part. Eventually, we end up with a family of functions $S_k(\Delta, t)$, where the index k denotes the specific initial configuration. For fixed Δ and t the values of S_k form a Gaussian-like distribution, for which we determined the mean $\langle S \rangle$ and standard deviation $\overline{S}$. As an example the results for $\Delta = 0$ are shown in fig. 3.

Results and discussions. – The penetration of small particles into a large-particle cloud can be sectioned into the following stages. After the initial equilibration of both species, the driving force was applied on small particles at time t_0. Small particles were driven toward the large-particle cloud until $t_1 \sim 50\%$ of the small particles entered the cloud of large particles. Both species formed lane structures during the penetration. For the convenience of analysis, we defined the time when the small particles moved into and out of ROI as t_2 and t_3, respectively. Eventually at t_4 50% of small particles moved out of the large-particle cloud.

Two snapshots of laning with non-additivity parameter $\Delta = 0$ and $\Delta = 0.5$ are shown in fig. 2. One can see the normal laning phenomenon in fig. 2(a), where narrow lanes —at most 2 particles across— can be observed for both small and large particles. Whereas in fig. 2(b), one can see the demixing-stimulated laning mode. Like particles try to cluster due to the non-additivity and a demixing-stimulated laning mode is achieved. The averaged kinetic energy of small particles (total kinetic energy divided by small particle number), K_S, is shown in fig. 2(c), where the normalized factor $u_0 = 1.2 \times 10^{-10}$ erg. One can also see that K_S increases significantly after applying the driving

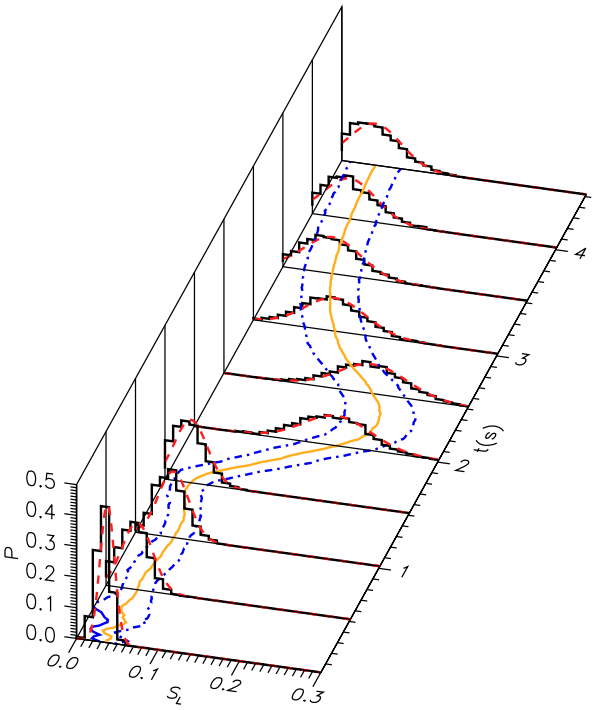

Fig. 3: (Color online) Role of the initial configurations. Temporal evolution of S_L, the global laning-order parameter for large particles, for $\Delta = 0$. The solid line (orange) shows the evolution of the mean value $\langle S_L \rangle$, the dash-dotted lines (blue) give the standard deviation $\overline{S}$. Normalized histograms of the original distribution of S_L at ten equidistant timesteps are displayed (solid black) for reference. Dashed lines (red) highlight the Gaussian fit to these histograms. For the first 0.5 s $\langle S_L \rangle$ shows some fluctuations due to incomplete thermalization. Small particles enter the ROI at $t \sim 1.5$ s. S_L has significant variance reflecting the strong influence of the initial particle configuration on lane formation.

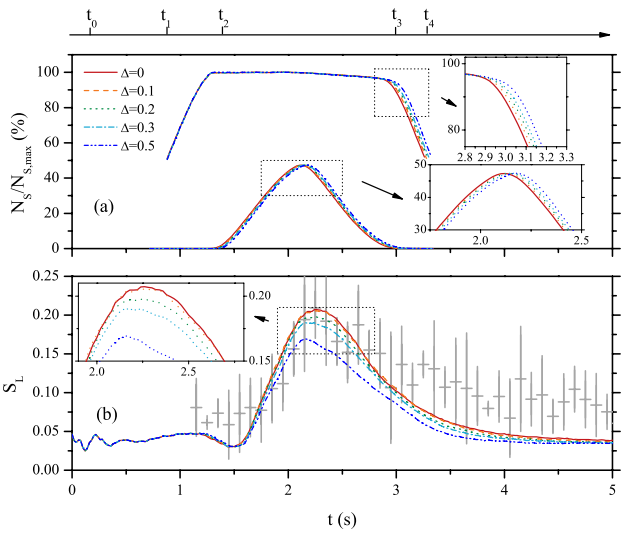

Fig. 4: (Color online) Dependance of lane formation on the non-additivity parameter Δ. (a) Percentage of small particles inside the cloud of large particles (upper curves) and the ROI (lower curves). Penetration speed depends on Δ, small particles need more time to cross the cloud of big particles for larger values of Δ. (b) The temporal evolution of $\langle S_L \rangle$. The values of $\langle S_L \rangle$ decreases systematically with increasing Δ. For comparison, the experiment results including error bars are overplotted.

force and then decreases when the initial contact between small particles and large-particle cloud occurs. Then K_S increases gradually between t_2 and t_3 when the lanes are formed. It is clear that the penetration speed $\langle v_S \rangle$ is slower in the case of $\Delta = 0.5$ than $\Delta = 0$ (both in the order of 1 cm/s), which can also be seen from the snapshots (cf. fig. 4(a)).

As mentioned in the simulation part, the initial configurations were varied. This resulted in different spatial configurations of the initial contact at t_1, which consequently leads to the variance of S_L, as shown in fig. 3. Initially at t_0 the distribution of $S_k(\Delta, t)$ for large particles in the ROI is peaked very strongly, and broadens slightly till the impact of small particles at t_1, mainly due to thermalization of the initial configurations. The distribution of S_k stays relatively stable until at t_2 small particles start to flow into the ROI, when the initial spatial deviations are magnified by the lane formation process. The standard deviation $\overline{S}_L$ is doubled. Even after t_3 when the small particles leave the ROI and the large particles approach their undisturbed equilibrium, the variance in the distribution of S_k is not decreased in this relaxation process. This information is critical for experimental and numerical studies since one should not make decisive conclusions based on a few events. A rather large ensemble is necessary to separate the random influence of initial configurations from the systematic derivation that researchers are interested in, such as the non-additivity effect in this letter.

The systematic influence of non-additivity on the laning mode is studied using the average speed of small particles inside the cloud of large paticles (fig. 4(a)) and the mean global order parameter for large particles $\langle S_L \rangle(\Delta, t)$ (fig. 4(b)). For $\Delta = 0$ small particles leave the large-particle cloud earlier than for higher non-additivity. This translates directly to a higher penetration speed $\langle v_S \rangle$. From the insert in fig. 4(a) it is clear that $\langle v_S \rangle$ decreases with Δ as we have shown in fig. 2(c).

The role of non-additivity can be very well probed by the mean global order parameter for large particles $\langle S_L \rangle(\Delta, t)$ as shown in fig. 4(b). The fluctuation of $\langle S_L \rangle$ between t_0 and t_1 are unrelated to the value of Δ. Small particles are not playing a role at this stage —due to the short range of the inter-particle interaction potential— and therefore non-additivity does not yet have any influence on $\langle S_L \rangle$. The cloud of large particles is still equilibrating, and reaches some intermediate plateau $\langle S_L \rangle \sim 0.02$ at $t \sim 0.5$ s. This finite initial value can be explained by the small number of large particles inside the ROI $\langle N_L \rangle \sim 100$, which limits the "homogeneity" of the ensemble.

Right before the penetration of small particles into the ROI at t_2, large particles inside this area are compressed by the wave front excited by small particles and $\langle S_L \rangle$ shows a dip. The damping length of acoustic waves in the large-particle cloud is estimated to be $l_D = \omega_L \lambda / \gamma_L = 110\,\mu$m (within 1 a_L), where ω_L is the dust plasma frequency of big particles. This explains why the dip of $\langle S_L \rangle$ starts to emerge slightly before the small particles entering the ROI. Between t_1 and t_2, lanes are formed inside the ROI and $\langle S_L \rangle$ peaks up. The main effect of non-additivity on the evolution of $\langle S_L \rangle$ is the decrease of the peak value from 0.21 for $\Delta = 0$ to 0.17 for $\Delta = 0.5$ (see insert in fig. 4(b)). This can be explained by the change in morphology of the lanes formed by the particles. The global order parameter is sensitive to structures as defined by the parameters $\xi = 1200\,\mu$m and $\epsilon = 5$ chosen for the ASIM. These values were taken from refs. [9,10], that were optimized for simulations of additive particle interactions. The peak value therefore relates to the deviation from long narrow lines in the cases of increasing non-additivity.

After t_4 when most small particles have left the ROI, the large particles relax towards thermal equilibrium, $\langle S_L \rangle$ slowly decaying towards its base value ($\langle S_L \rangle \sim 0.03$). Still the system is in a different state than before the penetration of small particles. This can be derived from the change of $\overline{S}_L$ and histogram of S_L at the initial stage of evolution as can be seen in fig. 3.

Conclusions. – Langevin dynamics simulations are employed to investigate the lane formation phenomenon with additive and non-additive particle interactions in binary complex plasmas under microgravity conditions. A crossover from the normal laning mode to a demixing-dominated laning mode is observed. This is similar to the transition from lane formation to classical Rayleigh-Taylor instability. For regular fluids this can be described in terms of the Weber number, which is the ratio of kinetic energy to surface tension [6]. However in mesoscopic systems hydrodynamic parameters like the surface tension are not well defined. Furthermore, for dissipative systems (such as complex plasmas or colloidal suspensions) the concept of a driving force (rather than energy) is more appropriate. Therefore F_{ext}/Δ, the ratio of the magnitude of the driving force to the non-additivity parameter (the microscopic source for surface tension), is the unambiguous way to describe the crossover, which is investigated for fixed F_{ext} by increasing Δ. For a vanishing non-additivity parameter, $\Delta = 0$, which would correspond to an infinite Weber number in the macroscopic case, small particles driven by an external force penetrate into large-particle clouds and form lane structures. When Δ is increased, the non-additivity–induced surface tension is built up, which would correspond to a decrease of the Weber number in a macroscopic system. Droplet-like lanes are formed and clear interfaces between unlike species emerge. A sensitive order parameter based on anisotropic scaling indices enabled us to measure the influence of non-additivity and to identify the critical value of the non-additivity parameter ($\Delta > 0.1$) for the crossover. A huge number of simulations is necessary not only to reduce the influence of random fluctuations, but also to highlight the importance of the initial configurations. Even though the initial configurations are thermodynamically equivalent, the minuscule details of single-particle kinetics define the dynamics of laning.

* * *

The authors would like to thank A. Wysocki, H. Löwen, L.-J. Hou and C. Räth for helpful discussions, the members of the theory group of Max-Planck-Institute for extraterrestrial physics, for supplying ample computing time on their XGRID cluster. This work was supported by "Die Raumfahrt-Agentur des Deutschen Zentrums für Luft und Raumfahrt e. V. mit Mitteln des Bundesministeriums für Wirtschaft und Technologie aufgrund eines Beschlusses des Deutschen Bundestages unter dem Förderkennzeichen 50 WP 0203".

REFERENCES

[1] Helbing D., Farkas I. J. and Vicsek T., *Phys. Rev. Lett.*, **84** (2000) 1240.
[2] Couzin I. D. and Franks N. R., *Proc. R. Soc. London, Ser. B*, **270** (2003) 139.
[3] Dzubiella J., Hoffmann G. P. and Löwen H., *Phys. Rev. E*, **65** (2002) 021402.
[4] Leunissen M. E., Christova C. G., Hynninen A.-P., Royall C. P., Campbell A. I., Imhof A., Dijkstra M., van Roij R. and van Blaaderen A., *Nature*, **437** (2005) 235.
[5] Rex M. and Löwen H., *Eur. Phys. J. E*, **26** (2008) 143.
[6] Wysocki A. and Löwen H., *J. Phys.: Condens. Matter*, **16** (2004) 7209.
[7] Schmittmann B. and Zia R. K. P., *Phys. Rep.*, **301** (1998) 45.
[8] Netz R. R., *Europhys. Lett.*, **63** (2003) 616.
[9] Sütterlin K. R., Wysocki A., Ivlev A. V., Räth C., Thomas H. M., Rubin-Zuzic M., Goedheer W. J., Fortov V. E., Lipaev A. M., Molotkov V. I., Petrov O. F., Morfill G. E. and Löwen H., *Phys. Rev. Lett.*, **102** (2009) 085003.
[10] Sütterlin K., Thomas H., Ivlev A., Morfill G., Fortov V., Lipaev A., Molotkov V., Petrov O., Wysocki A. and Löwen H., *IEEE Trans. Plasma Sci.*, **38** (2010) 861.
[11] Shukla P. K. and Mamun A. A., *Introduction to Dusty Plasma Physics* (Institute of Physics Publishing, Bristol, Philadelphia) 2002.
[12] Shukla P. K. and Eliasson B., *Rev. Mod. Phys.*, **81** (2009) 25.
[13] Morfill G. E. and Ivlev A. V., *Rev. Mod. Phys.*, **81** (2009) 1353.
[14] Thomas H. M., Morfill G. E., Fortov V. E., Ivlev A. V., Molotkov V. I., Lipaev A. M., Hagl T., Rothermel H., Khrapak S. A., Sütterlin R. K., Rubin-Zuzic M., Petrov O. F., Tokarev V. I. and Krikalev S. K., *New J. Phys.*, **10** (2008) 033036.

[15] Ivlev A. V., Zhdanov S. K., Thomas H. M. and Morfill G. E., *EPL*, **85** (2009) 45001.
[16] Wysocki A., Räth C., Ivlev A. V., Sütterlin K. R., Thomas H. M., Khrapak S., Zhdanov S., Fortov V. E., Lipaev A. M., Molotkov V. I., Petrov O. F., Löwen H. and Morfill G. E., *Phys. Rev. Lett.*, **105** (2010) 045001.
[17] Jiang K., Hou L. J., Ivlev A. V., Li Y. F., Sütterlin K. R., Du C.-R., Thomas H. M. and Morfill G. E., to be submitted to *EPL*.
[18] Allen M. P. and Tildesley D. J., *Computer Simulation of Liquids* (Clarendon Press, Oxford) 1987.
[19] Epstein P. S., *Phys. Rev.*, **23** (1924) 710.
[20] Konopka U., *Wechselwirkungen geladener Staubteilchen in Hochfrequenzplasmen,* PhD thesis, Ruhr-Universität-Bochum (July 2007).
[21] Lemons D. S., *An Introduction to Stochastic Processes* (John Hopkins University Press) 2002.
[22] Beeman D., *J. Comput. Phys.*, **20** (1976) 130.
[23] Hou L. J., Mišković Z. L., Piel A. and Shukla P. K., *Phys. Plasmas*, **16** (2009) 053705.
[24] Räth C., Bunk W., Huber M. B., Morfill G. E., Retzlaff J. and Schuecker P., *Mon. Not. R. Astron. Soc.*, **337** (2002) 413.
[25] Ivlev A. V., Morfill G. E., Thomas H. M., Räth C., Joyce G., Huber P., Kompaneets R., Fortov V. E., Lipaev A. M., Molotkov V. I., Reiter T., Turin M. and Vinogradov P., *Phys. Rev. Lett.*, **100** (2008) 095003.
[26] Räth C., Monetti R., Bauer J., Sidorenko I., Müller D., Matsuura M., Lochmüller E.-M., Zysset P. and Eckstein F., *New J. Phys.*, **10** (2008) 125010.

epl A Letters Journal Exploring the Frontiers of Physics

February 2009

EPL, **85** (2009) 45002 www.epljournal.org
doi: 10.1209/0295-5075/85/45002

Mach cones in a three-dimensional complex plasma

K. Jiang[1(a)], V. Nosenko[1], Y. F. Li[1], M. Schwabe[1], U. Konopka[1], A. V. Ivlev[1], V. E. Fortov[2], V. I. Molotkov[2], A. M. Lipaev[2], O. F. Petrov[2], M. V. Turin[3], H. M. Thomas[1] and G. E. Morfill[1]

[1] *Max-Planck-Institut für extraterrestrische Physik - D-85741 Garching, Germany, EU*
[2] *Joint Institute for High Temperatures, RAS - Izhorskaya Street, 13/19, Moscow, 125412 Russia*
[3] *RSC "Energia" Korolev - 141070 Moscow Region, Russia*

received 19 August 2008; accepted in final form 2 February 2009
published online 4 March 2009

PACS 52.27.Lw – Dusty or complex plasmas; plasma crystals
PACS 52.35.Fp – Electrostatic waves and oscillations (*e.g.*, ion-acoustic waves)
PACS 47.40.-x – Compressible flows; shock waves

Abstract – A three-dimensional hydrodynamic model has been applied to study the Mach cones in a three-dimensional complex plasma. Numerical results for the velocity distribution of dust particles showed the presence of compressional-wave Mach cones. The compressional Mach cones were excited when subjected to supersonic excitations. It was found that multi-cone structures became a single cone when the discharge pressure was increased. The experiment of Mach cones in a three-dimensional complex plasma under microgravity conditions on board the International Space Station was also reported. A single compressional-wave Mach cone in a three-dimensional complex plasma was observed and could also be obtained from our hydrodynamic model.

Introduction. – A complex plasma (or dusty plasma) [1–4] is a partially ionized gas (plasma) in which micron size dust particles are embedded. The dust particles in complex plasmas are electrically charged by collection of plasma electrons and ions. Microparticles in laboratory plasmas usually acquire negative charges of the order of 10^3 to 10^4 elementary charges and interact with each other in the direction perpendicular to the ion flow via a screened Coulomb (Yukawa) potential $\phi(r) = [(Z_d e)/r]\exp(-r/\lambda_D)$, where r is the distance, e is the electron charge, Z_d is the charge number of the particles and λ_D is the Debye screening length. Complex plasmas can be easily observed with a digital camera and therefore are used to investigate various physical phenomena dynamically [5].

Recently, wakes excited by a moving disturbance in a complex plasma have attracted much attention [6–22]. The structure of wakes is caused by constructive and destructive interference of waves excited by the moving disturbance, and their structures are determined by the wave dispersion properties of the medium as well as the details of the disturbance-medium interaction [13].

A Mach cone is a type of wake, which has a V-shaped structure in the two-dimensional (2D) case. The existence of Mach cones in complex plasmas was first predicted in theory by Havnes *et al.* [6,7] and later observed in a 2D plasma crystal by Samsonov *et al.* [8,9] and Melzer *et al.* [10]. Mach cones were excited by the electrostatic force from a charged particle moving spontaneously beneath a 2D lattice in refs. [8,9], and by the radiation force from a spot of focused laser beam scanned across the 2D complex plasma in ref. [10]. In these experiments, the observed Mach cones were composed of compressional waves. Shortly afterwards, shear-wave Mach cones composed of single cone, were observed in experiments by Nosenko *et al.* [11,12] by using a laser beam. Inspired by the studies above, various theoretical models [13–19] have been proposed to interpret these phenomena.

Mach cones in a three-dimensional (3D) complex plasma have been attracting attention since experiments under microgravity conditions were carried out [22], which generated 3D complex plasmas as expected. Recently, Bose *et al.* [23] presented a generalized hydrodynamic model to discuss the formation of a shear-wave Mach cone in a 3D complex plasma with the same excitation method as in refs. [11,12]. A single shear-wave Mach cone was reported and its formation was also studied. The wake patterns behind boulders in the rings of Saturn were studied by Brattli *et al.* [24] by using a fluid model. MD simulation was also utilized by Xin and Bhattacharjee [25] to study Mach cones in a 3D complex plasma. However, to

(a) E-mail: jiang@mpe.mpg.de

the best of our knowledge, experimental observations of Mach cones in 3D cases have not yet been reported.

The purpose of this paper is to develop a theoretical model to study Mach cones in 3D complex plasmas excited by a charged particle and report the observation of 3D Mach cones in complex plasmas from the PK-3 Plus project [26], which studies complex plasmas under microgravity conditions on the International Space Station (ISS) and offers a much better homogeneity of 3D complex plasmas than conventional studies. A hydrodynamic model similar as in ref. [24] is used to study Mach cones in a 3D complex plasma. In contrast to the previous theoretical account [24], we consider the neutral-gas drag force due to the collisions between particles and neutral atoms [27], which were shown to give rise to the exponential decay of waves and wakes [13]. The fluid model is generally believed to be strictly applicable in the weakly coupled complex plasma. However, it has been found out that even a fluid model could generate reasonable results [13] for the Mach cone formation in 2D dust crystals. The difference becomes significant only when the speed of the perturbation is very slow. This is due to the fact that in all these observations, the typical sizes of Mach cones in strongly coupled complex plasmas contain several tens of the dust lattice constants, so that a continuum limit may provide a reasonable approximation to some extent. The theory presented here has assumed a linear dynamics for the dust grains. The first-order perturbation approximation appears to be sufficient to explain qualitative aspects of the wake structure. The structure of wakes from linear theory has received close scrutiny in many studies [13,16,19,24]. However, nonlinear effects could play an important role if the interaction between the moving charge and the grains is sufficiently strong. For instance, the Earth's magnetotail formed by interaction with the solar wind, the shock wave behind a supersonic airplane. Besides, our intention with this work is not to reach a fully realistic and complete solution of the Mach cone study. A more complete theory should include nonlinearity to improve the precision in the near field close to the cone vertex. The results from our fluid model can only be regarded as approximations to the real wake pattern.

The paper is organized as follows. In the second section, the hydrodynamic model will be expressed in detail. The numerical results will also be shown in the third section. Experimental observation of Mach cones from PK-3 Plus in a 3D complex plasma will be shown in the fourth section. Finally, a short concluding remark is presented in the last section.

Theoretical model. – In the present work, we employ a fluid description of a 3D complex plasma, without considering the details of interactions among dust particles. Assuming that this fluid is immersed in a large volume of plasma, the continuity and momentum equations are, respectively,

$$\frac{\partial n_d(\mathbf{r},t)}{\partial t} + \nabla \cdot [n_d(\mathbf{r},t)\,\mathbf{u}_d(\mathbf{r},t)] = 0, \tag{1}$$

$$\frac{\partial \mathbf{u}_d(\mathbf{r},t)}{\partial t} + \mathbf{u}_d(\mathbf{r},t)\cdot\nabla\mathbf{u}_d(\mathbf{r},t) = \frac{Z_d e}{m_d}\nabla\Phi(\mathbf{r},t) + \frac{\mathbf{F}_{Ep}}{m_d}, \tag{2}$$

and the Poisson equation

$$\begin{aligned}\nabla^2\Phi(\mathbf{r},t)/4\pi e = {} & Z_d n_d(\mathbf{r},t) + Z_t\delta(\mathbf{r}-\mathbf{v}t) \\ & + n_e(\mathbf{r},t) - n_i(\mathbf{r},t),\end{aligned} \tag{3}$$

where $\Phi(\mathbf{r},t)$ stands for the electrostatic potential in a Cartesian coordinate system with $\mathbf{r}=\{x,y,z\}$, while $n_d(\mathbf{r},t)$, and $\mathbf{u}_d(\mathbf{r},t)$ represent the number density and the velocity field of the dust fluid. The forces exerted on the particles include electric force, and the Epstein drag force [27] $\mathbf{F}_{Ep}$ coming from the collisions of the dust particles with the neutral atoms and molecules in the plasma. Also in the equations, e is the elementary charge, m_d is the mass of a dust particle, Z_d is the average charge number on each particle in the complex plasma region. It is worth mentioning that we use a δ-function in the Poisson equation to stand for the test particle with velocity $\mathbf{v}$ and charge number Z_t.

The neutral drag force $\mathbf{F}_{Ep}$ is described as

$$\mathbf{F}_{Ep} = -\gamma_{Ep} m_d \mathbf{u}_d(\mathbf{r},t) = -\delta_{Ep}\frac{4\pi}{3} N_n m_n v_n r_d^2 \mathbf{u}_d(\mathbf{r},t), \tag{4}$$

where N_n, m_n and v_n are the neutral-gas density, mass and thermal velocity of the neutral molecules, and r_d is the radius of the microparticles, γ_{Ep} is the Epstein drag coefficient, and δ_{Ep} is a coefficient which depends on the interaction of the microparticles with the gas atoms.

In a complex plasma, the mobility of electrons and ions is sufficient to reach their respective local equilibria comparing with the massive dust particles. Therefore, the ion and electron densities are given by the Boltzmann relations $n_i = n_0\exp(-e\Phi/T_i)$ and $n_e = n_0\exp(e\Phi/T_e)$, with T_i and T_e being the ion and electron temperatures, respectively. The theory presented here has assumed linear dynamics for the dust particles, as this appoximation appears to be sufficient to explain the wake structure qualitatively [13]. Therefore, a first-order perturbation is employed here to study the particle behavior, in which $n_d(\mathbf{r},t) = n_{d0} + n_{d1}(\mathbf{r},t)$, $\mathbf{u}_d(\mathbf{r},t) = \mathbf{u}_{d1}(\mathbf{r},t)$, $\Phi(\mathbf{r},t) = \Phi_0 + \Phi_1(\mathbf{r},t)$, $n_e(\mathbf{r},t) \approx n_0 + n_0(e/T_e)\Phi_1(\mathbf{r},t)$, and $n_i(\mathbf{r},t) \approx n_0 - n_0(e/T_i)\Phi_1(\mathbf{r},t)$. Thus, the equations can be linearized as follows:

$$\frac{\partial n_{d1}(\mathbf{r},t)}{\partial t} + n_{d0}\nabla\cdot\mathbf{u}_{d1}(\mathbf{r},t) = 0, \tag{5}$$

$$\frac{\partial \mathbf{u}_{d1}(\mathbf{r},t)}{\partial t} = \frac{Z_d e}{m_d}\nabla\Phi_1(\mathbf{r},t) - \gamma_{Ep}\mathbf{u}_{d1}(\mathbf{r},t), \tag{6}$$

$$\nabla^2\Phi_1(\mathbf{r},t) = 4\pi e\left[Z_d n_{d1}(\mathbf{r},t) + Z_t\delta(\mathbf{r}-\mathbf{v}t)\right] + \lambda_D^{-2}\Phi_1. \tag{7}$$

In a plasma with $T_e \neq T_i$, the Debye length λ_D can be defined as $\lambda_D^{-2} = 4\pi n_0 e^2(1/T_e + 1/T_i)$.

By using a partial Fourier transform with respect to the $\mathbf{r}$ and t dependencies

$$A(\mathbf{r},t) = \int \frac{\mathrm{d}\mathbf{k}\mathrm{d}\omega}{(2\pi)^4} A(\mathbf{k},\omega)\, e^{i\mathbf{k}\cdot\mathbf{r}-i\omega t}, \tag{8}$$

we can obtain the following results:

$$n_{d1}(\mathbf{r},t) = \frac{\beta}{(2\pi)^4}\int \mathrm{d}\mathbf{k}\mathrm{d}\omega e^{i\mathbf{k}\cdot\mathbf{r}-i\omega t} \times\frac{\left[1-\varepsilon(k,\omega)\right]\delta(\mathbf{r}-\mathbf{v}t)}{\varepsilon(k,\omega)}, \tag{9}$$

$$\mathbf{u}_{d1}(\mathbf{r},t) = \frac{\beta}{(2\pi)^4 n_{\mathrm{d0}}}\int \mathrm{d}\mathbf{k}\mathrm{d}\omega e^{i\mathbf{k}\cdot\mathbf{r}-i\omega t} \times\frac{\omega}{k^2}\frac{\left[1-\varepsilon(k,\omega)\right]\delta(\mathbf{r}-\mathbf{v}t)}{\varepsilon(k,\omega)}\mathbf{k}, \tag{10}$$

where $\varepsilon(k,\omega)$ is the dielectric function of the complex plasma, which can be obtained by

$$\varepsilon(k,\omega) = 1 - \frac{\omega_{pd}^2}{\omega(\omega+i\gamma_{Ep})}\left(\frac{k^2\lambda_D^2}{k^2\lambda_D^2+1}\right) \tag{11}$$

with the dust plasma frequency $\omega_{pd}^2 = 4\pi(Z_d e)^2 n_{d0}/m_d$, and the ratio of charges $\beta = Z_t/Z_d$. Equations (9) and (10) are our main result and the numerical results will be shown in the next section.

The dispersion relation for the dust acoustic wave in our 3D fluid model can be easily obtained from eq. (11) and has been derived by Shukla [28,29], and Piel and Goree [30] as

$$\omega^2 = \omega_{pd}^2\frac{k^2\lambda_D^2}{k^2\lambda_D^2+1}. \tag{12}$$

Physically the difference between Mach cones in a 2D and in a 3D complex plasma lies in the dispersion relation of 2D and 3D Yukawa systems.

Numerical results. – Since the maps of particle velocity vectors $\mathbf{u}_{d1}$ [8–12] are usually used to study Mach cones, we then numerically solve eq. (10). The main parameters used in our numerical computations are all selected in accordance with our experiment on PK-3 Plus [26], which will be explained in detail later in next section. Since the wake structures depend sensitively on the perturbation velocity v, given in terms of the Mach number $M = v/C_s$ ($C_s = \lambda_D\omega_{pd}$ is the so-called dust acoustic speed), we will discuss the influence of the Mach number on the wake structures. In addition, the damping effect due to the neutral-gas friction is illustrated by adjusting the normalized damping coefficient $\gamma_0 = \gamma_{Ep}/\omega_{pd}$ (equivalently the discharge pressure p). The stationary spatial patterns of Mach cones from the view of a moving frame in the plane $z = 0$ in a Cartesian coordinate system with $\mathbf{r} = \{x, y, z\}$ will be presented. These patterns are caused by constructive and destructive interference of waves excited by the test particle, and their structures are determined by the wave dispersion properties of the medium as well as the details of disturbance-medium interaction.

We first consider the wakes with weak damping, *i.e.*, when $\gamma_0 = 0.01$, to study the influence of the velocity of disturbance on the wake structures. Multiple-cone structures due to the back and forth motion of particles in the disturbed regions have been shown in fig. 1, with, respectively, $M = 0.8$, $M = 1.1$, and $M = 2$. According to Dubin's theory [13] of Mach cones in complex plasmas, these multiple structures appear to be a consequence of the strongly dispersive nature of the dust acoustic waves. Furthermore, these Mach cones are composed of compressional waves, which can be clearly observed in the figure of the velocity field $\mathbf{u}_{d1}$. By comparing figs. 1(a), (b), and (c), one can conclude that with an increase in the Mach number, the opening angles of the Mach cones diminish due to the well-known Mach-cone–angle relation.

In order to illustrate the damping effect due to the neutral-friction, we then vary the neutral-gas damping rate. Figure 2 displays the velocity field in the wake region for $\gamma_0 = 0.01$, $\gamma_0 = 0.2$, and $\gamma_0 = 0.5$, respectively, while the Mach number is kept at $M = 2$. As expected, the wakes are sharply damped and oscillations in the wake region are soon smoothed out due to the decrease of the damping length $l_D = C_s/\gamma_{Ep}$. It is seen that damping at high pressures reduces the number of multiple-wake structures down to two or even one, as in fig. 2(c). Similar results have been achieved by the previous work [9,12,16] and it is also found that the discharge pressure plays the same role in the laser-excited Mach cones in dusty plasmas [12,16].

Experimental observation and analysis. – In order to support our semianalytic study on Mach cones in 3D complex plasmas, one recent experiment from PK-3 Plus is demonstrated here. The PK-3 Plus on the ISS is a parallel-plate capacitively coupled plasma chamber. Both electrodes are circular plates with a diameter of 6 cm. It can operate with argon, neon and mixture of gases at pressures between 5 Pa and 250 Pa and powers between 0.01 W and 1 W. Silica particles of $1.55 \pm 0.04\,\mu$m diameter and Melamine-Formaldehyde (MF) particles of five different sizes from 2.55 to 14.9 μm diameter can be dispersed into the chamber. As for the experiment described in this paper, 13.56 MHz RF power was used to partially ionize argon at a pressure of 9.6 Pa. The discharge power is approximately 0.3 W, with an amplitude of 46 V peak-to-peak RF voltage. After igniting the discharge, silica particles with a diameter of 1.55 μm were injected into the plasma. A low-frequency function generator with frequencies above the dust plasma frequency was used to close the void and finally form a homogeneous

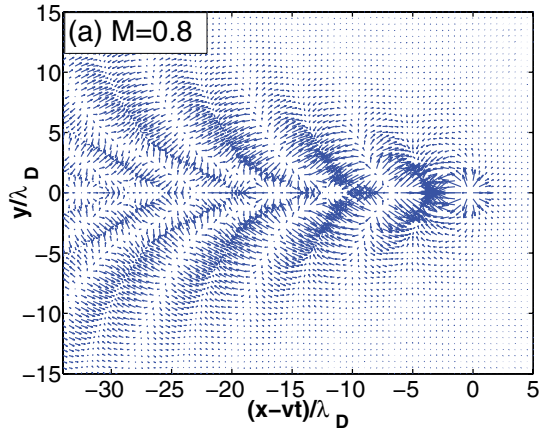

Fig. 1: (Color online) Map of particle velocity $\mathbf{u}_{d1}$ in the plane $z=0$, for different Mach numbers: (a) $M=0.8$, (b) $M=1.1$, and (c) $M=2$, with normalized damping rate $\gamma_0=0.01$.

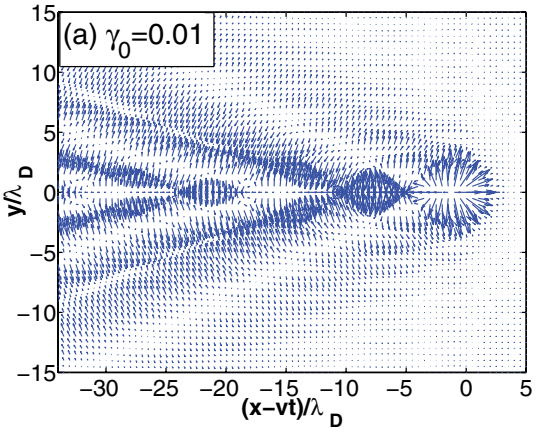

Fig. 2: (Color online) Map of particle velocity $\mathbf{u}_{d1}$ in the plane $z=0$, for different values of normalized damping rate: (a) $\gamma_0=0.01$, (b) $\gamma_0=0.2$, and (c) $\gamma_0=0.5$, with $M=2$.

3D complex plasma. There were also few bigger particles in the left-hand side pure plasma region, which were presumably from particle growth. The particles were illuminated from the side with a laser sheet and recorded by a CCD camera at a frame rate of 50 Hz. Viewing from the side we recorded a movie. The field of view (FOV) was $35.7\times26.0\,\mathrm{mm}^2$ with spatial resolution $49.6\,\mu$m/pixel horizontally and $45.05\,\mu$m/pixel vertically.

In order to determine the velocity of the cone's vertex, along the width of the sample region (we will term this direction as "x-direction", and the direction along the height as "y-direction"), we crop a $14.9\times4.5\,\mathrm{mm}^2$

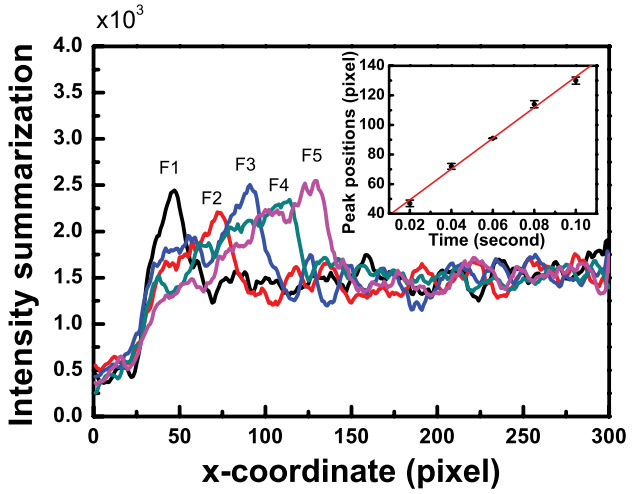

Fig. 3: (Color online) Intensity summarization of a $300 \times 100\,\mathrm{pixel}^2$ region in the center of the FOV along the x-direction at different heights. Shown are the results from five consecutive frames, F1 to F5, which are color-coded (the color varies from black, red, blue, green to pink). The inset shows the linear fit of the peak position.

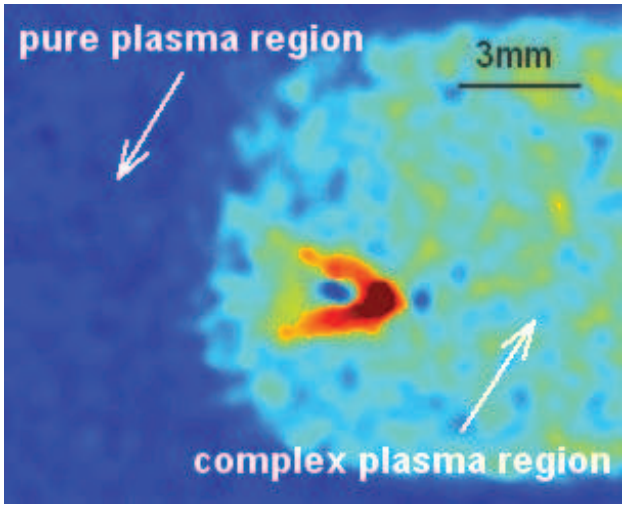

Fig. 4: (Color online) Mach cone in a 3D complex plasma. This figure is shown as a superposition of three consecutive frames shifted so that the cone vertexes in different frames coincide. The blue color region is a pure plasma region with few bigger particles. The green and yellow colors correspond to low dust number density, while the red color corresponds to high dust number density.

$(300 \times 100\,\mathrm{pixel}^2)$ region in the center of the FOV and summarize the pixel intensities for each value of x, for all possible values of y, similar as in ref. [31]. Figure 3 shows the intensity summarization. Higher intensities correspond to high particle densities, therefore the peak of different lines represents the x-coordinates of the cone vertex. Generally one can assume that the supersonic particles move in a straight line at a constant speed for a small path, which is about 3.2 mm in our case for 5 consecutive frames. The linear fit of the cone's vertex x-coordinates is used to determine $v_x = 1040\,\mathrm{pixel/s} = 51.61\,\mathrm{mm/s}$ of the supersonic particle, which is shown in the inset of fig. 3. Note that here we assume that the velocity of the vertex represents the velocity of the supersonic particle.

Examining the sample region in each frame, we then manually measured the x-y coordinates of the cone's vertex. Using a linear fit, the moving direction of the supersonic particle was obtained, which makes an angle of about $-10°$ with the x-direction. Therefore, the speed of the test particle can be obtained as $v \approx 52\,\mathrm{mm/s}$. Due to the high density of our particle cloud, the conventional particle tracking velocimetry (PTV) method could not be applied in our case since the particle positions could not be accurately obtained from the raw data. Alternatively, we simply use a superposition method to generate a clear cone structure [11,12]. A single compressional-wave Mach cone is clearly exhibited in fig. 4. The cone half-angle α, which is called the Mach-cone angle, is measured manually to be $27 \pm 3°$. Then we have $M = 1/\sin\alpha = 2.3 \pm 0.3$ and $C_s = 24 \pm 3\,\mathrm{mm/s}$ based on the definition of the Mach number. This single cone structure agrees well with the result from hydrodynamic model in the high discharge pressure case, see fig. 2(c).

In order to determine whether the complex plasma in our experiment was in a liquid or a crystalline state, we analyzed images from our high-resolution camera, which focused on another FOV close to the Mach-cone region at the same time while our quadrant view camera captured the Mach cone. After the analysis of 987 consecutive frames, only 43% of the cells are 6-sided by drawing Voronoi diagram for each frame, therefore we believe the complex plasma for this observation was within a liquid state since the degree of ordering was not too high. The average particle number density σ_{d0} in the whole 987 consecutive frames is calculated to be $61.4\,\mathrm{mm}^{-2}$ in a $2.1 \times 7.9\,\mathrm{mm}^2$ crop of the FOV by the high resolution camera. Therefore we have the average interparticle distance, $a = (\pi\sigma_{d0})^{-1/2} = 71\,\mu\mathrm{m}$.

The outline of the Mach cone formation was as follows. Bigger particles were trapped outside the main complex-plasma cloud, which was formed by small silica particles with a diameter of $1.55\,\mu\mathrm{m}$. Bigger charged particles can be seen accelerating due to a mechanism that is not well understood from the outer region towards the inner region of the complex plasma. Since the supersonic particles were charged, they scattered the nearby particles. This scattering effect launched compressional waves and formed the V-shaped structure, that is a Mach cone.

Concluding remarks. – This work presents a hydrodynamic model and observation of Mach cones in a three-dimensional complex plasma under microgravity conditions in the PK-3 Plus facility on board the ISS. Numerical results of the fluid velocity of particles showed

different structures of the Mach cone. Special attention was paid to the effect of the disturbance velocity and neutral-gas damping. Multiple-cone structures of compressional wakes have been found and the damping effect may reduce the number of multiple wakes down to a single cone. The observation of Mach cones in a three-dimensional complex plasma under microgravity conditions in the PK-3 Plus facility on board the ISS was reported. A single compressional-wave Mach cone in a 3D complex plasma was observed.

* * *

This work was supported by DLR/BMWi grant No. 50WP0203 and by RFBR grant No. 08-02-00444-a. KJ would like to thank T. Shimizu, Y. N. Wang and L. J. Hou for fruitful discussions.

REFERENCES

[1] Ikezi H., *Phys. Fluids*, **29** (1986) 1764.
[2] Thomas H., Morfill G. E., Demmel V., Goree J., Feuerbacher B. and Mohlmann D., *Phys. Rev. Lett.*, **73** (1994) 652.
[3] Hayashi Y. and Tachibana K., *Jpn. J. Appl. Phys.*, **33** (1994) L804.
[4] Chu J. H. and I Lin, *Phys. Rev. Lett.*, **72** (1994) 4009.
[5] Thomas H. and Morfill G., *Nature (London)*, **379** (1996) 806.
[6] Havnes O., Aslaksen T., Hartquist T. W., Li F., Melandsø F., Morfill G. E. and Nitter T., *J. Geophys. Res.*, **100** (1995) 1731.
[7] Havnes O., Li F., Melandsø F., Aslaksen T., Hartquist T. W., Morfill G. E., Nitter T. and Tsytovich V., *J. Vac. Sci. Technol. A*, **14** (1996) 525.
[8] Samsonov D., Goree J., Ma Z. W., Bhattacharjee A., Thomas H. M. and Morfill G. E., *Phys. Rev. Lett.*, **83** (1999) 3649.
[9] Samsonov D., Goree J., Thomas H. M. and Morfill G. E., *Phys. Rev. E*, **61** (2000) 5557.
[10] Melzer A., Nunomura S., Samsonov D., Ma Z. W. and Goree J., *Phys. Rev. E*, **62** (2000) 4162.
[11] Nosenko V., Goree J., Ma Z. W. and Piel A., *Phys. Rev. Lett.*, **88** (2002) 135001.
[12] Nosenko V., Goree J., Ma Z. W., Dubin D. and Piel A., *Phys. Rev. E*, **68** (2003) 056409.
[13] Dubin D., *Phys. Plasmas*, **7** (2000) 3895.
[14] Zhdanov S., Nunomura S., Samsonov D. and Morfill G., *Phys. Rev. E*, **68** (2003) 035401(R).
[15] Jiang K., Hou L. J., Wang Y. N. and Mišković Z. L., *Phys. Rev. E*, **73** (2006) 016404.
[16] Hou L. J., Wang Y. N. and Mišković Z. L., *Phys. Rev. E*, **70** (2004) 056406.
[17] Havnes O., Li F., Hartquist T. W., Aslaksen T. and Brattli A., *Planet. Space Sci.*, **49** (2001) 223.
[18] Mamun A. A., Shukla P. K. and Morfill G. E., *Phys. Rev. Lett.*, **92** (2004) 095005.
[19] Zhdanov S., Morfill G., Samsonov D., Zuzic M. and Havnes O., *Phys. Rev. E*, **69** (2004) 026407.
[20] Ma Z. W. and Bhattacharjee A., *Phys. Plasmas*, **9** (2002) 3349.
[21] Nosenko V., Zhdanov S. and Morfill G., *Phys. Rev. Lett.*, **99** (2007) 025002.
[22] Morfill G. E., Thomas H. M., Konopka U., Rothermel H., Zuzic M., Ivlev A. and Goree J., *Phys. Rev. Lett.*, **83** (1999) 1598.
[23] Bose A. and Janaki M. S., *Phys. Plasmas*, **13** (2006) 012104.
[24] Brattli A., Havnes O. and Melandsø F., *Phys. Plasmas*, **9** (2002) 958.
[25] Xin Q. and Bhattacharjee A., *Mach Cones in Three-Dimensional Yukawa Crystals* (unpublished).
[26] Thomas H. M., Morfill G. E., Fortov V. E., Ivlev A. V., Molotkov V. I., Lipaev A. M., Hagl T., Rothermel H., Khrapak S. A., Suetterlin R. K., Rubin-Zuzic M., Petrov O. F., Tokarev V. I. and Krikalev S. K., *New J. Phys.*, **10** (2008) 033036.
[27] Epstein P., *Phys. Rev.*, **23** (1924) 710.
[28] Rao N. N., Shukla P. K. and Yu M. Y., *Planet. Space Sci.*, **38** (1990) 543.
[29] Shukla P. K., *Phys. Scr.*, **45** (1992) 504.
[30] Piel A. and Goree J., *Phys. Plasmas*, **13** (2006) 104510.
[31] Schwabe M., Rubin-Zuzic M., Zhdanov S., Thomas H. M. and Morfill G. E., *Phys. Rev. Lett.*, **99** (2007) 095002.